
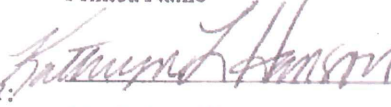



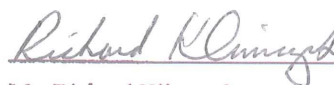
REPORT TITLE: Response to Administrative Law Judge's Decision Number
12-09-008 Regarding Dr. Douglas Hamilton's Concerns

SIGNATORIES

PREPARED BY:  DATE: August 1, 2014
Dr. William Page PG&E Geosciences Department
Printed Name Organization

GEOLOGY VERIFIED BY:  DATE: August 1, 2014
Ms. Kathryn Hanson AMEC Environment & Infrastructure, Inc.
Printed Name Organization

GEOPHYSICS VERIFIED BY:  DATE: August 1, 2014
Dr. Carlos Mendoza Fugro Consultants, Inc.
Printed Name Organization

APPROVED BY:  DATE: Sept. 10, 2014
Mr. Richard Klimczak PG&E Geosciences Department
Printed Name Organization

RECORD OF REVISIONS

Rev. No.	Reason for Revision	Revision Date
0	Initial Release. This work was defined and tracked under SAPN 50638223.	8/1/2014

TABLE OF CONTENTS

	Page
Signatories	1
Record of Revisions	2
Lists of Tables, Figures, and Attachments	5
Abbreviations and Acronyms	8
1.0 INTRODUCTION	10
1.1 Purpose	11
1.2 Intended Use of the Results	11
1.3 Scope of Work	11
1.4 Project Quality Assurance Program, Participating Organizations, and Responsibilities	12
2.0 ASSUMPTIONS	13
3.0 DATA.....	14
4.0 METHODOLOGY	17
4.1 MBES Data	17
4.2 Construction of Geologic Cross Sections	18
4.3 Seismic-Reflection Profiles.....	18
4.4 Interpretation of Diabase Intrusion Geometry from Tomographic Data	19
5.0 SOFTWARE	20
6.0 RESULTS AND ANALYSIS	21
6.1 Extent of PG&E's Investigations Addressing Concerns Raised by Dr. Hamilton.....	21
6.2 Diablo Cove Fault.....	22
6.2.1 Direct Observations of the Diablo Cove Fault	24
6.2.2 Diablo Cove Fault Model of Dr. Hamilton	28
6.2.3 Evaluation of the Diablo Cove Fault Model	31
6.2.4 Conclusion with Respect to the Diablo Cove Fault.....	40
6.3 San Luis Range/ IOF Thrust.....	40
6.3.1 Previous Interpretations of Seismic Sources.....	41
6.3.2 San Luis Range/ IOF Thrust Model of Dr. Hamilton	47
6.3.3 Analysis of Uplift Rate Boundaries.....	51

6.3.4	Analysis of Seismicity and Seismic-Reflection Data.....	58
6.3.5	Evaluation of Dr. Hamilton’s San Luis Range/ IOF Thrust.....	70
7.0	CONCLUSIONS	73
8.0	LIMITATIONS	75
9.0	IMPACT EVALUATION	76
10.0	REFERENCES	77

LISTS OF TABLES, FIGURES, AND ATTACHMENTS

Tables

Table 6-1	Number of Earthquakes as a Function of Magnitude in the Seismicity Analysis Box Shown on Figure 6-42
-----------	--

Figures

Figure 6-1	Onshore-Offshore Hillshade Image of the DCP.P Area Showing Improved Coverage in the Nearshore with the Kelpfly MBES data
Figure 6-2	Locations of Sources and Receivers in the DCP.P Area for the 2012 3D Seismic Survey
Figure 6-3	Interpretation of the Diablo Cove Fault Across the DCP.P Site and Diablo Cove from Hamilton (2012c)
Figure 6-4	Interpretation of the Diablo Cove Fault Across the DCP.P Site Area and Offshore to the Shoreline Fault Zone from Hamilton (2012c)
Figure 6-5	Geologic Map of the DCP.P Site Area Showing Faults Identified During Pre-Construction Studies: (a) Jahns et al. (1966-1973) and (b) PG&E (2014b)
Figure 6-6	Geologic Map of the DCP.P Site Showing Faults Identified During Pre-Construction Studies: (a) PG&E (1974) and (b) PG&E (2014b)
Figure 6-7	Explanation to Accompany Geologic Maps Based on PG&E (2014b)
Figure 6-8	Photograph of Mouth of Diablo Canyon Creek and Diablo Cove Fault Exposed in the Sea Cliff from Hamilton (2012c)
Figure 6-9	Diablo Cove Fault as Mapped in the Excavations for the Turbine Building, Unit 1 Containment, and Sea Cliff from Hamilton (2012c)
Figure 6-10	Photographs of Faulting in the Foundation Excavations for Unit 1 from Hamilton (2012c)
Figure 6-11	Interpretation of the Diablo Cove Fault Prior to Offshore Kelpfly Data from Hamilton (2012a)
Figure 6-12	Geologic Cross Section of the Irish Hills from Hamilton (2012c)
Figure 6-13	Geologic Map of the DCP.P Site Area Showing Locations of Seismic Lines and Shallow Geologic Cross Sections
Figure 6-14	Map of the DCP.P Area Showing Areas of High Seismic P-Wave Velocities Associated with Buried Diabase Bodies
Figure 6-15	Seismic Profile CL 395 and Geologic Interpretation, Cross Section E-E'

- Figure 6-16 Geologic Map of the DCP.P Area Showing Locations of Geologic Cross Sections F-F', G-G', and H-H'
- Figure 6-17 Shallow Geologic Cross Sections F-F', G-G', and H-H'
- Figure 6-18 MBES-LiDAR Hillshade Image of Diablo Cove: (a) Uninterpreted and (b) Showing the Diablo Cove and Headland Faults
- Figure 6-19 MBES-LiDAR Hillshade Image of the DCP.P and Offshore Area: (a) Uninterpreted and (b) Showing the Diablo Cove, Headland, and Shoreline Faults
- Figure 6-20 Seismicity Cross Sections Drawn Perpendicular to the Shoreline Fault
- Figure 6-21 Faults in the Irish Hills and Adjacent Area from Hamilton (2012a), with San Luis Range/ IOF Thrust and Shoreline Fault Highlighted
- Figure 6-22 Map of Seismic Sources by PG&E (2011)
- Figure 6-23 Previous Interpretations of the Inferred Offshore Fault (IOF)
- Figure 6-24 Onshore Faults Comprising the San Luis Bay Fault Zone and Offshore Faults and Folds East of the Hosgri Fault Zone
- Figure 6-25 Map of Coastal Uplift Rates as Determined During the LTSP from Hanson et al. (1994)
- Figure 6-26 Map of the San Luis Bay Fault Zone from Lettis et al. (1994)
- Figure 6-27 Map of Available Bathymetry (a) During the LTSP and (b) During the Shoreline Fault Investigation
- Figure 6-28 Maps and Profiles of the Central Segment of the Shoreline Fault from PG&E (2011)
- Figure 6-29 Maps Showing the Shoreline and N40W Faults with Bathymetric and Other Geophysical and Geomorphic Data from PG&E (2011)
- Figure 6-30 Maps and Profiles of the N40W Fault, Later Renamed the East Branch of the Point Buchon Fault, from PG&E (2011)
- Figure 6-31 Geologic Cross Sections Showing the Interpreted San Luis Range/IOF Thrust from Hamilton (2012c)
- Figure 6-32 Earthquake Focal Mechanisms, Epicenters, and Seismicity Profile Locations from Hamilton (2012a)
- Figure 6-33 Seismicity Cross Sections from Hamilton (2012a)
- Figure 6-34 Earthquake Epicenters, Focal Mechanisms, and Locations of Seismicity Profiles from Hamilton (2012c)
- Figure 6-35 Seismicity Cross Sections from Hamilton (2012c)
- Figure 6-36 Quaternary Faults and Sedimentary Basins in the Vicinity of the San Luis Range

- Figure 6-37 Uplift Rate Contour Map of the San Luis Range Area
- Figure 6-38 Maps and Profiles of the Shoreline Fault South of Point San Luis from PG&E (2011)
- Figure 6-39 Maps and Profiles of the Shoreline Fault Southeast of the DCP.P from PG&E (2011)
- Figure 6-40 Difference Between Hardebeck (2010) and Hardebeck (2014a) Epicenter Locations in the Vicinity of the Irish Hills
- Figure 6-41 Earthquake Location Difference Statistics Between Hardebeck (2010) and Hardebeck (2014a)
- Figure 6-42 Overview of Irish Hills Seismicity
- Figure 6-43 Northern Zone Seismicity
- Figure 6-44 Central Zone Seismicity
- Figure 6-45 Southern Zone Seismicity
- Figure 6-46 Seismicity Cross Sections Perpendicular to the Shoreline Fault
- Figure 6-47 OADC-FM Solution Planes Fit to Seismicity from Hardebeck (2014b)
- Figure 6-48 Structural Interpretation of OADC-FM Solution, Scenario 1, from Hardebeck (2014b)
- Figure 6-49 Structural Interpretation of OADC-FM Solution, Scenario 2, from Hardebeck (2014b)
- Figure 6-50 Structural Interpretation of OADC-FM Solution, Scenario 3, from Hardebeck (2014b)
- Figure 6-51 Geologic Map of the Point San Luis Area with Seismic Profile Lines
- Figure 6-52 Total Magnetic Field Anomaly, Helicopter Magnetic Survey, Point San Luis Area
- Figure 6-53 Seismic Reflection Profile, Line A-A'
- Figure 6-54 Seismic Reflection Profile, Line B-B'
- Figure 6-55 Seismic Reflection Profile, Line AWD 112-140

Attachments

Attachment 1a Report Verification Summary by Ms. Kathryn Hanson

Attachment 1b Report Verification Summary by Dr. Carlos Mendoza

ABBREVIATIONS AND ACRONYMS

2D	two-dimensional
3D	three-dimensional
A4NR	Alliance for Nuclear Responsibility
AB 1632	Assembly Bill 1632
AWD	accelerated weight drop
CEC	California Energy Commission
CL	crossline
CPUC	California Public Utilities Commission
CRADA	Cooperative Research and Development Agreement
CSUMB	California State University, Monterey Bay
DCPP	Diablo Canyon Power Plant
DEM	digital elevation model
ELP	early–late Pliocene
FCL	Fugro Consultants, Inc.
FSAR	Final Safety Analysis Report
ft.	feet <i>or</i> foot
GMP	Geologic Mapping Project (AB 1632 funded)
IOF	Inferred Offshore fault
ITR	Independent Technical Reviewer
ka	thousand years ago (<i>also</i> thousand years old)
kft/s	thousand feet per second
km	kilometers
LCI	Lettis Consultants International, Inc.
LESS	Low-Energy Seismic Study (AB 1632 funded)
LiDAR	light detection and ranging
LTSP	Long Term Seismic Program
m	meters
m/kyr	meters per thousand years
MBES	multibeam echosounder
mm/yr	millimeters per year

MSL	mean sea level
NCEDC	Northern California Earthquake Data Center
NRC	U.S. Nuclear Regulatory Commission
OADC	Optimal Anisotropic Dynamic Clustering
OADC-FM	OADC plus focal mechanism information (modification to algorithm)
ONSIP	Onshore Seismic Interpretation Project (AB 1632 funded)
PG&E	Pacific Gas and Electric Company
PSAR	preliminary safety analysis report
PSHA	probabilistic seismic hazard analysis
QA	quality assurance
SSER	supplemental safety evaluation report
SLRF	San Luis Range/ IOF thrust fault interpreted by Dr. Hamilton
SSC	seismic source characterization
SSHAC	Senior Seismic Hazard Analysis Committee
UNR	University of Nevada, Reno
USGS	U.S. Geological Survey
V_p	<i>P</i> -wave (or compressional-wave) velocity

1.0 INTRODUCTION

This report presents an evaluation of geologic interpretations made by Dr. Douglas H. Hamilton that have relevance for seismic hazard to the Diablo Canyon Power Plant (DCPP), located in San Luis Obispo County, California.

This evaluation was part of the work being done by Pacific Gas and Electric Company (PG&E) to comply with the recommendation of the California Energy Commission (CEC), as reported in the CEC's November 2008 report titled "An Assessment of California's Nuclear Power Plants: AB 1632 Report," that PG&E use three-dimensional (3D) seismic-reflection mapping and other advanced techniques to explore fault zones near the DCP.P.

On February 10, 2012, the Alliance for Nuclear Responsibility (A4NR) submitted testimony of Dr. Douglas H. Hamilton to support their concerns with PG&E's application for approval of ratepayer funding to perform additional seismic studies recommended by the CEC under AB 1632. Dr. Hamilton is a registered Professional Geologist and California Certified Engineering Geologist with BS, MS and PhD degrees earned at Stanford University. As stated in his testimony, between 1971 and 1991 he periodically worked as a consultant on PG&E's Diablo Canyon nuclear project. His testimony points out what he considers weaknesses in the (then) proposed AB 1632 investigations.

California Public Utility Commission (CPUC) Decision (D.) 12-09-008 stated the following with respect to Dr. Hamilton's testimony:

Dr. Hamilton's testimony focused on... two major gaps in PG&E's studies:

- "A continued lack of interest in the Diablo Cove Fault, a local fault on the Diablo Canyon Nuclear Power Plant site running from offshore directly under the turbine building and Unit 1 containment foundations." And,
- "The 'San Luis Obispo Range/Inferred Offshore Fault' in San Luis Obispo Bay, which A4NR says falls outside PG&E's target zone for enhanced studies. Dr. Hamilton testified that the existence of this structure is required in order to account for the level uplift of the Irish Hills/San Luis Range....PG&E said it will address the concerns of Dr. Hamilton. We expect PG&E to do so."

In response to this decision, PG&E committed to addressing the concerns of Dr. Hamilton through the AB 1632 program. Elements of the AB 1632 program that are used to address Dr. Hamilton's concerns include the following:

- Acquisition, processing, and interpretation of land seismic-reflection data throughout the Irish Hills, and high-resolution 3D land seismic-reflection data near the DCP.P and along the coastal terraces southeast of the DCP.P.
- Acquisition, processing, and interpretation of two-dimensional (2D) and 3D seismic-reflection data offshore along the northern and southern segments of the Shoreline fault.
- Analysis of the various data sets pertinent to assessing Dr. Hamilton's hypotheses.
- Preparation of this report.

1.1 Purpose

The purpose of this report is to formally respond to the CPUC D. 12-09-008, 13 September 2012, with respect to Dr. Douglas Hamilton's 10 February 2012 testimony regarding the Diablo Cove fault and his inferred San Luis Range / Inferred Offshore fault (IOF) thrust beneath the DCP.P.

This report has two objectives:

1. To evaluate whether the Diablo Cove fault is, or is not, a seismic hazard to the DCP.P.
2. To evaluate the existence of the San Luis Range/ IOF thrust as characterized by Dr. Hamilton.

1.2 Intended Use of the Results

The primary use of this study is to comply with CPUC D. 12-09-008. This study is also intended to inform state and federal stakeholders and regulators of PG&E's findings relative to Dr. Hamilton's testimony and ideas therein. In addition, information on the Diablo Cove and San Luis Range/ IOF thrust faults will contribute to the currently ongoing seismic hazard analysis for the DCP.P mandated by the U.S. Nuclear Regulatory Commission (NRC) through letter 50.54(f). This seismic hazard analysis is being conducted in accordance with the Senior Seismic Hazard Analysis Committee (SSHAC) Level 3 process and is designed to assess ground motion hazards to the DCP.P through probabilistic seismic hazard analysis (PSHA).

1.3 Scope of Work

PG&E performed the following activities to prepare this response:

- Review of the materials presented by Dr. Hamilton in the A4NR testimony (Hamilton, 2012a), at scientific conferences (Hamilton, 2010, 2012b), and at the DCP.P seismic source characterization (SSC) SSHAC workshop in November, 2012 (Hamilton, 2012c).
- Analysis of geomorphic, geologic, geophysical, and seismicity data from the DCP.P site area, the Irish Hills, and the southwestern San Luis Range.
- Analysis of geologic and seismic-reflection data, and interpretations of these data, performed as part of the AB 1632 studies.
- Interpretation of high-resolution bathymetric data from the DCP.P site area (CSUMB, 2007, 2009, 2010, 2011).

1.4 Project Quality Assurance Program, Participating Organizations, and Responsibilities

The work performed for this project was conducted under the PG&E Quality Assurance (QA) Program, in compliance with 10CFR50, Appendix B.

This report was prepared by Dr. William Page with the help of Dr. Stephen Thompson and Dr. Matthew Huebner of Lettis Consultants International, Inc., and Dr. Daniel O'Connell and Mr. James Turner of Fugro Consultants, Inc. (FCL). Dr. Stuart Nishenko (PG&E Geosciences) provided technical oversight. Ms. Kathryn Hanson of AMEC Environment & Infrastructure, Inc. served as Independent Technical Reviewer (ITR) for the geology part of the project, and Dr. Carlos Mendoza of FCL, served as the ITR for the geophysical part of the project. Ms. Marcia McLaren, Quality Assurance Manager for PG&E Geosciences, provided surveillance and oversight of compliance with QA requirements.

2.0 ASSUMPTIONS

The primary assumption made in this data report is that previously collected and published data and interpretations were done to a high technical standard: the materials mostly consisted of peer-reviewed publications, reports accepted by the NRC, the AB 1632 investigations that have been completed under a QA program, and other related studies conducted by qualified scientists within their field of expertise.

3.0 DATA

This report is based on analysis of information in the documents listed below. The list is organized by source.

Documents created or provided by Dr. Hamilton:

- Hamilton, D., 2010. Dual system tectonics of the San Luis Range and vicinity, Coastal Central California, Text and illustration from poster presented at the American Geophysical Union Fall Meeting, San Francisco, Calif., 15 December.
- Hamilton, D., 2012a. Direct Testimony of Douglas H. Hamilton. Written testimony submitted by the Alliance for Nuclear Responsibility to the Public Utilities Commission of the State of California, February 10.
- Hamilton, D., 2012b. The Diablo Canyon Nuclear Power Plant in South-Central Coastal California; Incremental Recognition of Seismic Hazard, 1965-2012. Abstract presented at the Association of Engineering Geologists Annual Meeting, Salt Lake City, Utah, PowerPoint file, September.
- Hamilton, D., 2012c. Irish Hills/San Luis Range Tectonic and Fault Model. Presentation by Dr. Hamilton at the 26 November 2012 Diablo Canyon SSC SSHAC Workshop 2, PowerPoint file.

Documents resulting from AB 1632 studies:

- Fugro Consultants, Inc. (FCL), 2014a. 2012 3D Onshore Seismic Survey Report, Project Report No. PGEQ-PR-21, Rev. 0, submitted to Pacific Gas and Electric Company.
- Fugro Consultants, Inc. (FCL), 2014b. 2011–2012 Onshore 2D-3D Data Processing Report, PGEQ-PR-08, Rev. 0, submitted to Pacific Gas and Electric Company.
- PG&E, 2014a. DCP.P 3D/2D Seismic-Reflection Investigation of Structures Associated with the Northern Shoreline Seismicity Sublineament of the Point Buchon Region. Technical Report GEO.DC.PP.TR.12.01, Rev. 1.
- PG&E, 2014b. Geologic Mapping and Data Compilation for the Interpretation of Onshore Seismic-Reflection Data, Technical Report GEO.DC.PP.TR.14.01, Rev. 0.
- PG&E, 2014c. Offshore Low-Energy Seismic-Reflection Studies in Estero Bay, San Luis Obispo Bay, and Point Sal Areas. Technical Report GEO.DC.PP.TR.14.02, Rev. 0.
- PG&E, 2014d. Onshore Seismic Interpretation Project (ONSIP) 2011 Data Report. Technical Report GEO.DC.PP.TR.14.03, Rev. 0.

Documents created as part of the original siting study for the DCP.P Units 1 and 2:

- Jahns, R.H., 1966. Geology of the Diablo Canyon Power Plant Site, San Luis Obispo County, California, December 5.
- Jahns, R.H., 1967a. Geology of the Diablo Canyon Power Plant Site, San Luis Obispo County, California, Supplementary Report, January 3.
- Jahns, R.H., 1967b. Geology of the Diablo Canyon Power Plant Site, San Luis Obispo County, California, Supplementary Report II, July 8.
- Jahns, R.H., 1968. Geology of the Diablo Canyon Power Plant Site, San Luis Obispo County, California, Supplementary Report III, June 19.
- Jahns, R.H., Johnson, A.M., Blum, R.L., Korbay, S.R., Hamilton, D.H., and Harding, R.C., 1973. Geologic Map of Diablo Canyon Power Plant Site. Unpublished(?) map based on mapping performed 1966-1973 for Pacific Gas and Electric Company, iterations of map used in PG&E (1974) FSAR for Units 1 and 2, approximate scale 1:500.
- PG&E, 1974. Final Safety Analysis Report, Figure 2.5-12: Geologic Map of Excavations for Plant Facilities, by Jahns, R.H., Hamilton, D.H., Korbay, S.R., and Blum, R., 1966-1971 and Figure 2.5-5: Geologic Map of Diablo Canyon Coastal Area, by R.H. Jahns, 12/65, 3/66, 7/66 supplemented by R.C. Harding, 1970, and S.R. Korbay, 1969, 1970.

Data and supporting documents provided to PG&E as part of its ongoing Long Term Seismic Program (LTSP), including results of U.S. Geological Survey activities supported by PG&E through a Cooperative Research and Development Agreement (CRADA):

- AMEC Environment & Infrastructure, Inc., 2012. *Preliminary Reevaluation of Emergent Shoreline Angles, San Luis Range, Diablo Canyon Power Plant, LTSP Update, San Luis Obispo, California*. Letter report to William Page, PG&E Geosciences Department, 28 February.
- California State University, Monterey Bay (CSUMB), 2007, 2009, 2010, and 2011. Multibeam echosounder (MBES) data for the California Central Coast; available at http://seafloor.csumb.edu/SFMLwebDATA_c.htm; accessed 16 May 2013.
- Hardebeck, J.L., 2010. Seismotectonics and fault structure of the California central coast, *Bulletin of the Seismological Society of America* **100** (3): 1031–1050.
- Hardebeck, J.L., 2013. Geometry and earthquake potential of the Shoreline fault, Central California, *Bulletin of the Seismological Society of America* **103** (1): 447–462.
- Hardebeck, J.L., 2014a. Updated seismicity relocation catalog, file hypoDD_combined_update_140218.reloc, written communication to Lettis Consultants International, Inc., 18 February.

- Hardebeck, J.L., 2014b. Seismicity and Fault Structure of Estero Bay and the Irish Hills. Presentation at the March 2014 Diablo Canyon SSC SSHAC Workshop #3, PowerPoint file.
- Johnson, S.Y., and Watt, J.T., 2012. Influence of fault trend, bends, and convergence on shallow structure and geomorphology of the Hosgri strike-slip fault, offshore central California, *Geosphere* **8** (6): 1632–1656.
- Langenheim, V.E., 2014. Gravity, Aeromagnetic and Rock-property Data of the Central California Coast Ranges: U.S. Geological Survey Open-File Report 2013-1282.
- Onshore-offshore composite DEM (version 7) based on onshore LiDAR data, offshore ship MBES data, and offshore Kelpfly MBES data.
- Sliter, R.W., Triezenberg, P.J., Hart, P.E., Watt, J.T., Johnson, S.Y., and Scheirer, D.S., 2009 (revised 2010). *High-Resolution Seismic Reflection and Marine Magnetic Data Along the Hosgri Fault Zone, Central California*, U.S. Geological Survey Open-File Report 2009-1100, version 1.1.

Recent investigations by PG&E not funded by AB 1632:

- PG&E, 2004. Final Safety Analysis Report of the Diablo Canyon Independent Spent Fuel Storage Installation. U.S. Nuclear Regulatory Commission Docket No. 72-26.
- PG&E, 2011. Shoreline Fault Zone Report: Report on the Analysis of the Shoreline Fault Zone, Central Coastal California. Report to the U.S. Nuclear Regulatory Commission, January.
- PG&E, 2013. Stratigraphic Framework for Assessment of Fault Activity Offshore of the Central California Coast Between Point San Simeon and Point Sal, Technical Report GEO.DCPP.TR.13.01.

4.0 METHODOLOGY

Our approach to evaluating the concerns raised by Dr. Hamilton is to treat his interpretations as proponent models for sources of seismic hazard to the DCP.P. Two types of seismic hazard are being proposed in his models:

- For the Diablo Cove fault, Dr. Hamilton suggests that it represents a surface-fault-rupture hazard to the DCP.P, and possibly an independent source of earthquakes that can generate vibratory ground motions at the plant.
- For the San Luis Range/ IOF thrust, Dr. Hamilton suggests that it is a source of earthquakes that could generate vibratory ground motions at the DCP.P.

Our evaluation of these proposed hazards focuses on evidence from the data for or against these hazards, the uniqueness of the interpretations, and the possibility that alternative interpretations provide a better explanation of the observations than those proposed by Dr. Hamilton.

In support of this general approach, a number of specific analyses were conducted as part of this study. Below, we briefly describe methodologies associated with the analysis of MBES bathymetric data, the construction of geologic cross sections, and the interpretation of seismic-reflection and tomography profiles.

4.1 MBES Data

The analysis of the projection of the Diablo Cove fault offshore used Global Mapper GIS software to create artificial hillshade images from a high-resolution DEM that merged various offshore MBES data sets. Artificial hillshade images used to interpret offshore geology and evaluate the geomorphic expression of the Diablo Cove fault offshore were generated using different illumination azimuths, illumination inclinations, and vertical exaggerations. Illumination azimuth refers to the map direction of the simulated illumination source, on an angular scale of 0 to 359 degrees, with 0 degrees for north, 90 degrees for east, 180 degrees for south, and 270 degrees for west. Illumination inclination is the angle from the horizontal, from 0 to 90 degrees, with 0 degrees representing illumination from the horizon and 90 degrees representing an illumination source directly overhead. Vertical exaggerations are multiples of the horizontal scale calculated from the DEM.

Images were created with azimuths of 0, 50, 70, 99, 310, and 330 degrees and inclinations of 30, 45, 70, and 75 degrees. Vertical exaggerations of zero (0), three times (3X) and ten times (10X) were also constructed and considered. After all the images were reviewed, the preferred artificial hillshade image for evaluating possible geomorphic expression of an offshore Diablo Cove fault was judged to have an azimuth of 0, inclination of 45 degrees, and a vertical exaggeration of 10X. This combination, discussed in Section 6.2.3.2, creates maximum contrast for seafloor features oriented generally east-west, or subparallel to the trend of the proposed offshore Diablo Cove fault.

4.2 Construction of Geologic Cross Sections

Three shallow geologic cross sections were drawn through and adjacent to the DCP.P. These cross sections are shown on figures discussed in Section 6.2.3.1, based on geologic map data provided in PG&E (2014b). The cross section lines were drawn in ArcMap 10.2, and topographic profiles were generated using the onshore-offshore 1-meter (m) DEM and 3D analyst tool. The profiles were exported to Adobe Illustrator for cross section construction. Lithologic contacts, structural data (bedding orientations), and other pertinent geologic information were transferred to the topographic profiles in Adobe Illustrator. Apparent dip of bedding orientations oblique to cross section lines were calculated using the Satin (1960) method. Arbitrary surfaces (form lines) were drawn to better illustrate structural continuity and to maintain stratigraphic thickness.

4.3 Seismic-Reflection Profiles

Seismic data are used in the evaluation of the Diablo Cove fault (discussed in Section 6.2.3) and San Luis Range/ IOF thrust (discussed in Section 6.3.4).

To evaluate the Diablo Cove fault, a north-south seismic-reflection and seismic velocity cross section was extracted from 3D seismic-reflection and tomography volumes in a location that crossed the Diablo Cove fault between the sea cliffs and the DCP.P. facilities. The seismic-reflection cross section, corresponding to crossline 395 (CL 395), was extracted from the 2012 Phase 1 SigSeis migration-amplitude-stack (rawstack) 3D volume in the DCP.P. site area (FCL, 2014a). The cross section was trimmed to a line extent within the source-receiver acquisition area between the sea cliffs on the south end of the line (inline 680) and the northern extent of the SigSeis receivers (inline 760). A high-pass filter was applied to provide a balance of shorter-wavelength and longer-wavelength reflections relative to the long-wavelength dominated reflections in the rawstack. The corresponding compressional wave (*P*-wave) velocity (V_p) cross section along crossline 395 was extracted from the highest resolution tomography volumes available as a function of elevation in FCL (2014a) at 5 foot (ft.) elevation and 30 ft. horizontal intervals. V_p was also extracted at constant elevations at 50 ft. horizontal intervals from the highest resolution tomography volumes in FCL (2014a) to show lateral variations in V_p throughout the DCP.P. area.

To evaluate the San Luis Range/ IOF thrust, seismic velocities from 3D tomography (FCL, 2014b) in the Point San Luis area were extracted along 2D seismic-reflection profile positions to compare and overlay on seismic-reflection data. Arbitrary 2D lines were extracted from 3D seismic-reflection volumes along profile positions of interest. Seismic-reflection and velocity data were displayed and interpreted in IHS Kingdom Suite software along with geologic and geophysical data imported into Kingdom Suite. In order to evaluate the presence or absence of the San Luis Range /IOF thrust, which has been postulated by Dr. Hamilton to dip to the northeast at 30–40 degrees and impinge on the Shoreline fault zone at depths between 1 and 2.5 kilometers (km) depth, the apparent dip range of the postulated fault orientation oblique to cross section lines was calculated and overlain on the seismic-reflection data for evaluating the presence or absence of the fault surface projected to depth.

4.4 Interpretation of Diabase Intrusion Geometry from Tomographic Data

The high-resolution land seismic data collected from the DCP.P site area feature areas of high velocity interpreted to be shallow magmatic intrusions of diabase. The high-resolution 3D V_P tomography model to 1,000 ft. below mean sea level (MSL) for the 2012 Phase 1 DCP.P data area (FCL, 2014b) had 5-ft.-thick vertical cells spaced horizontally 50 ft. apart. This 3D velocity model was used to estimate the diabase thickness near the DCP.P. The total thickness of 5-ft. cells with seismic velocities ≥ 11.5 thousand feet per second (kft/s) between elevations of 0 and 750 ft. below MSL was used to define the diabase thickness. The most appropriate cutoff velocity to use to measure diabase thickness is uncertain. A cutoff velocity of 12.5 kft/s exceeds measured velocities in the sedimentary Obispo Formation in the DCP.P area and provides a lower bound estimate of diabase thickness. A cutoff velocity of ≥ 11.5 kft/s may include altered rock adjacent to thin diabase sills in addition to the diabase intrusive material. However, a lower cutoff velocity is less likely to underestimate diabase thickness relative to a higher cutoff velocity. Thus, the cutoff velocity of ≥ 11.5 kft/s was used to estimate diabase thickness in this analysis. The median increase in diabase thickness for areas with nonzero thicknesses is 140 ft. for the cutoff velocity of ≥ 11.5 kft/s relative to using a cutoff velocity of 12.5 kft/s.

5.0 SOFTWARE

This project has no software validation requirements. The reader is directed to technical reports cited in this report to understand software programs used in developing those data and interpretations.

Six software programs (Global Mapper, ArcGIS, Adobe Illustrator, IHS Kingdom, Microsoft Excel, and IDL) were used to analyze the geologic and geophysical data and to prepare figures for this report.

Global Mapper (version 14) is an industry-standard GIS software application developed by Blue Marble Geographics. This software was used to create and analyze the onshore-offshore DEM through the rendering of various slope maps and hillshade images. Hillshade images used a variety of artificial sun azimuths and inclinations and variable amounts of vertical exaggeration for lineament analysis.

ArcGIS, developed by ESRI, is a software package used by industry, government, and academia to collate and map spatial data in an accurate georeferenced manner. This software (ArcMap version 10.2) was used to compile, integrate, and evaluate the geologic data and construct the technical information in several maps in this report.

Adobe Illustrator (Creative Suite 5) was used for computer drafting of geologic cross sections and other figures. Illustrator is a graphical illustration software package that is widely used by the earth sciences community.

IHS Kingdom Version 8.6 Hotfix 4 is a modular software package used by industry and academia to map 2D and 3D seismic-reflection, tomographic, and borehole data. Software modules used include 2D/3Dpak and VuPak. These IHS software modules are nuclear safety-related software that were used for the analysis and interpretation of seismic data. The software was validated in conformance with QA Procedure QAP-03C and documented in report PGEQ-PR-07 (FCL, 2012).

Microsoft Excel is a spreadsheet application developed by Microsoft for Microsoft Windows. Microsoft Excel Office 2010 version was used for analyses of seismicity, seismic velocity, and seismic-reflection data.

IDL (Interactive Display Language) is a software package used by industry, government, and academia for data analysis and visualization. IDL version 8.2 was used for visualization and analysis of seismicity, seismic velocity, and seismic-reflection data.

6.0 RESULTS AND ANALYSIS

The combined results and analysis of this technical report are divided into three main sections. Section 6.1 responds to the assertion made by Dr. Hamilton that PG&E has been deficient in addressing his concerns regarding interpreted seismic hazards. Section 6.2 evaluates the Diablo Cove fault. Section 6.3 evaluates the proposed San Luis Range/ IOF thrust. At the beginning of each section we present a summary of the analysis followed by the details used to make our conclusions.

6.1 Extent of PG&E's Investigations Addressing Concerns Raised by Dr. Hamilton

Dr. Hamilton raised the concern about whether the investigations performed to date by PG&E had been sufficient to address potential seismic hazards from the Diablo Cove fault and the San Luis Range/ IOF thrust (Hamilton, 2012a). As outlined below and discussed in this report, extensive investigations conducted or supported by PG&E provide sufficient high-quality data to evaluate the potential seismic hazards from both the Diablo Cove fault and proposed San Luis Range/ IOF thrust. These investigations include those conducted under the AB 1632 program, as well as other studies implemented by PG&E both before and during the AB 1632 program: obtaining and analyzing high-resolution MBES data offshore of the Irish Hills; gathering geologic data along transects across the Irish Hills in support of the seismic-reflection surveys; acquiring and interpreting 2D and 3D seismic-reflection survey data both offshore and onshore; analyzing earthquake hypocentral locations and focal mechanisms beneath the Irish Hills using double-difference methods; and analyzing late Quaternary patterns and rates of uplift in the continental shelf and coastal environments.

Beginning in the 1980s with the LTSP, PG&E has been consistently proactive in obtaining information to understand and assess the seismic hazard and risk for the DCP.P. After the identification of the Shoreline fault from analysis of seismicity data by Dr. Jeanne Hardebeck in 2008, through a PG&E-funded CRADA activity, PG&E has supported the following activities to investigate the Shoreline fault and structures beneath the Irish Hills:

- Obtaining and analyzing high-resolution MBES data offshore of the Irish Hills, including in the locations where Dr. Hamilton interprets the San Luis Range/Inferred Offshore fault and offshore Diablo Cove fault to be. In addition to acquiring and interpreting standard high-resolution ship data, PG&E helped fund the development of the R/V *Kelpfly*, a shallow-draft water craft equipped with instrumentation for obtaining MBES data in the extreme shallow-water nearshore environments of Diablo Cove and adjacent areas near the DCP.P (Figure 6-1).
- Gathering geologic data along transects across the Irish Hills in support of the seismic-reflection surveys. This work is presented in the Geologic Mapping Project (GMP) technical report (PG&E, 2014b), an AB 1632 activity. The GMP integrated earlier detailed geologic mapping of the stratigraphy and structures along the coast between Islay Creek and Point San Luis, with the detailed

interpretation of offshore geology using MBES data supplemented with diver samples conducted as part of the Shoreline fault zone investigation (PG&E, 2011). These coastal and nearshore investigations provide data that are directly relevant to the assessment of Dr. Hamilton's San Luis Range/ IOF thrust. Additionally, they provide structural context for evaluating the significance of the Diablo Cove fault.

- Completing 2D and 3D seismic-reflection surveys both offshore and onshore. The AB 1632 investigations offshore focused on the northern end (PG&E, 2014a) and the southern end (PG&E, 2014c) of the Shoreline fault. These surveys involved collecting data in the areas where Dr. Hamilton interprets the San Luis Range/ IOF thrust to intersect the Shoreline fault. The AB 1632 onshore seismic surveys collected data across the Irish Hills, along the coast, and within the DCP.P site area. This work is presented in the 2D land survey report (PG&E, 2014d) and the 3D land survey report (FCL, 2014a). These surveys were conducted in the areas directly overlying the proposed Diablo Cove fault and his hypothesized northeast-dipping San Luis Range/ IOF thrust. As an example, the 3D land seismic data acquisition configuration of the DCP.P site area is shown on Figure 6-2.
- Analyzing earthquake hypocentral locations using double-difference methods (Hardebeck, 2010, 2013, 2014a) and reviewing focal mechanisms information beneath the Irish Hills to locate potential faults by fitting planes using earthquake distance and misfit of *P*-wave first-motion polarities (Hardebeck, 2014b). These activities, supported by PG&E through the CRADA program, include both the creation of a high-quality seismicity data set and an innovative analysis of the data that can be used to evaluate Dr. Hamilton's hypothesized San Luis Range/ IOF thrust.
- Analyzing late Quaternary rates of uplift in the continental shelf and coastal environments. These activities include the USGS's evaluation of seismic-reflection data across the Hosgri Fault Zone through the CRADA program (Sliter et al., 2009; Johnson and Watt, 2012) and an evaluation of late Quaternary stratigraphy on the continental shelf (PG&E, 2013). The late Quaternary uplift rate boundaries (areas of an observed uplift rate gradient) for the Irish Hills and surrounding areas were analyzed by combining the onshore and offshore geology and geomorphology data to evaluate whether the Shoreline fault is an uplift rate boundary (Hanson et al., 1994; PG&E, 2011; AMEC, 2012). Understanding the locations, patterns, and rates of late Quaternary uplift is a critical component of the evaluation of Dr. Hamilton's hypothesized San Luis Range/ IOF thrust.

6.2 Diablo Cove Fault

In his written testimony (Hamilton, 2012a) and SSHAC workshop presentation (Hamilton, 2012c), Dr. Hamilton presents a proponent model in which the newly named "Diablo Cove fault" is a potential fault rupture and earthquake ground motion hazard to the DCP.P. Note that for clarity, PG&E uses the name Diablo Cove fault in this response to refer to the features noted by Dr. Hamilton and to his model of the fault's extent. The

faults that comprise the Diablo Cove fault were mapped beneath and adjacent to the DCP.P site prior to its construction, and were shown to pre-date the wave-cut platform and overlying marine terrace deposits estimated to be approximately 120,000 years old. Dr. Hamilton raises the issue of the Diablo Cove fault from his continued interest in the project since he helped map the geology of the DCP.P site in the 1970s. He has interpreted new information gained since the completion of LTSP studies reported in PG&E (1988, 1990) and points to the need to evaluate how the Diablo Cove fault might relate to the active Shoreline fault, a fault that was not recognized when the original site characterization work was completed.

Dr. Hamilton's concern is that the Diablo Cove fault connects to the Shoreline fault laterally and extends to seismogenic depth, and as such, is capable of causing surface rupture and possibly significant ground motion hazard. Dr. Hamilton connects the faults mapped onshore to the offshore Shoreline fault based on geomorphic expression he interprets from MBES bathymetry-derived hillshade images. His interpretation is shown on Figures 6-3 and 6-4.

PG&E's analysis of the Diablo Cove fault consisted of evaluating available data and figures and text provided by Hamilton (2012a, 2012c). The available data included information obtained prior to construction of the DCP.P, including photographs, trench and excavation logs, written statements by those who investigated the fault prior to construction of the DCP.P, detailed information on geologic structure, and figures and text provided by Hamilton (2012a, 2012c). Important new data that has become available since the discovery of the Shoreline fault zone include the Kelpfly MBES bathymetry data, relocated seismicity, and high-resolution seismic-reflection data obtained around the plant.

The evidence does not support Dr. Hamilton's contention that the Diablo Cove fault is a seismic hazard to the DCP.P. Where the fault is documented to occur on land, the fault consists of short, discontinuous strands in tuffaceous sandstone of the Miocene Obispo Formation with displacements on the order of a few feet. The offshore projection of the Diablo Cove fault postulated by Dr. Hamilton follows lineaments he interprets in the MBES data to the Shoreline fault, but these lineaments do not follow continuous features nor are they aligned with the fault trend documented at the coastline. Our interpretation of the MBES bathymetric data shows that potential lineaments along the offshore projection of the Diablo Cove fault from the sea cliff would intersect and be truncated by a north- to northwest-striking fault that is well expressed beneath Diablo Cove. This cross-cutting relationship demonstrates that the Diablo Cove fault would not continue west to the Shoreline fault zone.

Interpretations of geologic, seismic-reflection, and seismicity data do not support Dr. Hamilton's contention that the Diablo Cove fault extends to depth. Structural analysis using the extensive geologic information at the surface combined with images at depth created from the 3D seismic-reflection survey and tomography data collected around the plant support the interpretation—shared by the original mapper—that the minor faults associated with the Diablo Cove fault are related to shallow folding that occurred prior to the middle Quaternary (pre-Quaternary uplift of the Irish Hills). The faulting may be

related to an intrusive body of Obispo Formation diabase imaged at a depth of approximately 400 feet (120 meters) directly north of the fault. No credible association can be made between microseismicity at depth and the location of the Diablo Cove fault at the surface.

In the sections below, we present a detailed evaluation of the Diablo Cove fault as a potentially active structure through analysis of all the available geologic, seismological, and geophysical data. The assessment of Dr. Hamilton's interpretation is organized in four sections. Section 6.2.1 reviews the direct evidence for the Diablo Cove fault based on original mapping conducted for PG&E. Section 6.2.2 describes Dr. Hamilton's interpretations of the Diablo Cove fault in his testimony and workshop presentation. Section 6.2.3 evaluates Dr. Hamilton's interpretations using the available data and includes interpretations of the faulting made by the geologists at the time of the initial observations. Section 6.2.4 presents PG&E's conclusion regarding the viability of Dr. Hamilton's model.

6.2.1 Direct Observations of the Diablo Cove Fault

Dr. Hamilton defines the Diablo Cove fault as an approximately east-west-striking fault zone mapped in four locations (Hamilton, 2012a), as follows:

- In the sea cliff directly south of the outlet of Diablo Canyon Creek.
- Under the foundation of the turbine building.
- Under the foundation of the Unit 1 containment structure.
- In a road cut for the switchyard access road east of the DCP.P power block.

The locations of mapped faults and other structural features (joints and bedding orientations) are shown on Figures 6-5 and 6-6. These figures each have two panels: panel a shows original geologic maps, and panel b shows the digital geologic map created by the GMP, which was compiled from original geologic map data and supplemented with more recent mapping (PG&E, 2014b). Figure 6-7 provides an explanation of geologic units and symbols for Figures 6-5 and 6-6.

6.2.1.1 Locations of the Faulting

Figure 6-5a shows a geologic map created by Drs. R.H. Jahns, D.H. Hamilton, and colleagues that follows the original mapping from 1966 to 1973 for the DCP.P site. The map incorporated surface observations, excavation mapping for Units 1 and 2, and logging of trenches and road cuts for the proposed Units 3 and 4 and other facilities. Figure 6-5b shows the compilation geologic map of the DCP.P site area completed as part of the GMP, which integrated these original data with other geologic data collected during more recent studies (PG&E, 2014b). Figure 6-6 shows the excavation mapping of the DCP.P power block, including the turbine building and Unit 1 containment structure, in full detail: in panel a, as presented in the 1974 DCP.P Final Safety Analysis Report (FSAR; PG&E, 1974) and, in panel b, as compiled for the GMP.

As shown on Figures 6-5 and 6-6, the faulting below the Unit 1 containment structure consists of two small, discontinuous zones of faulting 10–20 m long mapped in bedrock.

Beneath the turbine building, a zone of faults is mapped in bedrock for a length of approximately 70 m. Between the faults mapped beneath the turbine building and Unit 1 containment structure, there is an approximate 50 m long gap that contains abundant structural observations of bedding and jointing but no mapped faulting. At the coastline, faults mapped in bedrock directly south of the Diablo Canyon Creek mouth are at least 25–40 m long. Between the coastline and turbine building fault exposures is a gap of approximately 80 m where unfaulted Quaternary terrace deposits obscure bedrock; these two exposures were tentatively connected by Jahns et al. (1973) on an approximately N80°E trend. Between the faults beneath the Unit 1 containment structure and the faults under the switchyard access road cut is a span of approximately 180 m. Although much of this distance was obscured by surficial deposits, continuous mapping of bedding along the cut slope east of the power block that is between Unit 1 and the access road suggests that no faults were observed along a continuous or near-continuous bedrock exposure there.

6.2.1.2 Nature of the Faulting

The faulting exposed in the sea cliff and beneath the DCP.P was described by Dr. Jahns in his original report, “Geology of the Diablo Canyon Power Plant Site” (Jahns, 1966) and in his first two supplementary reports (Jahns, 1967a, 1967b). The faulting beneath the DCP.P reported by Jahns (1967a, 1967b) was based on exploratory trench exposures. Additional information on these faults was later provided during the foundation excavation mapping. Hamilton (2012a) provides a description of faulting encountered during this later phase. Jahns (1966, 1967a, 1967b) describes the faulting as within thinly to thickly bedded, moderately hard to very hard sandstone of the Monterey Formation (Tm on Figure 6-3). We note that this bedded tuffaceous and dolomitic sandstone unit was later reclassified by Hall (1973) as part of the Obispo Formation, which is the stratigraphic scheme adopted by PG&E (1990, 2004, 2011, 2014b), and labeled as unit Tmofb on Figures 6-5b and 6-6b).

The fault zone exposed adjacent to the coastline directly south of the Diablo Canyon Creek mouth was considered by Jahns (1966) to be a “minor” fault that projects north of the DCP.P site. Figure 6-8 is an annotated photograph of the fault location taken from offshore looking east toward the plant during plant construction circa 1972. In his second supplemental report, Jahns (1967b) describes the relationship between the faulting recognized at the plant site and in the sea cliff near the mouth of Diablo Canyon Creek. He notes that the fault planes measured on the sea cliff and on the adjacent modern wave-cut platform strike more northerly than bedding, and project eastward to ground north of the DCP.P site.

The strike we infer based on mapping and this description is approximately N55°E to N60°E (Figures 6-3 and 6-5). The dip of the fault as recorded on a geologic map and sketch of the exposure shown on Figure 6-3 is approximately 40–60 degrees northwest. Steep, northerly plunging slickensides noted on the fault surfaces indicate north-side-up dip-slip displacement. Jahns (1967b) states that the total amount of movement is “probably no more than a few tens of feet and could well be less than ten feet.” To corroborate this, he notes the lack of continuity in the individual fault strands within the

exposure, the narrow fault planes, and the minor deformation of strata between the fault planes. He interprets the zone “to be a second-order feature related to a marked change in dip of strata to the south, and its general sense of movement is what one would expect if the breaks were developed during folding of the Monterey [sic] section against what amounts to a broad buttress of Obispo tuff farther south.”

The exploratory trenches mapped by Jahns (1967a) described discontinuities in the trenches that included “slip joints,” shear surfaces, and faults. Most of these surfaces that have experienced relative geologic displacements were described as hairline fractures with thin clay, and as displacements from “a small fraction of an inch to several inches.” Other surfaces were more prominent with narrow (less than half an inch thick) zones of gouge or breccia. The zones of faulting were observed in greater detail during the excavations for the power block foundation; the mapping that synthesizes the foundation excavation exposures, the trench logging, and the sea-cliff logging is the basis of the geologic maps on Figures 6-5a and 6-6a.

Hamilton (2012a) summarizes the history of geologic investigations at the DCP.P site up to and following information reported in Jahns’ 1966 and 1967 reports, and he refers to two figures in particular. The first figure is the detailed map of the geologic features exposed in the walls and, where accessible, floors of the Unit 1 foundation excavation that was completed circa 1969 (Figure 6-6a). The second figure is the four composite cross sections shown on Figure 6-9. For clarity, we modified Dr. Hamilton’s original figure (slide 18 from Hamilton, 2012c) by adding labels A-A’ to D-D’ to the four sections, and then show the locations of these cross sections on Figures 6-5 and 6-6.

Cross section A-A’ is located directly east of the Unit 1 containment structure and shows two subparallel, north-dipping faults with minor splays near the surface. Cross section B-B’ is located through the Unit 1 containment structure and shows an absence of faulting along a section through the middle of the Unit 1 containment structure. The note on this cross section, “Zone of Closely Spaced Fracturing Within Fault Trend,” appears to refer to the zone of fractures on the geologic map that strikes approximately N30°W, or nearly orthogonal to the trend of the Diablo Cove fault zone. Cross section C-C’ is located through the turbine building and shows a zone of faults from the exploration Trench A underlain by a narrower, steeply north-dipping fault. Cross section D-D’ is located across the mouth of Diablo Canyon Creek and shows the steeply north-dipping zone of faulting exposed at the sea cliff consisting of multiple branching and discontinuous strands (Figure 6-5).

Hamilton (2012a) describes an overall length (~400 ft., or 120 m) of faulting beneath the DCP.P site that aligns with the sea-cliff exposure. This length appears to be based on Figure 6-6a and would encompass the faulting beneath the turbine building, the faulting beneath the east side of the Unit 1 containment structure, and the area in between that is absent of faulting. Hamilton (2012a) notes that the zone crossing the turbine building was approximately 30 ft. (9 m) wide and consisted of three distinct strands that dip 45–50 degrees north. Hamilton (2012a) further notes that at the Unit 1 containment foundation, no distinct offsets were recognized in the west wall and floor, but two fault zones were mapped on the east wall, separated by about 100 ft. (30 m) and aligned with the zone

seen crossing the turbine-generator building. The faults also were observed to dip approximately 50 degrees north. Hamilton (2012a) notes that the dip-slip displacement across the faults crossing the turbine-generator building was between 1 and 5 ft., and the faults consisted of multiple shears in a zone from a few inches to approximately 2 ft. wide.

The amounts of stratigraphic separation on faults that we noted on the original geologic map (Figure 6-6a) ranged from 2 to 3 feet and were transferred onto the GMP geologic map (Figure 6-6b) for clarity. Annotated photographs presented by Hamilton (2012a) are reproduced on Figure 6-10. These photographs, taken during the excavation mapping, show zones of minor faults cutting bedding in a jointed, fractured rock mass with no apparent juxtaposition of different rock type or facies. Notes on the photographs, presumably by Dr. Jahns, appear to indicate the amount of displacement as 3–5 ft. (with a query) on one photograph, and 2 ft. on the other. Overall, Hamilton (2012a) reports that the general aspect of the faulting in the foundation excavation walls, where observed, was one of several distinct breaks that were much more coherent than the “diffuse” breaks recognized in the near surface seen in the overlying exploratory trenches.

The faults mapped along the switchyard access road are described by Hamilton (2012a) and shown on Figure 6-5a as, “small dislocations caused by north-side-up reverse faulting approximately along the trend of the headland and Unit 1 area faulting.” The faults as depicted on Figure 6-5a match the description given by Hamilton (2012a). Figure 6-5b, the map created as part of the GMP (PG&E, 2014b), shows a fault trace in this same location that was compiled from a geologic map of the DCP.P site area that was included in the FSAR for Units 1 and 2 (Figure 2.5-5 of PG&E, 1974). We presume that the slightly different depiction of the faults along the switchyard access road represents the same observations.

6.2.1.3 Activity of the Faulting

Direct observations of the faults that Dr. Hamilton collectively calls the Diablo Cove fault indicate a clear relationship between faulted bedrock and unfaulted top-of-rock surface and Quaternary marine terrace deposits overlying the faults (Jahns, 1966, 1967a, 1967b; Hamilton, 2012a, 2012c). Referring to the activity of faults mapped along the sea cliff, Jahns stated, “None of the faults observed in the mapped area extends upward from the bedrock section into overlying terrace deposits, nor have any of the wave-cut benches beneath these deposits been offset by such faults” (Jahns, 1966, p. 30). The following year, Jahns (1967a) reached a similar conclusion regarding the stratigraphic relationships between bedrock discontinuities mapped in the trenches and the overlying wave-cut platform and marine deposits. He estimated the age of the wave-cut bench and overlying marine terrace deposits to be “...at least 100,000 years, and more probably at least 120,000 years” based on their current elevation, the late Pleistocene sea-level curve, and radiometric dating from other similar terraces along adjacent stretches of the California coastline (Jahns, 1966, 1967a, 1967b).

An age of approximately 120,000 years (120 ka) is the current preferred age, based on the elevation of the terrace (back-edge elevation of 30–32 m), the observation and altitudinal

spacing of higher and lower emergent terraces, a well-constrained age determination of the last global sea-level highstand, and age dating of the equivalent terrace conducted during the LTSP (PG&E, 1988; Hanson et al., 1994). Hamilton (2012a, 2012c) suggests that the age of the unfaulted terrace platform and overlying marine deposits where trenched at the Unit 1 site is approximately 80 or 105 ka. Although the 105 ka age is permissible based on stratigraphic constraints, the 80 ka age is not consistent with the correlation and dating of the sequence of marine terraces adjacent to the DCP.P (Hanson et al., 1994). A lower terrace with a back edge elevation of approximately 10 m is mapped across the small headlands bordering both the northern and southern margins of Discharge Cove. The age of this terrace is estimated to be 80 ka based on fossil assemblage data and a U-series date ($\sim 76,000 \pm 4,000$ years) for samples collected from deposits overlying the correlative terrace at multiple sites within 1 to 2 miles of the DCP.P (PG&E, 1988; Hanson et al., 1994).

The clear crosscutting relationship between the fault and the overlying unfaulted terrace yields a minimum age constraint for the Diablo Cove fault, dictating that it must be older than approximately 120 ka (or possibly 105 ka). The maximum age of the faulting, Jahns (1967b) points out, is millions of years. This maximum age is bracketed by the depositional age of the Obispo Formation (Miocene), and the interpreted timing of onset of folding and contractional deformation (late Miocene to Pliocene; e.g., Luyendyk, 1991).

6.2.1.4 Summary

In summary, the direct evidence for the Diablo Cove fault consists of four approximately collinear locations of minor faulting within a rock mass that has local evidence for subordinate discontinuities and slip surfaces. The isolated exposures that comprise the Diablo Cove fault are demonstrated to be discontinuous beneath the power block, and the faults at the sea cliff have a more northerly trend (N55°E to N60°E) across the sea cliff and wave-cut platform than the overall trend of the tentatively correlated exposures (N80°E). Jahns (1967b) suggested that this difference in fault strike may indicate that the fault zone at the sea cliff may be separate from the small faults beneath the power block. The faulting is restricted to within a bedded tuffaceous sandstone unit that is 15–18 million years old, and observations suggest maximum displacements on any discontinuity of approximately 1 m to perhaps several meters (probably “not more than a few tens of feet,” according to Jahns, 1967b). Multiple direct observations clearly demonstrate that the faulting or any other bedrock discontinuities do not offset overlying deposits that are approximately 120 ka.

6.2.2 *Diablo Cove Fault Model of Dr. Hamilton*

Dr. Hamilton’s model of the Diablo Cove fault is presented in both his testimony (Hamilton, 2012a) and his SSHAC workshop presentation (Hamilton, 2012c). This model represents Dr. Hamilton’s interpretation regarding the fault’s location, along-strike length, downdip width, and seismic potential.

6.2.2.1 Location of the Faulting

Dr. Hamilton shows two map interpretations of the Diablo Cove fault—one in his testimony (Hamilton, 2012a) and another in his SSHAC workshop presentation (Hamilton, 2012c). The maps are shown on Figures 6-11 and 6-4, respectively. Both maps show a continuous fault over a distance of approximately 2 km that intersects the Shoreline fault on the west and terminates on the hillside east of the DCP.P on the east. The depiction of the faulting onshore is similar on both maps, with a solid, continuous trace drawn across the coastline and power block and a dashed line across the switchyard access road. The faulting offshore is different on the two figures, with the map presented at the SSHAC workshop (Figure 6-4) benefitting from the additional offshore data provided from the Kelpfly MBES survey data, and presumably, superseding the map from the testimony (Figure 6-11).

A larger-scale map showing greater detail of the interpreted trace of the Diablo Cove fault was also presented by Dr. Hamilton at the SSHAC workshop (Hamilton, 2012c) and is reproduced on Figure 6-3. The onshore depiction of faulting on this map is more consistent with the excavation mapping (Figures 6-5 and 6-6) in that it shows the discontinuous faulting within the DCP.P site and the original mapping of the faults at the sea cliff and wave-cut platform adjacent to the mouth of Diablo Canyon Creek. The larger-scale map on Figure 6-3 shows Dr. Hamilton's detailed interpretation of the fault offshore—guided by the MBES data and onshore bedding data. Dr. Hamilton draws the fault with a change in strike at the coastline, then a broad curve in the fault trace to cross the north headland of Diablo Cove (Figure 6-3). Directly east of the headland, Dr. Hamilton interprets the locally east-west-trending trace of the Diablo Cove fault to offset in a right-lateral sense the trace of a generally north-south-striking fault (Figure 6-3). We informally refer to this north-south fault herein as the “headland” fault. South of the Diablo Cove fault, the headland fault trace coincides with a strong lineament seen in the MBES data across Diablo Cove. North of the Diablo Cove fault, the headland fault trace is an extrapolation of a fault mapped in the sea cliff during pre-construction mapping. Farther offshore (Figure 6-4), Dr. Hamilton interprets the Diablo Cove fault to connect to the Shoreline fault along east-west-trending lineaments identified on an MBES image in the rocky seafloor.

6.2.2.2 Nature of the Faulting

Hamilton (2012a) summarizes the nature of the faulting characterized from the trench and foundation exposures as described in Section 6.2.1. Dr. Hamilton interprets the different description of the faulting in the trenches and the foundation exposures, as well as the overall geometry documented from the foundation exposures, to reflect faulting that developed near “a free surface” due to the, “pattern of upward splaying and near-surface secondary antithetic fault-bounded ‘pop-up’ wedges that characterizes the upper level of exposure of the Diablo Cove fault in both the natural headland exposure and the artificial exploratory trench and foundation exposures.” Dr. Hamilton further cites the results of a petrographic study by Jahns (1966) that observed brittle deformation mechanisms, including microfracture, in the faults at the headland exposure, and quotes Dr. Jahns as stating that “none [of the samples] appeared to have been smeared out or partially

obliterated by intense shearing or grinding.” Dr. Hamilton’s interpretation of this observation is that “The most recent faulting may have occurred when the now uplifted bedrock floor of the 80,000 year terrace surface was still the actively eroding surf zone platform” (Hamilton, 2012a).

In the offshore, Hamilton (2012c) described the fault as being apparent as a lineament in the MBES data. Based on the crosscutting relationship between the east-west Diablo Cove fault and the north-south headland fault, Dr. Hamilton estimates the total measured offset of the Diablo Cove fault as “about a 15 m right-lateral offset at the point of crossing” (Hamilton, 2012c).

The summary slide of the SSHAC workshop presentation by Hamilton (2012c) states, “The Diablo Cove fault shows reverse oblique displacement increasing from 1–2 m dip slip in DCNPP Unit 1 bedrock to ≥ 15 –20 m component of right slip near the Diablo Cove north headland.”

6.2.2.3 Activity of the Faulting

Hamilton (2012a, 2012c) recognizes the observed upward truncation of faulting at the wave-cut platform and the evidence for absence of faulting within overlying marine terrace deposits documented by Jahns (1966, 1967a, 1967b). However, Hamilton (2012a ,c) interprets the wave-cut platform to be associated with marine sea-level highstands at 80 ka or 105 ka, slightly younger than the 120 ka marine highstand interpreted by Jahns (1966) and Hanson et al. (1994). The basis for the younger age is not provided in Hamilton’s (2012a) testimony. Based on his interpretation of the brittle deformation mechanisms observed near the sea-cliff exposure and the pattern of faulting that developed “near a free surface,” Hamilton further suggests that faulting may have occurred when the wave-cut platform was actively eroding on the seafloor (Hamilton, 2012a).

6.2.2.4 Dip and Depth Extent

Hamilton (2012c, slide 11) presents a geologic cross section through the DCP.P and Irish Hills that extends to approximately 8 km depth; this slide is reproduced on Figure 6-12. The geologic cross section shows the Diablo Cove fault extending to a depth of approximately 7 km with a dip of approximately 45 degrees north. In his summary slide of the SSHAC workshop presentation, Hamilton (2012c) states that “a downdip projection of the Diablo Cove fault may presently be a locus of low level seismicity.” In his testimony, he does not draw a deep cross section that includes an interpretation of the Diablo Cove fault at depth, but rather correlates “a cluster of three epicenters of small earthquakes 0.5 km northwest of the offshore Diablo Cove fault” with the Diablo Cove fault, noting that these events, between 4 and 6 km deep, are “approximately down dip from the surface trace of the north-dipping Diablo Cove fault” (Hamilton, 2012a).

6.2.3 Evaluation of the Diablo Cove Fault Model

Our evaluation of Dr. Hamilton's model of the Diablo Cove fault consists of an assessment of its onshore location and style of faulting, offshore location, and interpreted style of faulting, activity, and depth extent based on available data.

6.2.3.1 Diablo Cove Fault Onshore

The evidence from the cliff exposure, pre-construction trenches, foundation excavation mapping, and mapping along the switchyard access road all demonstrate that the Diablo Cove fault is a laterally discontinuous zone of minor faults that is restricted to the tuffaceous, dolomitic sandstone of the Obispo Formation. The direct evidence from the onshore mapping does not support the characterization implied by Dr. Hamilton that the Diablo Cove fault has lateral continuity across the onshore reach as drawn on his summary maps (Figures 6-4 and 6-11). The detailed mapping of trench walls and foundation excavation exposures, discussed above, clearly demonstrates that the faulting is minor and discontinuous. For example, faults beneath the Unit 1 containment structure are limited to two separate zones of approximately 10 m and 15 m length in the eastern part of the containment footprint, and both of these faults are disconnected from the faults mapped under the turbine building (Figures 6-5 and 6-6). The implied continuity of the fault zone across the power block, suggested by the statement on cross section B-B' of Figure 6-9, "Zone of Closely Spaced Fracturing Within Fault Trend," appears misleading, as the fracture zone mapped across the Unit 1 containment that crosses B-B' clearly trends obliquely to the Diablo Cove fault (Figures 6-5 and 6-6).

The direct evidence from observations beneath the plant and at the sea-cliff exposure demonstrates that the amount of fault offset is minor—on the order of 1–2 m or less stratigraphic separation in places where offset equivalents were observed within the foundation excavations (Figures 6-5 and 6-10), and estimates of fault offset at the sea-cliff exposure of several meters or less (Jahns, 1967b). The steep, northerly plunging slickensides noted on the fault surfaces at the cliff exposure by Jahns (1967b) provide direct evidence that lateral offset is probably minor and that the estimated dip separation is probably close to net offset.

The evidence for the absence of lateral continuity and the minor amount of offset in the onshore has a direct bearing on assertions made by Dr. Hamilton that the fault has continuity at depth. It is not credible, from simple scaling arguments, that faults on the order of 10 m (or tens of meters) long and with a few meters or less of offset can have downdip widths of several kilometers as Dr. Hamilton's model proposes (Figure 6-12).

We present an alternative interpretation of the Diablo Cove fault to that of Hamilton (2012c) that fits better with the available data. This alternative interpretation draws on geologic data from the GMP (PG&E, 2014b) and recently acquired high-resolution 3D land seismic-reflection and tomography data from the DCP.P area (FCL, 2014a, 2014b).

Figure 6-13 shows a geologic map at 1:6,000 scale from the GMP (PG&E, 2014b). Seismic-reflection and tomography data collected during the 2012 3D seismic survey provide additional constraints for subsurface geologic interpretation, supplementing the

outcrop data. On this map are the locations of four geologic cross sections and the approximate limits of interpreted diabase bodies beneath the DCP.P as imaged from the high-resolution seismic data collected in the DCP.P area (FCL, 2014a). As described in Section 4.4, diabase bodies are interpreted to be approximately imaged in the 3D tomography as volumes with P -wave velocities (V_P) of 11.5 kft/s or greater; the extent of the diabase bodies in the DCP.P area are shown on Figure 6-14. The top panel (Figure 6-14a) shows a map of the approximate total thickness of the 3D volume that has velocities greater than or equal to 11.5 kft/s. The bottom panel (Figure 6-14b) shows a map of velocities at an elevation of -400 ft., which approximately represents the depth of greatest diabase extent, with warm colors (yellow, orange, and red) symbolizing velocities greater than or equal to 11.5 kft/s.

Cross-section E-E', which is coincident with crossline (CL) 395, is located between the discharge and land north of the DCP.P along a north-south trend (Figures 6-13 and 6-15). CL 395 is a vertical seismic display extracted from the 3D seismic data (FCL, 2014a). The cross section straddles the Diablo Cove fault in an area of good seismic source and receiver coverage (Figure 6-2) and has abundant structural control in the southern portion of the line from foundation excavation mapping (Figure 6-13). The top panel (Figure 6-15a) shows the seismic profile with reflectors overlain by P -wave velocities in kft/s (colors and contours). The seismic data provide subsurface information useful to help evaluate the structural context and interpret the fault. The bottom panel (Figure 6-15b) shows a geologic interpretation of cross section E-E' that incorporates surface geologic data and geophysical information. Details about the methodology for drawing the cross section are in Section 4.2.

The seismic-reflection data, represented by the gray undulating background image, provide little useful information along CL 395 (Figure 6-15a). The seismic-reflection data represent acoustic structure, which does not always correspond to geologic bedding or unconformity structure. In the DCP.P area, the steep to vertical bedding observed in outcrop is not represented in the seismic-reflection data due partially to the difficulty in detecting reflections from very steep reflectors and to the lack of strong acoustic contrasts along bedding within the Obispo Formation.

The tomographic data, however, show 3D contrasts in V_P that can indicate the presence and geometry of specific geologic materials in the subsurface (Figure 6-15a). The relatively low V_P material underlying the ground surface down to an elevation of approximately -300 ft. is consistent with the presence of weathered and unweathered Obispo Formation, similar to surface outcrops. From -300 to -500 ft. elevation, an elongated body of higher V_P material is present within the Obispo Formation. Based on tomographic data from the surrounding area, this high V_P body is interpreted as a zone of contact metamorphism or alteration associated with the intrusion of diabase magma into the Obispo Formation. Alteration is commonly accompanied by dolomitization, which increases the V_P of the rock.

Significant diabase bodies are located beneath the DCP.P area adjacent to either side of CL 395. The isopach map of the diabase bodies (Figure 6-14a) based on the thickness of material having a V_P greater than or equal to 11.5 kft/s above -750 ft., shows their

distribution and a range in thickness. In the vicinity of CL 395, the 3D tomographic volume images a well-constrained (up to 19.0 kft/s) diabase body that is several hundred feet thick east of CL 395, and a smaller body directly west of CL 395 (Figure 6-14a).

Along CL 395, a sliver of the western diabase body extends into the profile, surrounded by a thick altered contact aureole (Figures 6-14 and 6-15). The geometry of the diabase interpreted from the tomography depth slice is shown on Figure 6-14b, along with a projection of the approximate diabase extent from line CL 386, located approximately 82 m west of CL 395 (Figure 6-13). The subhorizontal geometry of the interpreted diabase is similar to the gently dipping to subhorizontal strata estimated at shallow depths based on surface bedding attitudes in Obispo Formation, suggesting that the diabase body was emplaced as a sill (Figure 6-15b).

The emplacement of a magmatic sill requires the upward displacement of overlying strata to accommodate the size and shape of the volcanic intrusive. This emplacement creates “forced folds” and small faults in the overlying sedimentary strata (Hansen and Cartwright, 2006). Multiple phases or pulses of magma emplacement can result in irregularly shaped forced folds. This may explain the high level of bedding dip variability in the Diablo Cove area, including northern Diablo Cove (Figure 6-13), and suggests an early phase of fold deformation during and/or immediately after the deposition of the Obispo Formation.

On CL 395 the V_p also decreases below the diabase alteration zone at about –500 ft. elevation (Figure 6-14a), and stays relatively low to a depth of –800 ft., consistent with the continuation of Obispo Formation strata below the contact aureole. Velocities increase again at –800 to –1,000 ft. depth. The velocity increase is fairly abrupt at the northern end of CL 395 and more gradual at the southern end. Interpretation of seismic-reflection and tomography data directly east of CL 395 suggests the presence of an angular unconformity at –1,000 ft. depth coincident with the strong increase in V_p (FCL, 2014a). The evidence in CL 395 for an unconformity is less clear. The abrupt increase in velocity at the north end of CL 395 may represent an unconformity and/or change in velocity within the Obispo Formation (as shown on Figure 6-15b), or alternatively it may be associated with an unconformity with an older unit such as Cretaceous sandstone.

The available data on geologic structure across the Diablo Cove fault is shown in greater detail on Figure 6-16, a 1:3,000 scale map, and on Figure 6-17, which shows three parallel geologic cross sections, F-F', G-G', and H-H'. These shallow cross sections, shown as an isometric drawing, are approximately 450 m long and evenly spaced at 125 m intervals drawn perpendicular to the Diablo Cove fault (Figure 6-17). Details about the methodology for drawing the cross sections are in Section 4.2. Cross section F-F' was drawn through the sea-cliff exposure of the fault, cross section G-G' was drawn through the faults exposed in the foundation excavation for the turbine building, and cross section H-H' was drawn directly east of the Unit 1 containment structure and east of the easternmost fault that was mapped beneath the power block.

The geologic cross sections illustrate the steeply north-dipping bedding in the south that gently shallows toward the north (Figures 6-16 and 6-17). At the coastline, on cross section F-F', the Diablo Cove fault cuts the flank of an asymmetric syncline and produces

minor north-side-up reverse faulting and shortening of the fold limb. Down dip the Diablo Cove fault projects to the interpreted diabase intrusion. The cross section shows the Diablo Cove fault terminating at or above the diabase body, suggesting that shortening of the Obispo Formation—largely accommodated by folding—was also accommodated by shallow faulting within the folded strata due in part to heterogeneity in the rock types (e.g., diabase, tuff, tuffaceous, dolomitized sandstone) and rock strengths within the Obispo Formation. On cross section G-G', the fault is again associated with a change in dip on the syncline limb, although the sharpness of the folding is less than at cross section F-F', and the cross section is east of the main diabase body. This is consistent with the interpretation that larger displacements estimated at the sea cliff may be related to more abrupt folding-related shortening and/or the presence of the mechanically strong and more brittle diabase body, and lesser displacements measured beneath the turbine building are associated with less abrupt fold-related shortening and/or the presence of thin diabase bodies or less mechanically strong alternation zones surrounding the diabase. On cross section H-H', the amplitude of folding is still lower, and no faulting is observed (Figures 6-16 and 6-17). Minor faults mapped along the east edge of the power block probably are related to short-wavelength parasitic anticlines and synclines much in the same way that the faulting to the west is related to larger-scale fold-related shortening.

Our structural interpretation of the Diablo Cove fault is that it accommodated shortening within a fold in Tertiary rock, and it is rooted at shallow depths within the fold (Figures 6-15 and 6-17). This type of structural interpretation—that the faulting is associated with folding—is consistent with the earlier interpretation by Jahns (1967b). This contrasts with Dr. Hamilton's model (Hamilton, 2012a, 2012c), which suggests that the fault is continuous downdip for several kilometers and is rooted in pre-Tertiary rock (Figure 6-12).

6.2.3.2 Diablo Cove Fault Offshore

Dr. Hamilton's evidence for the Diablo Cove fault in the offshore is speculative. As noted in Section 6.2.2, Dr. Hamilton's offshore trace of the Diablo Cove fault changed after he was provided with the Kelpfly MBES data (cf. Figures 6-11 and 6-4). Although it is understandable that an interpretation may change with additional information, it is important to observe that Dr. Hamilton's initial mapping of the offshore fault trace (Hamilton, 2012a) with a N80°E strike more closely honored the approximately N55°E to N60°E trend of faulting measured and mapped by Jahns (1966, 1967b) in the headland and wave-cut platform exposure near the mouth of Diablo Canyon Creek (Figure 6-11). The later mapping of the offshore fault trace by Hamilton (2012c) does not honor the fault trend measured by Jahns (Figures 6-3 and 6-4). In fact, to connect the fault mapped onshore, which is based on direct observation, to the lineament that he identifies in the offshore beneath Diablo Cove, Dr. Hamilton drew the fault trace to bend 30–40 degrees away from the observed fault strike (Figure 6-3). Thus, the more recent interpretation by Dr. Hamilton does not honor the fault data at the coastline.

A geologic structure is suggested in the approximate nearshore location of Dr. Hamilton's trace based on the northeast-striking, northwest-dipping beds mapped on the

wave-cut platform north of Dr. Hamilton's trace, and the westerly trending bedding-parallel lineaments seen in the seafloor image south of the trace (Figure 6-3). We consider that such a structure is more likely a small-scale fold in the Obispo Formation strata, similar to other folds mapped along the coastline of northern Diablo Cove (Figure 6-3). On this basis, we consider the evidence for Dr. Hamilton's connection of the onshore faulting observed near the mouth of Diablo Canyon Creek with his interpreted offshore faulting to be ambiguous.

We evaluated possible evidence for the Diablo Cove fault offshore based on its mapped location on the wave-cut platform and adjacent sea cliff, its projection into Diablo Cove, geologic mapping onshore, and the high-resolution seafloor MBES data. Our approach for selecting MBES imagery for interpretation is explained in Section 4.1. Figures 6-18 and 6-19 show what we consider to be the most useful image for assessing generally east-west structures, namely, an artificial hillshade with an illumination azimuth of 0 degrees (illuminated from the north), illumination inclination from the horizon of 45 degrees, and tenfold vertical exaggeration (vertical scale equal to 10 times the horizontal scale).

Our evaluation of the bathymetric data within Diablo Cove suggests that seafloor expression of the Diablo Cove fault is highly uncertain (Figure 6-18). This result, in and of itself, is not surprising because the faulting observed onshore appears to be too small to be associated with clear preferential erosion either on the exposed modern wave-cut platform (where the fault was directly observed by Jahns [1966, 1967b], indicating that it was not deeply etched) or on the ancient wave-cut platforms as recorded in the sea-cliff exposure and trench exposures (Figure 6-3 inset; Figures 6-8 and 6-9). Figure 6-18 shows the onshore-offshore hillshade image of Diablo Cove, both uninterpreted (panel a) and interpreted with the informally named headland fault, Diablo Cove fault, and notes about lineaments directly offshore of the mouth of Diablo Canyon Creek (panel b).

Directly along the N55°E to N60°E strike projection of the fault mapped at the coastline is a zone of short, discontinuous lineaments trending east-northeast that crosscut the more east-west bedding lineation (Figure 6-18b). This type of weak geomorphic expression is consistent with the minor amount of faulting and the weak expression observed onshore. Along the N80°E strike projection of the overall onshore Diablo Cove fault zone, there are no clear lineaments cutting the strong bedding lineation. The strongest lineaments seen in the data of northern Diablo Cove that are in the vicinity of the Diablo Cove fault projection are approximately east-west-trending lineaments that are consistent with differential erosion along strata (Figure 6-18b). We note that within uncertainty, one or more of these lineaments may be related to minor faulting. Dr. Hamilton's model, as shown on Figure 6-3, interprets the fault with apparent high confidence (solid line work on a geologic map indicates the existence and location of the feature is known with high confidence unless otherwise noted) along a lineament at the northern portion of this zone.

A very clear feature in the seafloor image is the north-northwest-trending lineament of the informally named "headland fault" that crosses Diablo Cove (Figure 6-18; see Section 6.2.2). Detailed geologic mapping by PG&E (2014b) interprets this lineament as a fault contact separating more massive and resistant Obispo Formation tuff (geologic map unit

Tmor) on the west and bedded dolomitic and tuffaceous sandstone (geologic map unit Tmofb) on the east (Figure 6-13). Onshore, the headland fault consists of at least two steeply dipping to subvertical fault strands, with a western fault strand that juxtaposes the map units Tmor and Tmofb, and an eastern fault strand that involves finer shale strata (geologic map unit Tmofc) but is fundamentally a fault within the bedded Tmofb (Figure 6-3, Figure 6-18b). The eastern fault strand is the same fault mapped by Dr. Jahns and shown by Dr. Hamilton (Figure 6-3). A straightforward map interpretation is that the north-northwest-striking headland fault zone is laterally continuous with the lineament in the MBES data offshore; the interpretation of the headland fault as offset in a right-lateral sense by 15 m or more, as proposed by Hamilton (2012c), is not well resolved within the data.

From our analysis, all likely offshore continuations of the Diablo Cove fault project to the north-northwest-striking headland fault, which shows no evidence of being offset. A Diablo Cove fault projected along a N55°E to N60°E strike, as mapped at the sea cliff, or along a N80°E strike, following the average strike of the onshore fault zone, would intersect the headland fault where it is well expressed as a linear fault (Figure 6-18). A Diablo Cove fault projected along an east-west strike from the sea-cliff exposure would likewise intersect the headland fault where it is well expressed. Thus, we interpret the most plausible offshore continuations of the Diablo Cove fault to intersect the headland fault where it is well expressed in the bathymetric data as a continuous, linear feature. This would strongly indicate that the fault, if it exists as far west as the headland fault, is crosscut by the headland fault and does not continue farther west. These observations strongly refute the assertion by Dr. Hamilton (2012a, 2012c) that the Diablo Cove fault has a clear lateral connection to the Shoreline fault.

Dr. Hamilton interprets the Diablo Cove fault to have a double right bend of approximately 60 m between its location onshore and its location where it crosses the headland fault (Hamilton, 2012c; Figure 6-3). His trace of the Diablo Cove fault through most of this right bend coincides with an absence of topographic or bathymetric data, due to either a sandy or rocky beach or an intertidal area where neither LiDAR nor MBES data were collected (Figures 6-3 and 6-18). Thus, the departure of the fault trace from its onshore trend cannot be evaluated in detail. Likewise, Dr. Hamilton's trace of the Diablo Cove fault crosses the headland fault where the MBES data do not resolve bedrock structure in the seafloor clearly, possibly due to sediment (cobbles and boulders) on the seafloor (Figure 6-18). Thus, Dr. Hamilton presents a fault trace that cannot be evaluated directly, either positively or negatively, against bedrock structural data. For this reason, Dr. Hamilton's depiction of the Diablo Cove fault in the offshore across Diablo Cove cannot be directly ruled out.

Farther offshore, Dr. Hamilton interprets the Diablo Cove fault to approach and connect with the Shoreline fault zone (Figure 6-4). The basis for the fault trace is a connection of lineaments in generally massive rock imaged on the seafloor from MBES data. A hillshade image of the MBES data in the area of this proposed trace is shown on Figure 6-19. Dr. Hamilton's trace, from east to west, coincides with the edge of the northern headland of Diablo Cove, east-west-trending lineaments in generally massive rock, and west-northwest-trending lineaments in generally massive rock (Figures 6-4 and 6-19).

While we recognize these features in the MBES data (Figure 6-19b), we consider them to be short and discontinuous and their alignment to be a poor basis for interpreting a continuous, throughgoing fault. We note that the massive, erosionally resistant rock, which is mapped as resistant tuff and possibly diabase of the Obispo Formation (Figure 6-13; PG&E, 2014b), is characterized by common lineaments with several distinct trends throughout the image (Figure 6-19). These lineaments are typical in a massive rock mass and reflect jointing, fracturing, and minor faulting within the rock mass. The alignment drawn by Dr. Hamilton is not a compelling feature that would be identified independently as a throughgoing fault, given the nature of the rock mass.

Furthermore, we note that one of the more prominent lineaments used by Dr. Hamilton to define the Diablo Cove fault, located directly west of the northern Diablo Cove headland, projects into the headland where geologic mapping has not identified any faulting (Figures 6-19b and 6-13). Dr. Hamilton instead shows the fault here to curve south and coincide with the south end of the headland where the resolution of the hillshade imagery is poor or the geomorphic expressions of geologic features becomes muted (Figures 6-4 6-19). Similar to the location of the fault drawn within Diablo Cove, we note that the Diablo Cove fault trace locally coincides with seafloor features that could reasonably be interpreted as related to jointing, fracturing, or faulting, but Dr. Hamilton's interpretation relies on connecting them by curving the fault trace through areas of poor or no interpretability or by crossing areas of no clear lineaments (Figures 6-4 and 6-19). In other words, the offshore depiction of the Diablo Cove fault proposed by Dr. Hamilton is viable only by ambiguities in the data and is not positively supported with direct evidence. Thus, the basis for the Diablo Cove fault as a laterally continuous fault offshore that connects to the Shoreline fault is not supported by the data.

6.2.3.3 DOWNDIP WIDTH OF THE DIABLO COVE FAULT

In his testimony (Hamilton, 2012a) and SSHAC workshop presentation (Hamilton, 2012c), Dr. Hamilton postulates that there is evidence for the Diablo Cove fault at seismogenic depths based on alignments of microseismicity. Based on the earthquake locations alluded to in his testimony (Hamilton, 2012a), the accuracy of the earthquake locations reported by Hardebeck (2010, 2013), and simple considerations of fault scaling, we consider this aspect of his model to be extremely poorly supported, if not factually inconsistent. Figure 6-20 presents maps and profiles of seismicity relative to the Diablo Cove fault, San Luis Range/ IOF thrust, and Shoreline fault as interpreted by Dr. Hamilton's testimony (Hamilton, 2012a) and SSHAC workshop presentation (Hamilton, 2012c) drawn perpendicular to the Shoreline fault zone. Panels (a) and (b) on Figure 6-20 presents seismicity locations from Hardebeck (2010), which were used by Dr. Hamilton for his testimony (Hamilton, 2012a). Panels (c) and (d) on Figure 6-20 show updated seismicity locations from Hardebeck (2014a) and fault geometries presented by Dr. Hamilton during the SSHAC workshop (Hamilton, 2012c). A more detailed evaluation of the spatial relationship between microseismicity and the San Luis Range/ IOF thrust is presented below in Sections 6.3.4.1 and 6.3.4.2.

In his testimony, Hamilton (2012a) correlates "a cluster of three epicenters of small earthquakes 0.5 km NW of the offshore Diablo Cove fault" with the Diablo Cove fault,

noting that these events, between 4 km and 6 km deep, are, “approximately down dip from the surface trace of the north-dipping Diablo Cove fault.” These earthquakes are shown on Figure 6-20 with a thick red outline to distinguish them from other microearthquakes on the map. The profiles clearly show that the earthquakes align with the Shoreline fault zone and not with the Diablo Cove fault, especially considering the stated uncertainty in the hypocenters (± 0.5 km relative location to 1 km absolute location per PG&E, 2011, and Hardebeck, 2010, 2013). In addition, we note that in order for the earthquake epicenters located 0.5 km horizontal distance from the Diablo Cove fault and at 4–6 km depth to be on the Diablo Cove fault, the fault would have an average dip (δ) of $\delta = \text{atan}(4/0.5) = 83$ degrees north to $\delta = \text{atan}(6/0.5) = 85$ degrees north. The implied average dips of 83 to 85 degrees are far steeper than Dr. Hamilton suggests, including in his SSHAC workshop presentation (Figure 6-12). The earthquakes suspected by Dr. Hamilton of being associated with the Diablo Cove fault in fact plot well below his suggested location of the San Luis Range/ IOF thrust, as described in both the testimony (Hamilton, 2012a) and Workshop 2 presentation (Hamilton, 2012c) and shown on Figure 6-20.

In his SSHAC Workshop 2 presentation, Dr. Hamilton states that “a downdip projection of the Diablo Cove fault may presently be a locus of low level seismicity” (Hamilton, 2012c). It is unclear whether Dr. Hamilton is referring to the same earthquakes described in his testimony (Hamilton, 2012a) or other earthquakes with epicenters beneath the Irish Hills (as would be predicted based on his geologic cross section shown on Figure 6-12). Regardless, we consider this statement to be conjecture based on the stated uncertainty in the hypocenters (± 0.5 to 1 km according to PG&E, 2011, and Hardebeck, 2010, 2013) and seismicity either aligned with recognizable structures (such as the Shoreline fault) or part of a more diffuse zone (such as earthquakes beneath the Irish Hills). The seismicity shown on Figure 6-20 clearly demonstrates that there is no compelling association between microseismicity and Dr. Hamilton’s inferred downdip continuation of the Diablo Cove fault.

The geological basis for showing the Diablo Cove fault as extending to 7 km depth and having a 10 km width, as Dr. Hamilton does in his cross section (Figure 6-12) is questionable. This model is inconsistent with simple fault scaling, in which a fault that Dr. Hamilton would assert is 2 km long, but which we suggest is likely limited to a few discontinuous faults over a distance of less than 0.5 km, has a width of 10 km. This length-to-width ratio, commonly called the aspect ratio, is typically considered to be close to 1 for dip-slip faults (e.g., Leonard, 2010). Dr. Hamilton’s Diablo Cove fault would have an aspect ratio of 0.2, implying an extremely unusual shape compared to known seismogenic faults.

6.2.3.4 Diablo Cove Style of Faulting

In his testimony, Hamilton (2012a) describes the Diablo Cove fault as a north-dipping reverse fault, which is consistent with the documented observations made in the onshore exposures (Jahns, 1967b). In his SSHAC workshop presentation, Hamilton (2012c) describes the Diablo Cove fault as an oblique fault with reverse and right-lateral components. The right-lateral component is inferred based on his interpretation that the

headland fault is offset by the Diablo Cove fault in a right-lateral sense (Figure 6-3). We find it improbable for the Diablo Cove fault to have a significant right-lateral component. First, Jahns (1967b) reports direct observations of steeply north-plunging slickensides on the faults at the coast exposure. There is no indication of west- or northwest-plunging slickensides, and no indication of gentle or moderate rakes on the fault surfaces. Thus, there is not direct geologic basis for oblique slip.

A component of right-lateral slip on the Diablo Cove fault would furthermore be inconsistent with the current tectonic regime. The current orientation of maximum principal stress is north-south to north-northeast/south-southwest, based on analysis of focal mechanism and GPS data (Lewandowski and Unruh, 2014), which is similar to the interpreted orientation of maximum principal stress from Tertiary folds (Vittori et al., 1994). This orientation is consistent with right-lateral slip on the steeply dipping and higher-slip-rate Hosgri fault and the subvertical and lower-slip-rate Shoreline fault. This orientation is also consistent with reverse slip on a northeast-dipping thrust plane such as Hamilton's proposed San Luis Range/ IOF thrust. This principal stress orientation would predict primarily reverse slip on an approximately east-west-trending fault such as the Diablo Cove fault or reverse displacement with a minor *left-lateral* component on faults trending east-west to east-northeast.

6.2.3.5 Diablo Cove Fault Activity

As discussed by Jahns (1966, 1967b), no faults observed at the sea-cliff exposure or in the trenches displaced the marine terrace surface or overlying marine terrace deposits. This conclusion was supported by independent peer review by E.C. Marliave (1966, letter to B.W. Shackelford at PG&E, included with PSAR v. II, part 2), who wrote as follows:

The trenches excavated at the site have been thoroughly examined, and there is no evidence of faulting by cutting of any of the marine materials or the alluvium or slope wash. This shows, therefore, that there has been no fault movement in this area for at least 100,000 years. The period of any fault activity in this area might well be gauged in terms of millions of years.

The most probable age of this marine terrace, mapped as the Q2 terrace by PG&E (1988) and Hanson et al. (1994), is approximately 120 ka. A similar age was suggested by Jahns (1966, 1967b). Longitudinal profiles of higher marine terraces east of the site do not show evidence of differential vertical separation (Hanson et al., 1994), although a fault that produces net dip separation of only a few feet would not be resolvable in the longitudinal terrace profile data.

In his testimony, Hamilton (2012a) asserts that the fault pattern mapped beneath the power block and at the sea-cliff exposure shows upward branching and splaying in a manner consistent with faulting near a free surface. He further notes the results of thin-section analysis from the sea-cliff exposure that suggest brittle faulting with little gouge development. Instead of clear evidence for upward branching and splaying, we instead suggest that the pattern of faulting in map view (Figures 6-5, 6-6, 6-13, and 6-16) and in cross section (Figures 6-9 and 6-10) is consistent with distributed slip over a zone of branching fault planes with little cumulative displacement. Such a pattern of faulting is

consistent with minor amounts of fault slip on a minor fault zone within a brittle environment. The change in fault pattern noted by Hamilton (2012a) between the broad zone of minor shearing and faulting documented in the trench exposures (based on an exposure 1 m high) and the narrower zone of faulting documented in the foundation excavations (based on an exposure 2–3 m high) is probably a result of the foundation excavations providing a larger and more complete bedrock exposure from which more developed faults could be distinguished from lesser features.

6.2.4 Conclusion with Respect to the Diablo Cove Fault

After evaluating the information above, we find that there is no technical basis for considering the Diablo Cove fault as proposed by Hamilton (2012a, 2012c) to be either a fault displacement hazard or a seismic source of strong ground motions. We conclude that the Diablo Cove fault does not represent a seismic hazard to the DCP.P, based on the following key points:

- Trench and excavation mapping conducted before construction of the DCP.P documented that the fault zone is discontinuous, is associated with minimal offset, and does not displace marine terrace deposits that are 120 ka. Thus the faulting, where observed directly, is minor and inactive in the late Quaternary.
- Geologic mapping and interpretation of MBES imagery do not support connecting the Diablo Cove fault offshore to the Shoreline fault zone.
- An evaluation of microearthquake locations and consideration of their location uncertainty do not provide a basis for correlating seismicity with the Diablo Cove fault.
- The short length of the fault zone—probably less than half a kilometer—is not consistent with a down-dip width of several kilometers that would extend the fault to seismogenic depths.
- Structural analysis of geologic map data and high-resolution seismic data supports an interpretation, shared by the original mapper of the faults, that the faulting is related to shallow fold deformation that pre-dates the late Quaternary. The faulting may be associated with heterogeneities within the Obispo Formation, including the diabase intrusion interpreted from the seismic data located directly north of the Diablo Cove fault. Based on this interpretation, the fault extends to only a few tens to hundreds of meters depth.

6.3 San Luis Range/ IOF Thrust

In his written testimony (Hamilton, 2012a), professional meeting presentations (Hamilton, 2010, 2012b), and SSHAC workshop presentation (Hamilton, 2012c), Dr. Hamilton interprets a northeast-dipping fault to underlie the Irish Hills and San Luis Range. Dr. Hamilton refers to this fault as the San Luis Range thrust, or San Luis Range/IOF (for Inferred Offshore Fault) thrust. A map of this fault from Hamilton (2012a) is shown on Figure 6-21. For brevity, we herein refer to the fault proposed by Dr. Hamilton as the San Luis Range fault (SLRF). Past seismic source characterizations for

PSHA by PG&E, including the LTSP (PG&E, 1988; 1991) and Shoreline Fault Zone Report (PG&E, 2011), have not included the SLRF as a seismic source, but instead have included separate sources along the southwestern margin of the San Luis Range, including the San Luis Bay fault source that dips moderately to steeply north beneath the Irish Hills. A map of the San Luis Bay fault and other seismic sources used by PG&E in the Shoreline Fault Zone Report (PG&E, 2011) is shown on Figure 6-22.

Dr. Hamilton raises the issue of the SLRF following the inference of a possible offshore fault along the straight coastline postulated during the LTSP. PG&E (1988, 1990) concluded it was not a viable seismic source, a conclusion agreed to by the NRC (NRC, 1991). Dr. Hamilton incorporated new information related to the Shoreline fault to develop the current SLRF interpretation (Hamilton, 2012a, 2012c). Dr. Hamilton proposes that the SLRF is required to explain the uplift rate pattern recorded in the coastal marine terraces and the seismicity pattern observed beneath the Irish Hills.

In response to Dr. Hamilton's concerns about the SLRF, we reviewed available information from the Irish Hills area that bear on Dr. Hamilton's interpretations about the fault location, subsurface dip, pattern of uplift resulting from fault slip, and slip rate. Information reviewed includes interpretations of offshore MBES bathymetric and seismic-reflection data, interpretations of seismicity data, and interpretations of land seismic-reflection data. Based on our review, we show that there is little supporting evidence for the SLRF as proposed by Hamilton (2012a, 2012c) from the available information on coastal and offshore uplift rates, microseismicity beneath the Irish Hills, and seismic-reflection data. Our interpretation of 3D land seismic-reflection data north of Point San Luis precludes its presence.

In the sections below we evaluate the SLRF as a potential active structure through analysis of available geologic, seismological, and geophysical data. Our evaluation of the SLRF is separated into five subsections. In Section 6.3.1, we review previous studies and interpretations of fault structures along the south or southwest margin of the Irish Hills. In Section 6.3.2, we restate Dr. Hamilton's proponent model of the SLRF, drawing mainly from his testimony (Hamilton, 2012a) and SSHAC workshop presentation (Hamilton, 2012c). Sections 6.3.3 and 6.3.4 present analyses by PG&E of key pieces of information that pertain to Dr. Hamilton's SLRF interpretation. Section 6.3.3 presents an evaluation of uplift rate data of the Irish Hills and adjacent areas, and Section 6.3.4 presents evaluations of double-difference relocated seismicity data and land seismic-reflection data. Section 6.3.5 summarizes our main findings that the SLRF interpretation is not well supported by the available data.

6.3.1 Previous Interpretations of Seismic Sources

Observations and interpretations of active reverse faulting along the southwestern margin of the Irish Hills and San Luis Range were developed during PG&E's LTSP in the mid to late 1980s. Different interpretations of faulting along the southern or southwestern margin of the Irish Hills were developed during that effort. Two interpretations were published, as follows:

1. A northwest-striking, northeast-dipping reverse fault called the Inferred Offshore fault (IOF) is located parallel to and offshore the coast of the Irish Hills (Figure 6-23).
2. A more west-striking, north-dipping reverse fault zone called the San Luis Bay fault zone is located between Avila Beach on the east and an uncertain location on the continental shelf near the Hosgri fault on the west (Figure 6-24).

We review the two interpretations below, with the goal of presenting an historical perspective on the development of alternative fault models.

6.3.1.1 University of Nevada, Reno Interpretation of the IOF

Researchers at the University of Nevada, Reno (UNR), funded by the NRC, interpreted a northwest striking, northeast dipping reverse fault offshore the coast of the Irish Hills (Figure 6-23). This interpretation was presented by Mr. Steve Nitchman in a UNR student's master's thesis (Nitchman, 1988), who called the fault the Inferred Offshore fault (IOF). This fault was shown on maps published in two papers coauthored by Mr. Nitchman and his advisor, Dr. Burton Slemmons, in the Geological Society of America Special Paper 292 (Nitchman and Slemmons, 1994; Vittori et al., 1994). In a review report for the NRC of the LTSP, which is provided in the DCP.P Supplemental Safety Evaluation Report 34 (SSER) issued by the NRC at the conclusion of the LTSP (NRC, 1991), Dr. Slemmons and a student provide additional information about the basis for the IOF (Slemmons and Clark, 1991).

Relatively little is written about the IOF in the UNR papers. The IOF is mentioned only by name by Vittori et al. (1994) in the caption of their Figure 1, a fault map of the area (Figure 6-23a). The paper does not focus on the basis for the fault mapping, but instead is an analysis of mesoscale fault-slip data to evaluate regional stress tensor orientations. The topic of Nitchman and Slemmons (1994) is a characterization of the Wilmar Avenue fault—the IOF is mentioned only briefly. Nitchman and Slemmons (1994) write, “

The south side of the [San Luis Range] is bound by a system of N60°W-trending, NE-dipping reverse faults, along the southwestern boundary of the Pismo/San Luis block including the Wilmar Avenue fault (Nitchman, 1988), the San Luis Bay fault (Lettis et al., 1990; Slemmons and Clark, 1991), and possibly by an inferred offshore range-bounding reverse fault (Nitchman, 1988).”

Figure 2 of Nitchman and Slemmons (1994) shows their interpretation, which is reproduced on Figure 6-23b.

In his thesis, Mr. Nitchman discusses the IOF briefly in four places (Nitchman, 1988). On his page 24, under “Mid Pleistocene Paleogeography,” he writes, “The southern margin of the San Luis Range has maintained a N60W orientation throughout the Pleistocene, as indicated by trends of uplifted marine terraces. The Wilmar Avenue fault has controlled the orientation of marine terraces east of Shell Beach. West of Shell Beach, the terrace trends have probably been maintained by an inferred offshore reverse fault which is a mirror image of the Los Osos fault.” This statement is accompanied by his Figure 7, which shows the IOF as a dashed and queried reverse fault offshore the Irish Hills and

subparallel to the coastline from Point Buchon in the north to south of Point San Luis in the south. On his page 30, under the heading “San Luis Range Tectonic Block,” he writes, “The [San Luis Range Tectonic Block] is topographically and structurally bounded by: (1) the Hosgri Fault Zone to the west; (2) a poorly-defined eastern border which may coincide with Arroyo Grande Creek [...]; (3) the Los Osos fault system along the north edge; and (4) by a complex southern boundary zone which consists of the Wilmar Avenue and San Luis Bay faults, as well an [sic] inferred NE-dipping reverse fault offshore of the southwestern San Luis Range (Figure 10).” His Figure 10 is presented on Figure 6-23c. We note that the Hosgri fault, which strikes approximately N27°W, is shown erroneously on this figure to strike north.

The longest discussion of the IOF in Nitchman (1988) is presented under the section titled, “San Luis Range Tectonic Block Boundary Faults,” and a subheading titled “Inferred Offshore Fault.” This text, from page 59 of his thesis, is presented in its entirety below:

The western part of the southern boundary zone is inferred to be composed of an offshore NW-trending (?), north-dipping reverse fault zone (Figure 10). Killeen (1988) suggests that the terraces that girdle the western San Luis Range between Point Buchon and Shell Beach are not appreciably tilted. The lack of tilting suggests that the San Luis Range has been uplifted as a block, and therefore is probably bound to the southwest by a reverse fault which is a mirror image of the western Los Osos fault.

The citation referenced in the thesis by Killeen is a second master’s thesis supervised by Dr. Slemmons at UNR—and completed in 1989—that included an evaluation of marine and fluvial terraces in the Irish Hills and surrounding areas (Killeen, 1989).

A final mention of the IOF is presented on p. 75 of Mr. Nitchman’s thesis, where he describes the fault on his cross section (his Figure 31). He writes, “The inferred offshore reverse fault is also depicted as a planar reverse fault within the Franciscan basement.” This cross section is reproduced on Figure 6-23d. On it, the IOF is shown as a planar, queried fault dipping approximately 60 degrees beneath the Irish Hills. The exact location of the cross section is unclear from his thesis.

In the Diablo Canyon SSER, the UNR review report (Slemmons and Clark, 1991) discusses the IOF, which was a topic discussed at NRC/PG&E meetings and a subject addressed in the response to Question GSG-Q16 (PG&E, 1990, and Section 6.3.1.2 below). Under the heading, “Inferred Coast-Parallel Fault,” the UNR review report (Slemmons and Clark, 1991, pp. 46–47) states,

This inferred fault is suggested by the steep and linear coastline, and by a late Quaternary slip deficit of 0.06 mm/yr...on the southwest margin of the Irish Hills subblock. It is also suggested by the steep, linear range front along the Point Buchon to Point San Luis part of the coastline. Other arguments for a coast-parallel offshore fault are summarized by Nitchman (1988).

Although the coastline linearity and slip deficit is consistent with a tectonic structure, the PG&E offshore investigations by a diver geologist...indicate that major geologic units and structures, including the Olson and San Luis Bay faults are oblique to the coastline and appear to preclude the existence of a coast-parallel fault. Accordingly, the UNR

model does not assume a coast-parallel surface fault for the southwestern boundary zone, although a somewhat similar southwestern boundary zone model is used.

In the SSER, under the heading of Regional Geology and Tectonics, the NRC staff write, “Although the presence of an undetected coastal fault cannot be completely ruled out, investigations and analyses by PG&E indicate that the probability of such a fault is very low.”

From the available information, the basis for the IOF by UNR researchers (Nitchman, 1988; Slemmons and Clark, 1991; Nitchman and Slemmons, 1994; Vittori et al., 1994) is as follows:

- The linear reach of outer coastline from Point San Luis to Point Buchon is hypothesized to be controlled structurally by the IOF.
- Paleostrandlines of late Pleistocene terraces are subparallel to the modern coastline, which is interpreted to suggest structural control by the coast-parallel IOF in the late Quaternary period.
- The lack of appreciable tilting of uplifted marine terraces on the outer coast of the Irish Hills supports an interpretation that it is underlain by a planar, subparallel, reverse-slip IOF.
- The general elongate form of the San Luis Range, and the interpretation that the Los Osos fault and Wilmar Avenue faults coincide with the topographic fronts of the eastern San Luis Range, suggests a comparable “mirror image” IOF is located along the southwestern margin of the Irish Hills opposite the Irish Hills segment of the Los Osos fault.
- The IOF dip beneath the western San Luis Range (i.e., Irish Hills) may be moderate (perhaps approximately 60 degrees) and within Franciscan Complex rocks.
- A bathymetric escarpment in the nearshore opposite the Irish Hills may be the surface expression of an active, northeast-side-up reverse fault.
- Offshore investigations by PG&E during the LTSP appeared to preclude the existence of a coast-parallel surface fault.

6.3.1.2 LTSP Interpretation of the San Luis Bay Fault Zone

An alternative explanation for the pattern of terrace deformation and uplift rate boundary on the southwestern margin of the Irish Hills was presented by PG&E Geosciences and its consultants in the LTSP Report (PG&E, 1988), LTSP Response to Question GSG 16 (PG&E, 1990), and published papers in the same Geological Society of America Special Paper 262 (Hanson et al., 1994; Lettis et al., 1994). This collection of work contended that the approximately east-west-trending San Luis Bay fault zone (consisting of a southern trace called the San Luis Bay or Rattlesnake fault and a northern trace called the Olson fault; Figure 6-24) was associated with a change in the coastal uplift rates from approximately 0.2 meters per thousand years (m/kyr; equivalent to mm/yr) north of the fault zone to 0.06 m/kyr south of the fault zone (Figure 6-25). This change in uplift rate of approximately 0.14 m/kyr was recorded in detailed mapping of the marine terrace paleostrandlines on the outer coast, with similar but slightly lower amounts suggested

across the San Luis Bay fault zone mapped near Avila Beach across northern San Luis Obispo Bay (Hanson et al., 1994; Lettis et al., 1994; Figure 6-26). The evidence for an offshore continuation of the San Luis Bay fault zone was equivocal in the available seismic-reflection and other data, “because of very low slip rates and generally poor data quality” (p. 19 of PG&E, 1990; Figure 6-24). The PG&E group interpreted that additional changes in uplift rate along the southwestern margin of the Irish Hills—needed to decrease the rate from 0.06 m/kyr to a rate of approximately zero or slightly negative in the Santa Maria Basin—occurred on one or more low slip rate reverse faults, including the Pecho located offshore Point San Luis (Figure 6-25). The Wilmar Avenue fault was recognized as the primary uplift rate boundary at the southwestern margin of the San Luis Range east of the Irish Hills, and was associated with a differential uplift rate of approximately 0.12 m/kyr (Hanson et al., 1994). The near-uniform pattern of uplift rates recorded on the Irish Hills coastline between approximately Olson Hill to the south and Montaña de Oro State Park to the north was attributed to block uplift accommodated by multiple planar fault sources, including the Hosgri Fault Zone to the west, the Los Osos fault zone to the north and east, and the north-dipping San Luis Bay fault on the south (Lettis et al., 1994).

As stated above, the UNR interpretation for a reverse-slip IOF was considered during review of the LTSP Report, but rejected in response to Question GSG Q16 by PG&E (1990). The bases for rejecting the interpretation of a coast-parallel IOF were evaluations of diver geology results and the bathymetry along the near shore from which it was concluded that the bathymetric escarpment was a series of closely spaced, submerged shoreline features (Attachment GSG Q16-E of PG&E, 1990). The interpretation that the southwestern margin of the San Luis Range was being uplifted by a broad Southwestern Boundary fault zone, consisting of the San Luis Bay fault zone (the Olson and Rattlesnake faults), Pecho fault, Wilmar Avenue fault, and Oceano fault, was accepted by the NRC staff and by the USGS and UNR reviewers in the SSER (NRC, 1991). Although both the USGS and UNR reviewers considered alternative structural configurations of the Southwestern Boundary fault zone to those preferred by PG&E (1988), neither group in its review reports considered the IOF to be a preferred interpretation and a seismic source that needed to be considered for hazard analysis (USGS staff, 1991; Slemmons and Clark, 1991).

6.3.1.3 PG&E Interpretation of the Shoreline Fault Zone

After the discovery of the Shoreline fault seismicity lineament by Dr. Hardebeck and the collection of both high-resolution seismic-reflection data (Sliter et al., 2009) and MBES bathymetric data (CSUMB, 2007, 2009, 2010), the escarpment discussed during the LTSP as possible evidence for the IOF could be evaluated using much higher resolution data (e.g., Figure 6-27). In the Shoreline Fault Zone Report, PG&E (2011) performed a detailed analysis of the MBES data that consisted of geologic interpretation (Appendix B in PG&E, 2011) and geomorphic interpretation of submerged paleostrandlines (Appendix I in PG&E, 2011). The investigations interpreted a narrow zone of well-defined lineaments subparallel to the coast from south of Point San Luis to offshore Point Buchon. Between offshore Point San Luis and a location directly west of the DCP, the

lineaments coincided closely with seismicity epicenters that defined the Shoreline fault, and these lineaments were interpreted to be the surface expression of the subvertical Shoreline fault. Although locally the mapped Shoreline fault coincided with an escarpment (e.g., Figure 6-27), on detailed profiles where the fault crossed interpreted submerged wave-cut platforms or crossed other areas of the eroded seafloor, no or minimal differential uplift was interpreted across the fault (e.g., Figure 6-28). Northwest of the DCP.P and offshore Point Buchon, a linear escarpment was noted in the bathymetry coinciding with an abrupt transition from eroded rock at the seafloor to sand-wave deposits (Figure 6-29). A fault informally named the N40W fault (and since renamed the East Branch of the Point Buchon fault during the AB1632 studies; PG&E, 2014a), was interpreted as a subvertical fault adjacent to this escarpment that possibly branches from the Shoreline fault (PG&E, 2011). From mapping of wave-cut platforms and submerged paleoshoreline angles, PG&E (2011) interpreted there to be a negligible differential uplift rate across the N40W fault (Figure 6-30). The conclusion made from several profiles and mapping across the Shoreline fault and N40W fault was that the local coincidence of the faults with rock escarpments was due to marine erosion rather than a measurable change in uplift rate (PG&E, 2011).

The geologic and geomorphic interpretation of the MBES data performed for the Shoreline Fault Zone Report (PG&E, 2011) included changes to the characterization of the Pecho fault and the San Luis Bay fault zone from those presented during the LTSP (PG&E, 1988; 1990). The rocky seafloor exposed on the shelf between offshore Point San Luis and areas south of the DCP.P revealed evidence that demonstrated the absence of the Pecho fault at the surface where mapped previously (cf. Figures 6-24 and 6-29). The rocky seafloor also revealed evidence that suggested that the faults mapped at the coast interpreted to be part of the San Luis Bay fault zone—the Rattlesnake, Olson south, and Olson north—did not cross the shelf along westerly trends but rather merged asymptotically with the Shoreline fault zone (cf. Figures 6-24 and 6-29). This observation appears to contradict the interpretation of paleoshoreline data that the differential uplift observed along the coast across the San Luis Bay fault zone cross-cuts the Shoreline fault zone (Appendix I in PG&E, 2011; Figure 6-22). The interpreted offshore uplift rate boundary would separate the continental shelf west of the Shoreline fault between a northern “Islay” shelf and a southern “Santa Rosa Reef” shelf (Appendix I in PG&E, 2011). If the differential uplift rate offshore on the shelf is due to dip slip on a local fault subparallel to the uplift rate boundary, PG&E (2011) proposed that this fault may be the lateral continuation of the San Luis Bay fault west of the Shoreline fault zone as a blind, north-dipping reverse fault to account for the absence of a surface-fault trace in the offshore.

PG&E (2011) included two alternative model interpretations of the San Luis Bay fault seismic source to explain the observations. In one model, the San Luis Bay fault seismic source ends on the west at the Shoreline fault, as suggested from mapping of fault traces. This model suggests that any change in uplift rate on the continental shelf could be accommodated by changes in dip or uplift across the Hosgri Fault Zone. In the alternative model, the San Luis Bay fault seismic source is a continuous seismic source across the Shoreline fault zone that terminates on its western end at the Hosgri Fault Zone (Figure

6-22). This model is consistent with the interpretation that the differential uplift rate observed along the coast and offshore on the shelf is accommodated by a single seismic source that crosses the Shoreline fault zone. This interpretation requires that the San Luis Bay fault is a blind, north-dipping reverse fault to account for the absence of a surface-fault trace in the offshore. Additional changes in uplift rate south of the San Luis Bay fault source were attributed to the Oceano fault for purposes of seismic source characterization in the Shoreline Fault Zone Report (PG&E, 2011).

In summary, the main pieces of information considered by PG&E (1988; 1990; 2011) for interpreting the San Luis Bay fault zone as the primary uplift rate boundary for the southern margin of the Irish Hills, and not considering the IOF as a seismic source, are as follows:

- The coastal marine terraces show a significant change in uplift rate coincident with the east-west trending San Luis Bay fault zone.
- Uniform uplift rate of the coastal terraces between approximately Olson Hill and Montaña de Oro State Park is accommodated by block uplift bounded on the north and northeast by the Los Osos fault, on the west by the Hosgri Fault Zone, and on the south by the north-dipping San Luis Bay fault.
- During the LTSP (PG&E, 1990), the nearshore escarpment was interpreted to be non-tectonic, and a series of closely spaced, submerged shoreline features.
- For the Shoreline Fault Zone Report (PG&E, 2011), this interpretation was revised, with the escarpment locally coinciding with a subvertical Shoreline fault and (inferred subvertical) N40W fault. Detailed mapping suggested the escarpment was related to differential erosion (i.e., fault line erosion, locally) rather than differential tectonic uplift across the Shoreline and/or N40W faults.

6.3.2 San Luis Range/ IOF Thrust Model of Dr. Hamilton

Dr. Hamilton further develops the interpretation of the IOF published by the UNR group (e.g., Nitchman, 1988; Nitchman and Slemmons, 1994) by incorporating additional observations and drawing more detailed interpretations of its lateral and down-dip geometry and late Quaternary activity (Hamilton, 2012a, 2012b, 2012c). His names for the interpreted fault—the San Luis Range/ IOF thrust—recognizes the UNR interpretation for the Irish Hills-parallel fault as well as the continuity of a range-front-parallel structure farther south along the western margin of the eastern San Luis Range (Hamilton, 2012b, his slide 31). As stated previously, Dr. Hamilton’s proponent model is referred to as the SLRF for brevity.

6.3.2.1 Location of the Faulting

The location of the SLRF in the direct vicinity of the Irish Hills and the DCP.P is presented on Figure 6-21, taken from his written testimony (Hamilton, 2012a). For clarity, we have added a yellow “highlight” to the original figure on the SLRF trace and a blue “highlight” on the Shoreline fault trace. According to the description in the testimony (Hamilton, 2012a, p. 32), the SLRF is interpreted to coincide with the Wilmar Avenue fault at the coastline in Pismo Beach (in the southeast corner on Figure 6-21),

cross the seafloor beneath San Luis Obispo Bay along an east-west trend, and then intersect the Shoreline fault south of Point San Luis. Between the intersection with the Shoreline fault zone south of Point San Luis and a location south of Point Buchon, the SLRF is interpreted to intersect the Shoreline fault zone at shallow depths—estimated to be 1 to 2 km in his written testimony (Hamilton, 2012a). Along this portion of the fault, which is indicated on Figure 6-21 where the yellow and blue highlights are adjacent and parallel, the fault would strike approximately N55°W, subparallel to the strike of the Shoreline fault zone. Directly east of Point Buchon, the SLRF diverges from the Shoreline fault zone and strikes more northerly (approximately N33°W). For this portion, the SLRF coincides approximately with the N40W fault interpreted by PG&E (2011; later renamed the East Branch of the Point Buchon fault) and follows the rock escarpment observed during the LTSP (PG&E, 1990). Although the northern end of the SLRF is not defined explicitly by Hamilton (2012a), we stop the yellow highlight on Figure 6-21 where Dr. Hamilton shows the offshore Los Osos fault intersecting the SLRF trace. The southern end of the SLRF is inferred to coincide with the southeastern end of the San Luis Range. The total lengths reported for the SLRF by Hamilton (2012a) are 60 km to 80 km.

6.3.2.2 Dip and Width

The down-dip geometry of the SLRF is presented on Figures 6-12 (Hamilton, 2012c) and 6-31 (Hamilton, 2012a). Based on his testimony, the fault is interpreted to be approximately 20 km wide and extend beneath the Irish Hills at a dip of approximately 35 degrees northeast (Hamilton, 2012a, his Table A). The subsurface location of the SLRF as stated by Dr. Hamilton is, “clearly delineated by the hypocenters of numerous small earthquakes” (Hamilton, 2012a, p. 16). He later states that the earthquake hypocenters, “...approximately define the San Luis Range/"IOF" thrust” (Hamilton, 2012a, p. 17).

The seismicity data used by Dr. Hamilton to support this interpretation is shown on Figure 6-32 in map view and on Figure 6-33 as a series of sections (Hamilton, 2012a, 2012b). An additional seismicity map (Figure 6-34) and sections (Figure 6-35) using locations determined by double-difference relocation methods were presented at the SSHAC workshop presentation (Hamilton, 2012c). Interpreted fault dips measured from the seismic sections from his testimony (Figure 6-33) and SSHAC workshop presentation (Figure 6-35) range between approximately 30 and 40 degrees, with generally planar to slightly curved faults drawn, and slightly steeper dips on average shown on the sections presented at the workshop (Figure 6-35).

6.3.2.3 Nature of the Faulting

The SLRF is interpreted by Hamilton (2012a, 2012c) to be a thrust or reverse fault based on the interpreted northeast-southwest directed direction of maximum compression and shortening (e.g., Vittori et al., 1994) and reverse focal mechanisms in the Irish Hills (Figures 6-32 and 6-34).

Where the SLRF impinges on the Shoreline fault, Dr. Hamilton interprets movement of the hanging-wall block to be “deflected” by the Shoreline fault and locally produce abrupt, localized uplift on the Shoreline fault (Hamilton, 2012a; Figure 6-31, see note on inset). Dr. Hamilton interprets, “the scarp along the trace of the central reach of the Shoreline fault” to be the surface expression of the reverse slip on the SLRF along the margin of the Irish Hills where the SLRF impinges on the Shoreline fault (Hamilton, 2012a, p. 32). Thus, Hamilton (2012a) makes a very clear prediction for the SLRF model, that the central portion of the Shoreline fault is a localized uplift rate boundary that accommodates the vertical movement attributed to the SLRF, and that the N40W fault is a northeast-dipping fault and an uplift rate boundary.

Hamilton (2012a) interprets that several other structures mapped and recognized by others are secondary structures to the SLRF. Specifically, he considers the Olson and Rattlesnake faults that offset late Quaternary terraces at the coastline to be “minor features of apparent late Quaternary deformation” (Hamilton, 2012a, p. 17), or upward splays from the underlying SLRF (Hamilton, 2012a, p. 33). Dr. Hamilton omits a source characterization of the San Luis Bay fault in his testimony, stating that he does not consider it, “as significant a threat” (Hamilton, 2012a, p. 29). The Los Osos fault is also considered a secondary feature to the SLRF by Hamilton (2012a). On p. 32, he states, “Additionally, it seems likely that significant movements along the Los Osos fault can occur only as back thrust events linked to movements along the San Luis Range/“IOF” thrust. The Los Osos fault, by itself, would therefore appear to provide very little contribution to the seismic hazard to the DCNPP” (Hamilton, 2012a).

Hamilton’s (2012a) strongest language in support of his SLRF model relates to his interpretation that reverse movement on the SLRF is required to explain the observed pattern of terrace uplift along the Irish Hills. On page 31, Hamilton (2012a) states, “The existence of [the SLRF] is required in order to account for the level uplift of the Irish Hills/San Luis Range, as was noted by both the USGS’s Brown and UNR’s Slemmons each in both 1989 and 1991 and by Slemmon’s student Nitchman in 1988 and (with Slemmons) in 1994.” Later in the testimony, on pages 49-50, Hamilton (2012a) paraphrases this same information, and goes on to state,

Instead, the undeniable tectonic requirement to explain the level uplift of the Irish Hills was replaced with a vaguely defined “Southwest Boundary Zone” consisting of a “—diffuse complex zone of northwest-trending reverse faults and flexures. Principal structures within the zone include the San Luis Bay, Wilmar Avenue, Pecho, and Oceano faults”. This zone conveniently omitted any “IOF” and its only component extending into the offshore opposite the DCNPP site was the “Pecho” fault which was shown (LTSP Figure 2.53) as parallel to but slightly more than 4 km from the Irish Hills shoreline. This safely distant “Pecho” fault—PG&E’s rationalization [sic] for the southwest side level uplift of the Irish Hills—was not accorded the importance of an earthquake magnitude assessment. By ignoring Nitchman’s “IOF,” PG&E deprived the real life tectonic model of undeniable uplift of the mechanism along its necessary southwest side reverse fault.

This highlights a second very important aspect of Dr. Hamilton’s proponent model—that the SLRF is an “undeniable tectonic requirement” and is a “real life tectonic model of undeniable uplift” to account for the pattern of “level uplift of the Irish Hills.”

6.3.2.4 Slip Rate

The slip rate of the SLRF and overall uplift rate of the Irish Hills are discussed briefly in Dr. Hamilton's testimony (Hamilton, 2012a) and SSHAC workshop presentation (Hamilton, 2012c). The estimated slip rate on the SLRF reported by Hamilton (2012a) in his seismic source parameters (his Table A) is 0.6 to 0.9 mm/yr. In his SSHAC workshop presentation, Hamilton (2012c) considers the slip rate of the SLRF to be approximately 0.5 mm/yr, based on a 0.24 mm/yr long-term rate of vertical uplift of the Irish Hills and a 30 degree dipping SLRF. No basis is provided in his testimony to support the slip rate values, and no basis is given in his workshop presentation to support the long term uplift rate value (Hamilton, 2012a, 2012c). Hamilton (2012a, 2012c) does note his interpretation that the geomorphology of stream valleys draining the Irish Hills suggests an increase in uplift rate in the past approximately half million years. Based on these rates, we infer that Hamilton (2012a, 2012c) interprets the shelf west of the SLRF to be subsiding or at a near-zero uplift rate. Data from the MBES and the Point Buchon 3D study show that the shelf is not subsiding because the sediment cover is thin (PG&E, 2011, 2014a).

Although Dr. Hamilton does not explicitly state it, the suggested slip rate of 0.5 mm/yr is consistent with a differential vertical uplift rate of approximately 0.25 mm/yr. If he considers the uplift rate of the coastal Irish Hills (and his hanging wall block) to be 0.24 mm/yr—which is approximately 20 percent higher than the published late Quaternary uplift rate of approximately 0.2 m/kyr (Hanson et al., 1994)—the uplift rate of the footwall block southwest of the SLRF must be approximately zero. The higher uplift rates presented in his testimony (0.6–0.9 mm/yr) would imply differential uplift rates of 0.3–0.45 mm/yr for a 30-degree-dipping SLRF, or differential uplift rates of 0.35–0.5 mm/yr for a 35-degree-dipping SLRF as listed in his Table A (Hamilton, 2012a). From these numbers, we infer that Dr. Hamilton interprets the shelf west of the SLRF to be subsiding at a rate of 0.05–0.24 mm/yr. We note that it is not clear whether Dr. Hamilton intends to interpret the shelf southwest of the SLRF to be subsiding as implied by his testimony, or whether some other rationale was used to derive the estimated slip rates.

6.3.2.5 Summary of the Proponent Model

Dr. Hamilton's interpretation of the SLRF may be summarized with the following six key points:

1. The SLRF is a continuous, northeast-dipping thrust fault connecting the coastal Wilmar Avenue fault with a fault interpreted to impinge at shallow depths along the central portion of the Shoreline fault, and with the N40W fault (East Branch of the Point Buchon fault).
2. The SLRF is marked by abrupt uplift rate boundaries and local scarps across the seafloor beneath San Luis Obispo Bay, along the central portion of the Shoreline fault, and along the N40W fault.

3. The SLRF is delineated by hypocenters of numerous small earthquakes beneath the Irish Hills, yielding an estimated dip of 30–40 degrees, and projects to intersect the Shoreline fault at approximately 1–2 km depth.
4. The SLRF is required to explain the observed pattern of coastal uplift rates.
5. The Los Osos, San Luis Bay, and other faults are secondary features to the SLRF and are significantly less hazardous to the DCP.P.
6. The model implies that the SLRF is the uplift rate boundary between the uplifting Irish Hills and a non-uplifting or subsiding block seaward.

6.3.3 Analysis of Uplift Rate Boundaries

Dr. Hamilton's interpretation of the SLRF implies patterns and rates of uplift within and surrounding the Irish Hills that can be tested or evaluated. Examples include the prediction for abrupt uplift rate boundaries along the trace of the SLRF, the prediction for either no uplift or subsidence on the shelf southwest of the SLRF, and the assertion that the SLRF uniquely explains the observed pattern of coastal terrace uplift.

Below we present an analysis of uplift rate boundaries for the San Luis Range based on available data. We then specifically evaluate the evidence for abrupt uplift rate changes along the SLRF as proposed by Dr. Hamilton.

6.3.3.1 San Luis Range Uplift Rate Boundaries

Uplift of the San Luis Range was evaluated during the LTSP (PG&E, 1988) and the major findings were published by Lettis et al. (1994), Lettis and Hall (1994), and Hanson et al. (1994). Figure 6-25, from Hanson et al. (1994), summarizes the key findings in a map of faults and locations of measured uplift rate. The LTSP work identified the Los Osos fault on the northeast side of the San Luis Range as a structure accommodating significant differential vertical uplift. On the southwestern side of the San Luis Range, a series of faults, including the Wilmar Avenue, Oceano, Pecho, and San Luis Bay faults, were interpreted to accommodate differential uplift rate changes. The Hosgri fault was also identified during the LTSP as accommodating differential vertical uplift of the western Irish Hills relative to the subsiding offshore Santa Maria Basin to the west (Lettis et al., 1994; Hanson et al., 2004). Whereas the uplift rate boundaries onshore have been evaluated and constrained using flights of emergent marine terraces with relatively high degrees of confidence (e.g., Hanson et al., 1994), comparable definition of offshore uplift rate boundaries have been more challenging. Recently acquired high-resolution data, including detailed MBES bathymetric data (CSUMB, 2007, 2009, 2010), 2D single-channel seismic data (Sliter et al., 2009), and AB 1632-funded 3D and 2D high-resolution, multichannel seismic data (PG&E, 2014a, 2014c), have provided an opportunity to re-evaluate the location and nature of offshore uplift rate boundaries. Recent interpretations of these data have helped refine uplift rate boundaries in the shelf and upper slope areas (PG&E, 2011, 2013, 2014a, 2014c), and have resulted in an updated summary map showing Quaternary sedimentary basins and structures (Figure 6-36). From this summary map, we have created a simplified uplift rate contour map that

reflects currently recognized uplift rate boundaries (expressed as gradients in uplift rate) (Figure 6-37).

Below we describe modifications to the uplift rate boundaries defined by the LTSP (Figure 6-25) based on our new assessment (Figures 6-36 and 6-37). The modifications are presented from north to south, and include the following uplift rate boundaries:

- the northwestern reach of the Los Osos fault zone in Estero Bay
- the Hosgri fault
- the San Luis Bay fault zone and offshore extension
- the Los Berros and Oceano faults in San Luis Obispo Bay

Northwestern Los Osos Fault in Estero Bay

The northwestern end of the Los Osos fault has been mapped in Estero Bay where recent offshore investigations have better located a fault zone in the near-surface (Johnson and Watt, 2012; PG&E, 2013; Figure 6-36). The revised location of the offshore Los Osos fault zone has a more northerly strike than the previously defined offshore segment of the Los Osos fault (Figures 6-24b and 6-25). The fault zone is not an abrupt uplift rate boundary, but does coincide with the transition from the rock-exposed Islay shelf (in an area inferred to be actively uplifting) to areas of greater aggradation of Quaternary deposits in Estero Bay (and a lower or slightly negative uplift rate; Figure 6-37). North of the rock-exposed Islay shelf, faults in the offshore Los Osos fault zone appear to bend and merge asymptotically with the Hosgri Fault Zone. The bend in trend of these faults coincides with the change in direction of vertical separation across the Hosgri from west-side-down vertical separation to east-side-down vertical separation (Figure 6-36).

Hosgri Fault Zone

The recent offshore geophysical investigations of the Hosgri Fault Zone have built on interpretations made during the LTSP (Hanson et al., 2004; Willingham et al., 2013), that while the fault zone is dominantly strike slip, uplift and subsidence is occurring along the fault. Opposite the Irish Hills, the Hosgri Fault Zone has a clear east-side-up component of slip (Johnson and Watt, 2012; PG&E, 2013, 2014a) and a steep northeast dip (Hardebeck, 2010, 2013). Using unconformities mapped in seismic-reflection data estimated to be approximately 240 ka or older and 130 ka, a late Quaternary vertical separation rate across the Hosgri fault in the reach opposite the Irish Hills is estimated to be approximately 0.05–0.2 m/kyr west-side down, with the higher approximate rate of 0.2 m/kyr estimated opposite Point Buchon and the northern end of the Irish Hills (PG&E, 2013; Figure 6-36). These rates are comparable to the earlier estimates of 0.1–0.4 m/kyr by Hanson et al. (2004), which were based on depths of the early-late Pliocene (ELP) unconformity west of the fault zone (published later in Willingham et al., 2013), depths of the ELP unconformity east of the fault observed locally, and an assumed range of uplift rates in areas of stripped bedrock platforms east of the fault zone inferred from Quaternary marine terrace data. The east-side-up vertical rate has been interpreted to be due to a component of reverse slip and fault-normal shortening across the Hosgri Fault Zone where the fault zone exhibits a restraining bend geometry and intersects the

uplifting Irish Hills and San Luis–Pismo structural block (PG&E, 1988; Lettis et al., 1994).

The relative rates of uplift east of the Hosgri Fault Zone and subsidence west of the Hosgri Fault Zone have been difficult to quantify, but evidence suggests a modest rate of east-side uplift of the continental shelf east of the Hosgri Fault Zone, and a similar rate of uplift on the shelf as is present at the coastline (Figure 6-37). Flights of submerged paleostrandlines mapped on the shelf surrounding the Irish Hills based on the MBES data were interpreted to show two distinct areas of uplift—the Islay shelf to the north and the Santa Rosa Reef shelf to the south (PG&E, 2011; Figures 6-36 and 6-37). Both rock-exposed shelves (and adjacent areas where the shelves are covered with a thin veneer of sand overlying rock) suggest late Quaternary uplift of the entire shelf out to the Hosgri Fault Zone. Geomorphic distinctions, correlation of paleoshorelines, and comparison to uplift blocks onshore, suggest that the Santa Rosa Reef shelf and Islay shelf represent separate blocks that are uplifting at different rates (Appendix I in PG&E, 2011). Differences in the elevations and altitudinal spacing of paleostrandlines between the two shelves broadly constrain an uplift rate boundary between them, and the spacing within flights of marine terraces is shown to be compatible with uplift rates for adjacent onshore regions calculated from the emergent marine terraces (i.e., approximately 0.2 m/kyr for the Islay shelf and approximately 0.06 m/kyr for the Santa Rosa shelf; PG&E, 2011). Although it is recognized that there is uncertainty in the exact location and nature of the boundary zone between the two shelf blocks, the boundary appears to cross the entire shelf from the San Luis Bay fault onshore to the Hosgri fault. These observations, however, clearly demonstrate that the boundary between the Santa Rosa Reef shelf and Islay shelf is not localized along the Central segment of the Shoreline fault zone coincident with the SLRF as defined by Dr. Hamilton (Appendix I in PG&E, 2011).

As illustrated on Figures 6-36 and 6-37, the most significant boundary between uplifting areas within the Irish Hills block as indicated by emergent and submerged flights of marine terraces and associated abrasion platforms and accommodation space filled with sediments is the Hosgri Fault Zone. The inferred age of the highest erosional platforms in the Irish Hills that appear to be stripped marine terraces of Quaternary age is on the order of 1 Ma (Hanson et al., 1994). The marine wave-cut platforms present across the entire shelf region at the western end of the Irish Hills attest to a long history of fluctuating sea level and multiple periods of marine erosion in the Quaternary superimposed on an uplifting block.

San Luis Bay Fault Zone and Offshore Extension

The southwestern boundary of the San Luis Range and the uplifting San Luis–Pismo block was interpreted during the LTSP to be accommodated by a series of faults, including the San Luis Bay fault zone, Pecho fault, Wilmar Avenue fault, and Oceano fault (Figure 6-25). The San Luis Bay fault zone and offshore extension have been investigated further by PG&E (2011, 2014b, 2014c, 2014d) using geologic mapping, the MBES bathymetric data, and seismic-reflection data. Interpretations of those data have resulted in modifications to the location and style of the faulting and uplift rate boundaries associated with the San Luis Bay fault zone (Figures 6-36 and 6-37).

As stated above in Section 6.3.1.3, geologic interpretation of the MBES data showed that faults associated with the San Luis Bay fault zone mapped at the surface—namely, the Rattlesnake fault to the south and the Olson faults to the north, may terminate against and/or asymptotically merge with the Shoreline fault zone (PG&E, 2011). In addition, the northern portion of the Pecho fault interpreted during the LTSP (Figure 6-25) was not observed in the MBES data (Figures 6-36 and 6-29).

Although the faults mapped at the surface appear to terminate and/or merge with the Shoreline fault zone, the uplift rate boundary associated with the San Luis Bay fault zone appears to cross rather than terminate against the Shoreline fault zone (PG&E, 2011; Figure 6-37). Further analysis of the marine terrace data and field mapping along the Olson fault by PG&E (2011) suggested that the differential uplift across the San Luis Bay fault zone was better represented by broader fold deformation, rather than discrete steps in terrace elevation at a northern Olson fault and a southern Rattlesnake fault as was interpreted during the LTSP (PG&E, 1988). The broader zone of deformation of the terraces suggested that the causative fault is mostly blind, with the discrete offset at the Rattlesnake fault perhaps representing a fault splay that reaches the surface (PG&E, 2014b). Such a pattern of deformation inferred onshore is consistent with available data offshore. Profiles of the seafloor across the Shoreline fault zone suggest that negligible vertical separation has occurred across the fault zone south (Figure 6-38) or north (Figure 6-39) of the intersection with the San Luis Bay fault zone offshore. Profiles drawn parallel to the Shoreline fault and across the projection of the Rattlesnake fault suggest that the uplift rate boundary seen onshore continues in the offshore (PG&E, 2011). The boundary between the Islay and Santa Rosa shelves—each interpreted to have a more-or-less consistent uplift rate compatible with the adjacent coastal uplift rates—is not a clearly delineated boundary in the offshore, but generally follows a west-northwest trend subparallel to the strike of the San Luis Bay fault zone (PG&E, 2011; Figure 6-37).

Offshore Los Berros and Oceano Faults in San Luis Obispo Bay

The characterization of the Wilmar Avenue fault at the coast and onshore has not significantly changed since the LTSP (Lettis et al., 1994; Hanson et al., 1994). The offshore continuation of the Wilmar Avenue and the other offshore faults, including the Oceano and Los Berros faults, have been investigated further by PG&E (2011, 2013, 2014c) using high-resolution data, including the MBES bathymetric data, single-channel 2D seismic-reflection data, and 2D and 3D multichannel seismic-reflection data (PG&E, 2014c). The intersection offshore of the southern Shoreline fault zone with a set of northwest-striking faults east of the Shoreline fault, summarized on Figure 6-36, is presented in more detail in the Low-Energy Seismic Survey (LESS) Report (PG&E, 2014c). This mapping shows late Quaternary active Oceano and Los Berros faults terminating against and/or asymptotically merging with the Shoreline fault zone. The mapping also shows the Wilmar Avenue fault ending beneath San Luis Obispo Bay, with the subparallel Los Berros fault located directly to the south. Near the intersection with the Shoreline fault zone, the Los Berros fault is interpreted to be a north-dipping thrust fault, with a curved and locally unclear trace where it intersects the top-of-rock surface (PG&E, 2014c). The LESS mapping also mapped faults west of the Shoreline fault that were interpreted to be the southern portion of the Pecho fault zone (PG&E, 2014c).

The geomorphic and geologic evaluation of the 3D seismic data interpreted late Quaternary north-side-up vertical displacement resulting from reverse slip on the Oceano and Los Berros faults (PG&E, 2014c), but the implied vertical displacement rates are low. The 3D seismic volume imaged buried paleochannels that cross the Shoreline, Oceano, and Los Berros faults. No paleochannels show evidence for lateral offset across either the Oceano or Los Berros faults. Several paleochannel thalwegs are interpreted to show a north-side-up step across the Oceano fault of one to several meters, with an estimated slip rate of approximately 0.1 mm/yr, although the LESS report suggests the slip rate may be as high as approximately 0.2 mm/yr or as low as approximately 0.01 mm/yr (PG&E, 2014c). No north-side-up steps are observed across the Los Berros fault, although a change in channel gradient across the fault is noted. The slip rate uncertainties offshore suggest rates comparable to or lower than the differential slip rate of approximately 0.1 m/kyr observed across the Wilmar Avenue fault at the coastline (Hanson et al., 1994; Lettis et al., 1994).

Contours on the top of pre-Quaternary rock across San Luis Obispo Bay constructed from high-resolution seismic-reflection data (PG&E, 2013, 2014c) show the absence of abrupt escarpments or steps associated with any particular fault or fault trend (Figure 6-36). These data suggest the uplift rate boundary between the San Luis–Pismo block to the north and the subsiding onshore Santa Maria Basin to the south may be gradual and not clearly associated with near-surface faulting offshore, which would be consistent with the lower slip rates estimated from the paleochannel measurements (Figure 6-37).

6.3.3.2 Evaluation of the San Luis Range/ IOF Thrust as an Uplift Rate Boundary

The SLRF interpreted by Dr. Hamilton is predicted to coincide with an uplift rate boundary of approximately 0.24 mm/yr (Hamilton, 2012c) and perhaps higher (Hamilton, 2012a). Below we evaluate evidence for the presence or absence of an uplift rate boundary and estimated vertical displacement rates along the three offshore sections of the SLRF shown on Figure 6-21: the offshore Wilmar Avenue fault, the Shoreline fault opposite the Irish Hills, and the East Branch of the Point Buchon fault (PG&E, 2014a), called the N40W fault in the Shoreline Fault Zone Report (PG&E, 2011).

Wilmar Avenue fault

As described in Section 6.3.3.1, the LESS study interpreted the Wilmar Avenue fault to end in northern San Luis Obispo Bay, and the Los Berros and Oceano faults south of the Wilmar Avenue fault to terminate to the west against the Shoreline fault zone (PG&E, 2014c; Figure 6-36). For purposes of evaluating Dr. Hamilton's hypothesis, we assume that the intersections of the Los Berros and Oceano faults with the Shoreline fault zone represents (i.e., are a proxy for) the interpretation by Dr. Hamilton that the offshore Wilmar Avenue fault intersects the Shoreline fault (Figure 6-21). Therefore, the offshore data are consistent with the geometry proposed by Dr. Hamilton for the southern offshore portion of the SLRF.

The LESS data provide evidence for multiple paleostream channel thalwegs to have north-side-up offset across the Oceano fault, and a change in gradient associated with the

Los Berros fault. These observations support Dr. Hamilton's kinematic prediction that localized uplift observed at the coastline also occurs offshore. The rates proposed by the LESS study, although uncertain by an order of magnitude, are consistent with the approximate rate of vertical change observed at the coast across the Wilmar Avenue fault. Considering the broad, generally south-facing slope of the top-of-Quaternary surface, the lack of association between the faulting and that surface (Figure 6-36), and the permissible low slip rates on the Oceano and Los Berros faults, the available data are also consistent with an interpretation that the primary uplift rate boundary across San Luis Obispo Bay is not localized on an SLRF, but instead is broad. Accordingly, the vertical displacement rates localized on recognized offshore faults at the surface may be a minor portion of the overall differential uplift rate across the southern margin of the San Luis–Pismo block. Thus, within uncertainties, the available data broadly support Dr. Hamilton's kinematic model for the southern offshore portion of the SLRF, but on a detailed scale the same data also support an alternative interpretation that uplift rates on offshore reverse faults at the surface are low relative to the total differential uplift rate across the southern margin of the San Luis–Pismo block.

Shoreline Fault Opposite the Irish Hills

Dr. Hamilton interprets the SLRF to impinge on the Shoreline fault zone at shallow depths of approximately 1 to 2.5 km for an along-strike length of approximately 20 km (Figure 6-21). A prediction of this interpretation is that differential uplift from reverse slip on the SLRF at depth would be localized at the surface along the Shoreline fault zone (Hamilton, 2012a). As described above in Section 6.3.1.3, the MBES bathymetric data across and along the Shoreline fault was analyzed during the Shoreline fault investigation to evaluate whether there was direct evidence for localized differential vertical uplift (PG&E, 2011). It is recognized that locally the Shoreline fault zone coincides with a west-facing scarp (Figure 6-27), but elsewhere the fault does not coincide with a clear scarp (Figure 6-28), and locally the fault coincides with discontinuous, low scarps that are both west and east facing that bound an erosional trough (PG&E, 2011).

Three locations were identified and evaluated in the Shoreline Fault Zone Report (PG&E, 2011) where the Shoreline fault zone is crossed by a wave-cut platform. These wave-cut platforms are interpreted to have been modified only slightly during the last marine transgression, and mainly formed prior to the last glacial maximum about 22 ka, and probably formed about or prior to 75 ka (Appendix I in PG&E, 2011). Such platforms are valuable as strain markers for evaluating deformation or deformation rates in that they have an original uniform (approximately planar) shape. Two of these locations, shown on Figure 6-36, are across the Shoreline fault zone south of Point San Luis (Figure 6-38) and southeast of the DCP.P entrance (Figure 6-39). Both locations are interpreted to show zero vertical separation across the mapped fault trace with an uncertainty of approximately ± 1.5 m. Using an estimated minimum wave-cut platform age of 75 ka yields vertical slip rates that are less than 0.02 mm/yr (PG&E, 2011). Thus, the preferred evaluation of the available data is that the vertical rate across the Shoreline fault zone is less than approximately 0.02 mm/yr, and may be zero. This is an order of magnitude (or more) less than the 0.24 mm/yr differential vertical rate across the Shoreline fault zone interpreted by Hamilton (2012c). We acknowledge that the PG&E (2011) interpretation of the wave-

cut platform ages is subject to uncertainty, and that, if incorrect, there is less of a constraint on the age and initial shape of the seafloor across the Shoreline fault zone. Thus, we do not consider the evidence from the wave-cut platforms strong enough to reject the interpretation by Dr. Hamilton that the Shoreline fault zone may accommodate some amount of vertical displacement, but we consider the evidence to strongly suggest that the vertical displacement rate of 0.24 mm/yr proposed by Hamilton (2012a) is inconsistent with the available data.

East Branch of the Point Buchon Fault Zone

Dr. Hamilton interprets the northern portion of the SLRF to separate from the Shoreline fault zone in map view southwest of Point Buchon, and lie along the boundary between bedrock on the east and unconsolidated sediment on the west (Figure 6-21). This northern portion of the SLRF coincides approximately with the East Branch of the Point Buchon fault zone interpreted from the high-resolution MBES bathymetry and seismic-reflection data (Figure 6-36; PG&E, 2014a). As noted above, this same fault was recognized in the Shoreline fault zone study and informally named the N40W fault (Figure 6-29; PG&E, 2011). Similar to the SLRF to the south, a prediction of Dr. Hamilton's interpretation is that differential uplift occurs on this fault at a rate of approximately 0.24 mm/yr (Hamilton, 2012a).

As described above in Section 6.3.1.3, the MBES bathymetric data was analyzed during the Shoreline fault zone investigation to evaluate whether there was direct evidence for localized differential vertical uplift across mapped faults (PG&E, 2011). PG&E (2011) identified a location south of Point Buchon, shown on Figure 6-36, where the then-called N40W fault zone crosses an interpreted wave-cut platform (Figure 6-30). Revised mapping using bathymetry and high-resolution 2D and 3D seismic-reflection data (PG&E, 2014a) interprets this location to coincide with the intersection of the main Point Buchon fault and the East Branch of the Point Buchon fault (Figure 6-36). The wave-cut platform overlying the fault zone is interpreted to have been modified only slightly during the last marine transgression, and mainly formed prior to the last glacial maximum about 22 ka, and probably about 49 to 60 ka (Appendix I in PG&E, 2011). The wave-cut platform is interpreted to show zero vertical separation across the mapped fault trace with an uncertainty of approximately ± 2 m. Using an estimated minimum wave-cut platform age of 50 ka yields a vertical slip rate that is less than 0.04 mm/yr (PG&E, 2011). A low vertical slip rate is supported by interpretations of seismic-reflection data, which show the East Branch of the Point Buchon fault to dip steeply to vertical and be overlain by a thin veneer of sediment with no change in elevation of the top-of-rock surface (Foldouts C and D in PG&E, 2014a).

Based on the above, the preferred evaluation of the available data is that the vertical slip rate across a fault zone interpreted by Dr. Hamilton to be the SLRF is less than approximately 0.04 mm/yr, and may be zero. This is a fraction of the 0.24 mm/yr differential vertical rate across the SLRF interpreted by Hamilton (2012c). Furthermore, interpretations of seismic-reflection data are consistent with a steeply dipping to subvertical East Branch of the Point Buchon fault near the surface rather than a moderately or gently east-dipping fault as interpreted for the SLRF. We acknowledge

that the PG&E (2011) interpretation of the wave-cut platform ages is subject to uncertainty, and that, if incorrect, there is less of a constraint on the age and initial shape of the seafloor across the fault zone. Thus, we do not consider the evidence from the wave-cut platforms strong enough to reject the interpretation by Dr. Hamilton that the East Branch of the Point Buchon fault zone may accommodate some amount of vertical displacement, but we consider the evidence to strongly suggest that the vertical displacement rate of 0.24 mm/yr proposed by Hamilton (2012a) is inconsistent with the available data. In addition, the gently east-dipping thrust fault geometry proposed by Hamilton (2012a) for the SLRF in this area is inconsistent with interpretations of high-resolution seismic-reflection data at shallow depths (PG&E, 2014a).

6.3.4 Analysis of Seismicity and Seismic-Reflection Data

Dr. Hamilton's interpretation of the SLRF included a very specific basis for interpreting the fault at depth—the presence of well-defined seismicity lineaments seen in seismicity cross sections beneath the Irish Hills (Hamilton, 2012a, 2012c). Based on his interpretation of the hypocenters in several cross sections, Dr. Hamilton delineated the SLRF and connected it to the Shoreline fault zone at approximately 1 to 2.5 km depth (Figures 6-32 to 6-35).

This section includes analyses of two datasets that are central to Dr. Hamilton's interpretation of the presence and location of the SLRF. First, the seismicity data are reviewed and analyzed to assess the degree to which Dr. Hamilton's interpretation is defensible or "clearly delineated" in his words (Hamilton, 2012a), or whether the seismicity data permit alternative tectonic interpretations. This analysis uses double-difference relocated seismicity data from Hardebeck (2010, 2014a), and considers both PG&E's assessment of the data (presented in Section 6.3.4.1) and that of Dr. Hardebeck (Hardebeck, 2014b; presented in Section 6.3.4.2). Second, high-energy land seismic data from the Irish Hills are analyzed and evaluated in Section 6.3.4.3 to determine whether there is evidence for or against the SLRF in the locations predicted by Hamilton (2012a, 2012c). These land seismic data include the data interpreted across the Irish Hills in PG&E (2014d).

6.3.4.1 Seismicity Evidence for an East-Dipping Fault Beneath the Irish Hills—PG&E's Assessment

Introduction

This section re-examines the evidence provided by the seismicity data—including earthquake locations and fault plane solutions—that bear on the presence or absence of the proposed SLRF by Hamilton (2014a, 2014c). The seismicity analyses focus on an approximately 15 km long central section of the Shoreline fault and areas to the northeast where Dr. Hamilton shows the proposed SLRF intersecting the Shoreline fault at shallow depth (Figure 6-21).

Comparison of the Hardebeck (2010) and (2014a) Seismicity Data

The seismicity data Dr. Hamilton used in his analyses include catalog data from the Northern California Earthquake Data Center (NCEDC) and earthquake location data through the end of 2008 from Hardebeck (2010; Figures 6-32 to 6-35). More recent earthquake data are available from Hardebeck (2014a) that include earthquakes through the end of 2013. In addition, Hardebeck (2014a) has relocated all the earthquakes based on an updated 3D velocity model. As this constitutes a larger and higher quality seismicity dataset, we use the Hardebeck (2014a) earthquake location data in the seismicity analyses of this section. As Dr. Hamilton included interpretations based on the earlier data set, we start the analysis with a comparison of the Hardebeck (2010) and Hardebeck (2014a) earthquake locations.

The Hardebeck (2014a) earthquake locations were produced with an updated tomDD joint velocity inversion and earthquake relocation that used the original Hardebeck (2010) data plus new events through the end of 2013. Additional constraints from more earthquake data and refined velocities typically reduce absolute earthquake location uncertainties and biases (Husen et al., 2003). The Hardebeck (2014a) earthquake locations are most likely to have the lowest absolute and relative earthquake uncertainties and biases and provide the most complete earthquake hypocenter data set for analyses of seismicity near the Shoreline fault and within the Irish Hills. We only consider the earthquake location differences for the seismicity associated with the 15 km long portion of the Shoreline fault shown on Figure 6-40, where the proposed SLRF would join the Shoreline fault.

The differences in epicenter locations between 169 common earthquakes from Hardebeck (2010) and Hardebeck (2014a) within this area are less than 0.7 km for 84 percent of the events but exceed 2 km for only a few events as shown on Figure 6-40. The median epicentral shift between the 2010 locations and the 2014 locations is relatively small, less than 0.3 km (Figure 6-41a), but there are three epicenters that moved more than 3 km that are not included on Figure 6-41; the three longest epicentral-difference vectors have lengths of 4.4, 6.7, and 7.7 km on Figure 6-40. The maximum epicentral shift shown on Figure 6-41 is truncated at 3 km to show more detail in the main portion of the epicenter shift density distribution.

The larger epicenter shifts occur onshore in the Irish Hills (Figure 6-40) while all the epicenters near the Shoreline fault moved less than 1 km. The differences in epicenter positions are fairly systematic with most epicenters moving west to southwest (Figures 6-40 and 6-41b).

Systematic depth differences are larger than median horizontal distance differences with median 2014 hypocenter depths about 0.5 km deeper than 2010 hypocenter depths (Figure 6-41c). Hardebeck (2014a) states that the 3D velocity model changed very little between the Hardebeck (2010) model and the new velocity model. Depth estimates are thus much more sensitive to small changes in velocity structure compared to horizontal position because the 84th percentile depth shift of 2 km (Figure 6-41c) is observed to be three times greater than the 84th percentile epicenter shift of 0.68 km (Figure 6-41a). Thus, to first order a reasonable conclusion is that depth uncertainties are about three

times larger than horizontal position uncertainties. The Hardebeck (2014a) earthquake locations are used in all the seismicity analyses presented below.

Table 6-1. Number of Earthquakes as a Function of Magnitude in the Seismicity Analysis Box Shown on Figure 6-42

Magnitude Range	No. of Earthquakes
0 to <1	56
1 to <2	122
2 to <3	24
3 to <4	3

Fault Analysis Based on Updated Seismicity Distribution

Hardebeck (2013) shows that the Shoreline fault is essentially a vertical right-lateral strike-slip fault based on focal mechanisms and analyses of best-fitting planes to earthquake locations. Earthquake locations from Hardebeck (2014a) are plotted in map view and in depth cross sections perpendicular to a vertical Shoreline fault through the 15 km long central section along the southwest coast of the Irish Hills (Figure 6-42). Seismicity is plotted as a function of horizontal distance from the Shoreline fault in three cross sections that show seismicity within 5 km wide zones oriented perpendicular to the strike of the Shoreline fault. The objective of plotting seismicity in this way is to evaluate to what extent seismicity is located near known Quaternary or Tertiary faults, and to what extent there is seismicity not located near known faults that could therefore be associated with the proposed SLRF interpreted by Hamilton (2012a, 2012c). This evaluation does not provide a basis to uniquely associate seismicity with a particular fault, and cannot be used to preclude the SLRF, but it does provide a test of whether there is evidence in the microseismicity data for yet-unidentified faults beneath the Irish Hills.

The known Quaternary or Tertiary fault zones for this analysis consist of the Shoreline fault (Hardebeck, 2010, 2013; PG&E, 2011), the Los Osos, Edna, San Miguelito, and San Luis Bay fault zones (PG&E, 2011, 2014b, 2014d; FCL, 2014a), and buried faults within the Pismo Syncline identified from the land seismic data (PG&E, 2014d). For this analysis the southernmost extent of the buried normal faults interpreted from the land seismic-reflection data that dip inward (north) toward the axis of the Pismo syncline as mapped in PG&E (2014d) is used to define the southern boundary of a system of faults. These buried normal faults accommodated extension and subsidence in the ancestral Pismo Basin during deposition of the Obispo Formation (PG&E, 2014d). This boundary is referred to as the south margin of the blind north-dipping faults below the Pismo syncline on Figures 6-40, 6-42, 6-43, 6-44, 6-45, and 6-46 and in subsequent text. The south margin of the blind north-dipping faults below the Pismo syncline is approximated as a simple linear boundary (Figures 6-40, 6-42, 6-43, 6-44, 6-45, and 6-46) to separate seismicity proximal to faults mapped to the north in the Irish Hills from the onshore area

north of the Shoreline fault. In the following analysis, all seismicity north of the south margin of the blind north-dipping faults below the Pismo syncline is considered to be spatially associated with faults delineated and identified in PG&E (2014d).

Hardebeck (2013) fits fault planes to a 25 km long extent of Shoreline fault seismicity located from near the Hosgri Fault Zone to east of Point San Luis (Figure 6-42). To focus on seismicity directly south of the Irish Hills relevant to this analysis of the SLRF, a vertical plane striking N55°W and consistent with the Shoreline seismicity extending 15 km along the southwest coast of the Irish Hills is used as the reference to calculate perpendicular distance from the Shoreline fault for the seismicity depth cross sections (Figure 6-42). This straight vertical plane denoted as the white line on Figure 6-42 is consistent with Hardebeck's (2013) estimated fault positions within her uncertainties of several degrees in strike and dip (Figure 6-42). In particular, the straight vertical plane location honors the most eastward positions of the shallowest seismicity along this 15 km long section of the Shoreline fault zone (Figures 6-43 to 6-45) while avoiding deep seismicity at the northern end of the 15 km segment that Hardebeck (2013) cautions may be associated with seismicity on an east-dipping Hosgri fault.

Earthquake locations are uncertain so it is necessary to use absolute earthquake location uncertainties to quantitatively identify earthquakes that may not be associated with known Quaternary or Tertiary faults or fault zones. The criterion is that an earthquake located farther than its location uncertainty from known faults or fault zones becomes a member of the pool of earthquakes not associated with known faults and fault zones. Hardebeck (2013) uses synthetic testing to estimate earthquake location uncertainties but only for an offshore seismicity data set dominantly located more than 2 km from shore (Figure 5a in Hardebeck, 2013). Thus, the Hardebeck (2013) offshore earthquakes will tend to have larger estimated location uncertainties than onshore seismicity because the offshore seismicity is located outside of the confines of the onshore seismographic stations. Hardebeck (2010) presented earthquake location uncertainty analyses for the entire San Luis Obsipo subregion including the onshore seismicity in the Irish Hills. Consequently, we use the Hardebeck (2010) earthquake uncertainty analyses along with the earthquake location shifts between the Hardebeck (2010) and Hardebeck (2014a) earthquake locations to assess earthquake location uncertainties for the area near the Shoreline fault and extending inland into the Irish Hills. This area is shown as the seismicity analysis area on Figure 6-42.

Absolute earthquake location uncertainties are greater than relative location uncertainties as discussed in Hardebeck (2010). Hardebeck (2010) estimates absolute-position horizontal location uncertainties of <1.2 km for the onshore earthquakes in the Irish Hills with uncertainties increasing offshore. Since the Shoreline fault is relatively close to shore, it is reasonable to assign absolute-position horizontal location uncertainties of <1.2 km for earthquakes along and northeast (landward) of the Shoreline fault. This assumption is supported by the consistently small epicentral differences between Hardebeck (2014a) and Hardebeck (2010) epicenters close to the Shoreline fault on Figure 6-40. Hardebeck (2010) estimates median relative location uncertainty of 0.4 km horizontally and 0.36 km vertically for the area containing the Shoreline fault and

onshore Irish Hills. Thus, absolute horizontal location uncertainties for these earthquakes are bounded to first order to be greater than 0.4 km and less than 1.2 km.

For purposes of illustration, it is useful to employ a relatively small estimate of absolute horizontal location uncertainty to maximize the number of earthquakes that are located farther from known faults or fault zones than their location uncertainty. Such earthquakes comprise a pool of seismicity that could be considered to identify and characterize possible additional unknown faults. An absolute horizontal location uncertainty of 0.6 km is used here to identify earthquakes not associated with known faults or fault zones. A 0.6 km epicenter location uncertainty is probably optimistically small based on the discussion of absolute horizontal location uncertainty in Hardebeck (2010) that simply states such uncertainties are less than 1.2 km. However, as discussed above the comparison of common Hardebeck (2014a) and Hardebeck (2010) epicenter locations indicates median epicenter shifts of <0.3 km and shifts <0.7 km for 84 percent of the epicenters. This suggests that Hardebeck (2014a) achieved some reduction of absolute earthquake location uncertainties from <1.2 km although maybe not to a 0.6 km epicenter location uncertainty. We note that underestimating location uncertainties only increases the number of earthquakes not associated with known faults in this analysis, thus providing a conservative assessment of the amount of seismicity that could be assigned to unknown faults.

Depth cross sections perpendicular to the Shoreline fault plane are constructed encompassing the area extending from 1 km southwest of the Shoreline fault to 15 km northeast of the Shoreline fault across much of the Irish Hills. Three depth cross sections include seismicity within rectangular areas in map view that each span 5 km in the strike direction (Figures 6-43 to 6-45). The three rectangular areas are referred to in the following discussion as the northern, central, and southern seismicity zones. The location of the boundary between the central and southern seismicity zones is selected to encompass the northern onshore limit of the San Luis Bay fault zone within the southern seismicity zone. The central seismicity zone encompasses the DCP.P and the central section of the Shoreline fault zone. The northern seismicity zone encompasses the northern portion of the Shoreline fault that includes the last northern stretch of relatively linear seismicity along the fault before seismicity becomes increasingly diffuse farther north toward the intersection of the Shoreline fault trend with the Hosgri Fault Zone. Hardebeck (2013) notes the more diffuse distribution of seismicity north of the northern seismicity zone used in this analysis. Hardebeck (2013) concludes that more fault complexity is required in this area such as a nonplanar fault geometry for the Hosgri fault and/or an additional third fault.

Color contours of Bouguer gravity anomaly (from Langenheim, 2014) delineate the approximate extent of the south margin of the blind north-dipping faults below the Pismo syncline at the transition from light blue to darkest blue on Figures 6-42 to 6-45. Typically, the southern margin of the blind north-dipping faults below the Pismo syncline interpreted by PG&E (2014d) is located approximately 3.4–3.6 km north of the Shoreline fault. A line parallel to the Shoreline fault is placed 3.7 km northeast from it on Figures 6-42 to 6-45 to denote a position that is consistently slightly north of the southern margin of the blind north-dipping faults below the Pismo syncline. The areas in the northern and

central seismicity zones extending from 0.6 km to 3.7 km northeast of the Shoreline fault plane represent a volume where seismicity would not be associated with known Quaternary or Tertiary faults. In contrast, in the southern seismicity zone, the region from 0.6 km to 3.7 km northeast of the Shoreline fault plane encompasses the steeply dipping San Miguelito fault zone and the north-dipping San Luis Bay fault zone, the northern structure within the late Quaternary active Southwestern Boundary fault zone (PG&E, 2011) (Figure 6-45).

The seismicity depth cross sections show very few earthquakes in the area between the Shoreline fault and southern margin of the blind north-dipping faults below the Pismo syncline within the northern and central seismicity zones compared to the southern seismicity zone (Figure 6-46). Of the 125 total earthquakes located in the northern and central seismicity boxes, 2.4 percent of the seismicity (three earthquakes) is not located within 0.6 km of a known Quaternary or Tertiary fault zone. In contrast, 25 percent of the seismicity (20 of the 80 earthquakes) in the southern seismicity box is located within the area extending from 0.6 km to 3.7 km northeast of the Shoreline fault plane that includes the San Miguelito and the San Luis Bay fault zones.

The seismicity depth cross sections perpendicular to the Shoreline fault illustrate that there is very little seismicity outside the extent of known mapped Quaternary and Tertiary fault zones. In particular, three microearthquakes, all with magnitudes of 1.1, distributed over a 31 km² area (Figures 6-43, 6-44, and 6-46) do not provide a basis to require or determine the geometry of an additional fault (such as the SLRF) spanning the area between the Shoreline fault and the southern margin of the blind north-dipping faults below the Pismo syncline in the central and northern seismicity zones. Over the entire 15 km strike extent of the central Shoreline fault examined here, only 1.5 percent of the seismicity is located more than 0.6 km from a currently recognized Quaternary or Tertiary fault zone (Figures 6-43 to 6-46). Consequently, there is no significant residual seismicity to support or require the SLRF interpreted by Hamilton (2012a, 2012c) northeast of the Shoreline fault in the central and northern seismicity zones (Figures 6-43, 6-44, and 6-46).

Review of Focal Mechanisms

Focal mechanisms were examined to determine whether individual earthquakes provide data on geometry and sense of motion consistent with thrust faulting as proposed by Hamilton (2012a, 2012c). Hardebeck (2010) estimated single-event focal mechanisms for the California central coast, including focal mechanisms for 26 earthquakes located within the seismicity analysis area delineated on Figure 6-42. Hardebeck (2010) assigned each single-event focal mechanism a quality rank from A to D, with A being the best resolved focal mechanisms and D being the worst. Hardebeck (2010) states that quality A–C focal mechanisms are those with ≤ 30 percent of polarities incorrect, $\leq 45^\circ$ uncertainty in the nodal plane orientations, and a ≥ 50 percent probability that the given solution is better than any other solution if multiple solutions are found. Hardebeck (2010) also manually selected and retained a subset of D-quality focal mechanisms based on visual inspection of polarity constraints but does not provide quantitative estimates of uncertainties in nodal plane orientations for the retained D-quality focal mechanisms.

Among the 26 earthquakes with single-event focal mechanisms determined within the seismicity analysis area on Figure 6-42, there are no earthquakes with A-quality focal mechanism solutions and just 3 B-quality and 4 C-quality focal mechanism solutions. Thus, 19 of the 26 earthquake focal mechanisms have D-quality solutions. Six of the 26 solutions—all of D quality—are located along the Shoreline fault. Of the 20 earthquake focal mechanism solutions located in the area northeast of the Shoreline fault, 3 are B quality, 4 are C quality, and 13 are D quality. Hardebeck (2010) computed composite focal mechanisms for events in the poorly sampled offshore and southern parts of the study area including the Shoreline fault because the single-event focal mechanisms were poorly constrained.

Quantitative assessments of focal mechanism properties requires $\leq 30^\circ$ uncertainties in the nodal-plane orientations to distinguish between strike-slip, oblique-slip, and dip-slip focal mechanisms and to resolve first-order nodal-plane dips. There are just two focal mechanisms from Hardebeck (2010) in the seismicity analysis area on Figure 6-42 that have nodal-plane uncertainties of $\leq 30^\circ$ and would be considered reliable enough to distinguish between strike-slip, oblique-slip, or dip-slip faulting mechanisms. In our judgment, two well-constrained single-event focal mechanisms do not provide a sufficient database to use individual focal mechanisms to evaluate whether focal mechanism data support the presence or absence of the SLRF. However, we note that, in aggregate, inversions of focal mechanism and geodetic data from the Irish Hills vicinity show a consistent orientation of maximum shortening strain (and maximum compressive stress) of approximately N10°E to N20°E, with an approximate N30°W orientation of macroscopic dextral shear (Lewandowski and Unruh, 2014). While these results suggest that the SLRF interpreted by Hamilton (2012a, 2012c) would be well oriented to accommodate shortening and thickening, the constraints on the directions of principal stresses do not provide evidence to support its existence.

6.3.4.2 Evaluation of Seismicity Beneath the Irish Hills by Dr. Hardebeck

Dr. Hardebeck (2014b) independently evaluated the seismicity in the Irish Hills area for evidence of laterally continuous faults using her double-difference relocated seismicity data set (Hardebeck, 2014a). Previously, Hardebeck (2013) used an algorithm called Optimal Anisotropic Dynamic Clustering (OADC; Ouillon et al., 2008) to evaluate the geometry of the Hosgri and Shoreline faults through the seismogenic crust with the stated advantage that it provides an objective means of evaluating planar fits to data based on earthquake distances. Whereas the analysis of the Shoreline and Hosgri Fault Zone seismicity was relatively straightforward, due to a clear spatial relationship between the relatively abundant seismicity along these steeply dipping faults and the relative absence of seismicity in areas adjacent to the faults (Figure 6-42), the analysis of alignments of seismicity beneath the Irish Hills, where seismicity is diffuse and there are a variety of slip types, is more problematic. At the Diablo Canyon SSHAC Workshop #3 in March, 2014, Dr. Hardebeck presented results extending the OADC method to evaluate seismicity alignments northeast of the Shoreline fault and beneath the Irish Hills (Hardebeck, 2014b). Dr. Hardebeck used a modification of the OADC algorithm, called OADC-FM, that constrains planar fits to earthquakes based on focal mechanism

information as well as distance. The OADC-FM algorithm fits planes to an earthquake data set using earthquake distance and misfit of *P*-wave first motion polarities (Hardebeck, 2014b). Dr. Hardebeck identified several candidate planar alignments of seismicity beneath the Irish Hills that were repeatable solutions in her OADC-FM inversion (Figure 6-47). Her presentation included interpretations of laterally continuous fault planes from single or multiple OADC-FM planes, and three alternative configurations, projections, and cross-cutting relationships of the interpreted fault planes beneath the Irish Hills that were intended to help evaluate possible seismic source configurations (Figures 6-48 to 6-50; Hardebeck, 2014b).

From this analysis, Hardebeck (2014b) interprets two north-northeast-dipping faults beneath the northern and eastern Irish Hills that she names the North Irish Hills structure (Figures 6-48 to 6-50). She shows three “scenario” configurations of the interpreted fault planes with different projections and crosscutting relations that are intended to help evaluate possible seismic source configurations beneath the Irish Hills (Figures 6-48 to 6-50). Scenario 1 shows the case where a northeast-dipping SLRF-type fault is the main reverse fault beneath the Irish Hills (Figure 6-48). Scenario 2 shows the case where a southwest-dipping Los Osos fault is the main reverse fault beneath the Irish Hills, with the condition that the fault cannot crosscut a plane defined by the OADC-FM solution (Figure 6-49). Scenario 3 shows the case where a vertical strike-slip Los Osos fault is a crustal-penetrating structure on the eastern margin of the Irish Hills, and reverse faults and other strike-slip faults west of the Los Osos fault are present (Figure 6-50). Dr. Hardebeck concluded that there is “no strong preference for any one of the scenarios from the seismicity” (Hardebeck, 2014b).

To further evaluate whether the OADC-FM solution supports the SLRF interpretation by Hamilton (2014a, 2014c), additional interrogation of Dr. Hardebeck’s scenario 1 is relevant (Figure 6-48). This analysis is based on the OADC-FM planes on Figure 6-47, a data table provided to the Diablo Canyon SSHAC team by Dr. Hardebeck showing the results and uncertainties of the analysis (Hardebeck, pers. comm., 27 March, 2014), and the interpretation of the OADC-FM planes on Figure 6-48. The North Irish Hills structures (labeled NIH on Figure 6-48) strike approximately N70°W to N80°W and dip moderately north, with a steepening of dip to the east noted in the solution (Figure 6-47). The northern of the two North Irish Hills structures on Figure 6-48 is based on a single OADC-FM plane (NIH 1 on Figure 6-47), and the southern of the structures is a composite of three planes (NIH 2–4 on Figure 6-47). The northern structure has a strike and dip of N78°W ±18°, 40° ± 5°N (NIH 1). The three planes that are merged to define the southern structure are oriented, from west to east, N74°W ±18°, 45° ± 9°N (NIH 2); N47°W ±11°, 65° ± 7°N (NIH 3); and N70°W ±11°, 60° ± 6°N (NIH 4; Figure 6-47). The merged southern North Irish Hills structure has a strike of N69°W, dips approximately 42 degrees at its west end, and dips approximately 62 degrees north at its east end (Figure 6-48).

Figure 6-48 shows three seismicity profiles—A, B, and C from northwest to southeast—with the structures interpreted from the OADC-FM solution plotted as solid lines and projections as dashed lines. Up-dip projections of the northern plane on profile A and of the southern plane on profile B intersect up-dip projections of the Shoreline seismicity

lineament planes at or above the ground surface (Figure 6-48), in approximate agreement with Hamilton (2014a). However, the North Irish Hills structure along profile A has a N78°W preferred strike, in contrast to a N32°W interpreted strike for the SLRF along its northern portion, and the N55°W preferred strike along its southern portion where it impinges on the Shoreline fault zone (Figure 4-21). Within the strike uncertainty of $\pm 18^\circ$, the North Irish Hills structure along profile A is not compatible with the northern portion of the SLRF, and only toward the clock-wise limit of the solution uncertainty (N60°W) would the North Irish Hills structure be near-parallel to the Shoreline fault opposite the Irish Hills (N55°W; Figure 6-48). The best-fit dip of the Northern Irish Hills structure on profile A—40 degrees north—is greater than the stated dip of 30–35 degrees interpreted by Hamilton (2014a, 2014c).

The OADC-FM solution and interpretation by Dr. Hardebeck along profile B on Figure 6-48 is in general agreement with Hamilton (2014a, 2014c), but disagrees in detail. The projection of the southern—and lower—of the two North Irish Hills structures intersects the surface approximately 1 km east of the surface projection of the seismicity lineament and approximately 2 km east of the mapped fault trace at the surface. In order for the North Irish Hills structure along profile B to fit the 30- to 35-degree dip of the SLRF of Hamilton (2012c) and impinge on the Shoreline fault at 1 to 2.5 km depth (Hamilton, 2012a, 2012c), the North Irish Hills structure—most closely represented by NIH 2 on Figure 6-47—would have to have a dip near or beyond the lower limit of its uncertainty range of $45 \pm 9^\circ$ (Figures 6-47 and 6-48).

Up-dip projection of the southern North Irish Hills structure on profile C (Figure 6-48) does not align with the SLRF interpreted by Hamilton (2012a, 2012c; Figure 6-21 and profile B on Figure 6-35). Profile C on Figure 6-48 shows the North Irish Hills structure intersecting the surface approximately 2 km east of a point labeled “SLB/WAF.” This “SLB/WAF” label coincides with the north-striking offshore continuation of the San Miguelito fault in eastern San Luis Obispo Bay, north of the Wilmar Avenue fault, and is marked by a yellow triangle on the map and profile (Figure 6-48). The intersection of profile C with the offshore Los Berros and Oceano faults, near where Hamilton (2012a) interprets the SLRF (Figure 6-21), is shown on the map and profile on Figure 6-48 as a small magenta star. This point is approximately 12 km west of where the North Irish Hills structure intersects the surface, showing that at this location the OADC-FM analysis does not identify an alignment of seismicity to support the SLRF.

The OADC-FM analysis by Dr. Hardebeck (Figure 6-48) is generally consistent with an alternative interpretation that north- to northeast-dipping structures underlie the Irish Hills and are defined by alignments of microseismicity (Figure 6-48). In detail, however, the OADC-FM analysis provides marginal or no support for the SLRF interpretation, and suggests that Dr. Hamilton’s assertion that the seismicity data show clear lineaments supporting his SLRF fault geometry at depth is not well supported by the data.

6.3.4.3 Evaluation of the SLRF from Seismic-Reflection Data near Point San Luis

Seismic-reflection data were used to evaluate the presence or absence of the SLRF at the longitude of Point San Luis and at the depth ranges proposed by Hamilton (2012a, 2012c). The seismic data evaluated are 3D Vibroseis data from a larger 2011 3D Vibroseis volume collected in 2011 (Figure 6-51; FCL, 2014b). These data were acquired in the field with a source-to-receiver configuration acceptable for 3D processing. Details pertaining to the acquisition, processing and interpretation of the broader data set can be found in the report by FCL (2014b). It is noted that many of Dr. Hamilton's cross sections (e.g., Figures 6-12 and 6-31) were drafted at the longitude of the DCP.P, whereas these Vibroseis data evaluated herein are at the longitude of Point San Luis, approximately 9 km to the southeast. Based on his testimony (Hamilton, 2012a) and interpreted seismicity cross sections presented at the SSHAC workshop (Hamilton, 2012c) (Figures 6-34 and 6-35), it is clear that Dr. Hamilton interprets the SLRF to be at shallow depths beneath the Point San Luis area.

To evaluate the presence or absence of the SLRF, the 3D seismic data were used in two ways:

1. The data were analyzed for direct evidence of a gently to moderately northeast-dipping fault at a depth range of approximately 2–6 km.
2. High-angle features observed in the data—interpreted to be faults—were used as strain markers. The down-dip continuity of these faults were used to assess the presence (or absence) of a gently to moderately northeast-dipping fault at depths of approximately 2–6 km.

Coarse mapping of these data was performed at a scale of 1:30,000 (horizontal equal to vertical) using IHS Kingdom software. Criteria used to identify throughgoing, low- or high-angle boundaries within the reflection data include: abrupt lateral changes in reflector amplitude, continuity, and orientation; localized disruption of lateral continuity of reflector horizons; and the juxtaposition of disparate reflector sequences or packages. The 3D volume was mapped using “arbitrary profiles,” or profiles oblique to the inline and crossline orientations of the 3D volume. These were extracted at various angles relative to the local structural fabric; for each orientation, a series of parallel transects were mapped to capture spatial and geometric trends.

A geologic map of the Point San Luis area is shown on Figure 6-51. Within the area of the 3D volume useful for evaluating the presence or absence of the SLRF most of the geology on the surface consists of Cretaceous sandstone and various rocks of the Franciscan Complex, including serpentinite, mélangé, and ophiolite (Figure 6-51). These geologic units form the basement rock of the Irish Hills. Exposures of topographically high ophiolite north of Point San Luis along the west side of San Luis Obispo Bay indicate that the Cretaceous sandstone is not very thick locally. In addition to the basement rocks, Miocene sedimentary, volcanic and volcanoclastic strata of the Obispo, Monterey and Pismo Formations outcrop along the northern portion of the 3D Vibroseis data (Figure 6-51).

The principal faults that traverse the 3D Vibroseis data as mapped by PG&E (2014b) include (from south to north): the San Luis Bay fault zone, the informally named Irish Canyon fault, and the San Miguelito fault zone (Figure 6-51). The San Luis Bay fault zone is shown by a queried trace and is located wholly within Franciscan Complex or Cretaceous sandstone (i.e., it juxtaposes similar rock types against one another). The Irish Canyon fault is concealed beneath the Squire Member of the Pismo Formation locally, but where exposed the fault separates Cretaceous sandstone (and locally, underlying Franciscan complex ophiolite) on the south from Franciscan Complex mélangé and serpentinite on the north (Figure 6-51). The Irish Canyon fault is associated with a relatively strong positive magnetic anomaly seen in the helicopter magnetic survey data (Langenheim et al., 2012), which is expressed by a “ridge” of pink-to-purple colors directly north of the fault on Figure 6-52. The magnetic susceptibility high on the north side of the fault corresponds to serpentinite and other rocks with high magnetic susceptibility within the mélangé. The San Miguelito fault zone trends more northwesterly than the other faults in the volume, and consists of several mapped splays (Figure 6-51). Collectively, the fault zone separates rocks of the Franciscan complex to the south from Miocene rocks to the north; this fault contact defines the southern margin of the ancestral Pismo Basin (PG&E, 2014d).

From the 3D volume, two north-south arbitrary profiles were selected for presentation in this report. The profiles are labeled A-A' and B-B', and are shown with respect to the surface geologic and regional magnetic anomaly maps on Figures 6-51 and 6-52. These profiles were chosen because they span the entire length of the volume, they are spaced far enough apart to provide an overview of acoustic (and, by proxy, geologic) features along strike, and they provide the clearest imaging of the deeper acoustic structure. The vertical profiles are shown to depths of –29,000 ft. (–8.8 km) for profile A-A' and –25,000 ft. (–7.6 km) for profile B-B'—the overall depths of interpretability on Figures 6-53 and 6-54, respectively.

The reflection profiles can be subdivided into two first-order seismic domains based on overall assemblages of reflection sequences, or packages, and acoustic expression. For example, the reflections on the left-hand side (southern half) of each profile on Figures 6-53 and 6-54 are predominantly flat-lying, planar, bright (i.e., high-amplitude), widely spaced (i.e., low-frequency), and laterally continuous. These reflectors are informally referred to as Domain 1, which, in turn, is subdivided into 1A and 1B based on alignments of reflection and amplitude terminations; these subdivisions are discussed below. Domains and subdomains are labeled on Figures 6-53 and 6-54. In contrast, reflections on the right-hand side (northern half) of the profiles are flat-lying to gently-tilted, planar to slightly curved, high-amplitude, moderate- to low-frequency, and laterally discontinuous. These reflections are informally referred to as Domain 2 (Figures 6-53 and 6-54).

The boundary between Domains 1 and 2 is important because it persists throughout the volume both laterally and to depth. The location of this boundary in the subsurface coincides with the surface trace of the Irish Canyon fault (Figures 6-51 and 6-52). In the reflection data, the Irish Canyon fault is expressed by a subvertical alignment of reflection and amplitude terminations, and the juxtaposition of disparate reflection

packages. Collectively, the alignment of terminations defines a steeply north-dipping to subvertical and planar contact. Similarly, the 1A/ 1B boundary (Figures 6-53 and 6-54) persists throughout the volume, both laterally and to depth. This boundary coincides with the mapped surface trace of the San Luis Bay fault (Figure 6-51). In the reflection data, the San Luis Bay fault is expressed by a subvertical alignment of reflection and amplitude terminations. Collectively, the alignment defines a planar to undulating contact. The similarity in reflection packages between subdomains 1A and 1B likely reflects the presence of the same rock type at depth on either side of the fault—interpreted as ophiolite based on the high-amplitude reflectivity and lateral continuity. This interpretation is consistent with the mapped surface relations, which show ophiolite and Cretaceous sandstone faulted against themselves (Figure 6-51). In contrast, the more pronounced change in the reflective character that occurs across the Irish Canyon fault likely indicates greater cumulative displacement on the fault—enough to juxtapose different rock units. This interpretation is consistent with the mapped surface geology, which shows relative north-side-up displacement across the Irish Canyon fault (placing stratigraphically lower Franciscan Complex rocks over higher Cretaceous sandstone), (Figure 6-51). The high angle of the Irish Canyon fault interpreted from the seismic volume is consistent with forward modeling of the magnetic data (Figure 6-52) performed for the Shoreline Fault Zone Report (Appendix D in PG&E, 2011), which matched the observed magnetic data across the Irish Canyon fault well with a modeled subvertical boundary between magnetic rocks to the north against non-magnetic rocks to the south.

Results from the evaluation of the 2011 3D Vibroseis data subset are consistent with results from analysis of 2D land seismic-reflection data (PG&E 2014d) that interpreted seismic-reflection data from a higher-resolution accelerated weight drop (AWD) source in this area. The seismic line AWD 112-140 is located along the eastern boundary of the Vibroseis subset and directly east of profile B-B' as shown on Figure 6-51. An interpretation of the line AWD 112-140 from PG&E (2014d) is shown on Figure 6-55. In these 2D data, both the Irish Canyon and San Luis Bay faults were mapped as subvertical to steeply north-dipping structures (PG&E, 2014d), and lie along trend with the equivalent structures mapped herein. These data were interpreted to a depth of approximately –8,000 ft. (–2.4 km), and provide an independent evaluation of geologic structure within the upper portion of the Vibroseis data (Figures 6-53 and 6-54).

The white transparency overlays on Figures 6-53 and 6-54 show the expected locations of the SLRF on the seismic profiles A-A' and B-B', respectively, based on the dips and depths interpreted by Hamilton (2014a, 2014c). The upper limit of the white overlays are based on an SLRF dipping 30 degrees northeast (perpendicular to the Shoreline fault zone) and intersecting a vertical Shoreline fault zone at a depth of –1 km (–3,280 ft.). The northern-most trace of the Shoreline fault zone closest to the profile lines on Figure 6-51 was used for the analysis. When resolved along the north-south orientation of profiles A-A' and B-B', the apparent dip of the SLRF at its upper limit is approximately 26 degrees (Figures 6-53 and 6-54). The lower limit of the white overlays on Figures 6-53 and 6-54 are based on an SLRF dipping 40 degrees northeast and intersecting a vertical Shoreline fault zone at a depth of –2.5 km (–8,200 ft.). The southwestern-most trace of the

Shoreline fault zone near the profile lines on Figure 6-51 was used for this geometry. When resolved along the north-south orientation of profiles A-A' and B-B', the apparent dip of the SLRF is approximately 33 degrees (Figures 6-53 and 6-54).

Based on the review and analysis of the Vibroseis data, there is no direct evidence of a gently to moderately dipping SLRF as proposed by Hamilton (2012a, 2012c) (Figures 6-53 and 6-54). Direct evidence of a thrust fault in seismic-reflection data might include reflections off the fault plane itself, gently to moderately dipping alignments of reflection and amplitude terminations, a hanging wall anticline, and/or growth strata. These types of features have been successfully imaged in seismic-reflection data collected elsewhere across blind thrust faults (e.g., Shaw and Shearer, 1999). No such features are apparent in the data, particularly within the white transparency areas where the SLRF is interpreted to be located (Hamilton, 2012a, 2012c).

Consistent with the lack of such direct evidence of a gently to moderately dipping fault, the down-dip continuity of the Irish Canyon and San Luis Bay faults precludes the presence of a lower-angle fault, such as the SLRF, within the depth of interpretability (approximately -29,000 ft./ -8.8 km to -25,000 ft./ -7.6 km) that includes the depths where the fault is interpreted to be located (Hamilton, 2012a, 2012c). This interpretation is based on the continuity of reflection and amplitude terminations, and the abrupt juxtapositions of disparate seismic-reflection packages that are used to delineate the Irish Canyon and San Luis Bay faults at depth.

6.3.5 Evaluation of Dr. Hamilton's San Luis Range/ IOF Thrust

In this section we summarize our conclusions regarding whether the SLRF interpretation by Dr. Hamilton is supported by available data based on analyses presented in Sections 6.3.3 and 6.3.4.

6.3.5.1 Fault Location at the Surface

Interpretations of available data are generally consistent with the SLRF surface trace proposed by Hamilton (2012a, 2012c). Analysis of seismic-reflection data, including new high-resolution 3D seismic data from San Luis Obispo Bay, suggest that faults at or near the surface cross San Luis Obispo Bay and intersect the Shoreline fault zone south of Point San Luis (PG&E, 2014c). New high resolution 2D and 3D data from the Point Buchon area show that a fault zone named the East Branch of the Point Buchon fault coincides with the boundary between bedrock and unconsolidated sediment, and continues north of Point Buchon as shown by Hamilton (2012a) on Figure 6-21 (PG&E, 2014a).

6.3.5.2 Fault Dip and Location at Depth

Whereas there is general support for north-dipping reverse faults beneath the Irish Hills, the data do not support specific fault geometries proposed by Dr. Hamilton for the SLRF. In the near surface, interpretation of high-resolution seismic-reflection data near Point Buchon suggests a subvertical East Branch of the Point Buchon fault and not an east-dipping fault (PG&E, 2014a). As shown in Section 6.3.4.3, the land seismic data do not

provide evidence for a gently dipping thrust fault in the general area of the SLRF proposed by Hamilton (2012a; 2012c) north of Point San Luis. Instead, interpretations of seismic-reflection data to depths of approximately 7 km or deeper identify steeply north-dipping San Luis Bay and Irish Canyon faults through the area where Dr. Hamilton would predict the SLRF to occur, demonstrating the absence of evidence for the SLRF in the data (Figures 6-53 and 6-54).

Within the seismogenic crust (2–12 km depth), there is little evidence that would support the interpretation of the SLRF. Review of the seismicity northeast of the Shoreline fault and beneath the Irish Hills in Section 6.3.4.1 shows scant earthquake activity not associated with known Quaternary or Tertiary faults, and does not support the existence of a buried east-dipping fault extending north from the Shoreline fault beneath the Irish Hills within 3.5 km of the DCP.P. An examination of the distribution of earthquakes shows that only 1.5 percent of the seismicity (three $M \sim 1$ microearthquakes) over a 31 km² area could potentially be associated with unknown faults.

Available single-event focal mechanisms have large nodal-plane orientation uncertainties and thus do not have sufficient resolution to evaluate the spatial properties of microearthquake faulting in the Irish Hills. Only two focal mechanisms within the 225 km² Irish Hills region are well enough constrained to delineate detailed microearthquake faulting properties.

Using approaches designed to identify planar features from seismicity independent of known or hypothesized faults, such as the OADC-FM approach used by Hardebeck (2014b), north-dipping alignments of seismicity with compatible first motion polarities are identifiable in the data. However, as shown in Section 6.3.4.2, the preferred alignments of planes fit to the data suggest the SLRF interpretation is neither a unique fit to the data nor fits the data well in detail.

6.3.5.3 Uplift Rate Boundary

The available data do not support the vertical displacement rate of 0.24 mm/yr proposed by Dr. Hamilton (2012c), and clearly do not support the 0.6 to 0.9 mm/yr fault slip rates proposed by Dr. Hamilton in written testimony (Hamilton, 2012a). The preferred uplift rate for the coastal terraces near the DCP.P and Point Buchon is 0.2 m/kyr (Figures 6-25 and 6-36), and evidence strongly suggests the continental shelf directly adjacent to the Irish Hills is also uplifting, rather than subsiding as Dr. Hamilton would suggest, with the primary uplift rate boundary on the west side of the San Luis–Pismo block being the Hosgri Fault Zone (Figure 6-36). Preferred interpretations of the shelf offshore the Irish Hills, discussed in Section 6.3.3.1, suggest that the Islay and Santa Rosa Reef shelves are uplifting at comparable rates as recorded by the coastal terraces. The primary uplift rate boundary observed onshore has a general east-west trend coinciding with the San Luis Bay fault zone, and the preferred interpretation of offshore data suggests the gradient in uplift rate extends offshore onto the shelf and does not bend and coincide with the Shoreline fault zone as predicted by the SLRF model (Figure 6-37). East-west-trending uplift rate boundaries are interpreted south of the San Luis Bay fault zone and across San Luis Obispo Bay. This southern uplift rate boundary between the continental shelf south

of the Irish Hills and the Santa Maria Basin may be broad and/or localized on east-west-trending faults such as the Oceano and Los Berros faults (Figures 6-36 and 6-37). As discussed in Section 6.3.3.2, interpretation of available multibeam data suggest the Shoreline and East Branch of the Point Buchon faults have no to very low differential uplift rates (Figures 6-28, 6-30, 6-38, 6-39) that are an order of magnitude (or more) lower than the rate interpreted for the SLRF by Hamilton (2014c).

6.3.5.4 Fit to Coastal Terrace Data

Dr. Hamilton states that the SLRF is required to fit the observed uniform uplift of the coastal terraces (Hamilton, 2012a). We disagree with this assertion, and instead suggest that there are several fault geometry solutions that can match the observed pattern of terrace uplift, including the proposed solutions by PG&E (1988, 2011). The SLRF, in contrast, does not appear to recognize the approximately 0.14 m/kyr, east-west-trending change in uplift rate coinciding with the San Luis Bay fault zone (Figure 6-37), which represents approximately 75 percent of the 0.2 m/kyr uplift rate of the Irish Hills coast between approximately the DCP.P and Montaña de Oro State Park. This uplift rate change is a key component to the fault source characterization by PG&E for the Shoreline Fault Zone Report (PG&E, 2011; Figure 6-22), but is not a recognized key element in Dr. Hamilton's model (Hamilton, 2012a).

7.0 CONCLUSIONS

The amount and concentration of geologic and geophysical data collected has been extensive and thorough allowing a confident assessment of the Diablo Cove fault and San Luis Range/ IOF thrust fault vis-à-vis the interpretations presented by Dr. Hamilton.

We conclude that the Diablo Cove fault does not represent a seismic hazard to the DCP.P, and there is no basis for considering the Diablo Cove fault as proposed by Hamilton (2012a, 2012c) to be either a fault displacement hazard or a seismic source of strong ground motions. We make this conclusion based on the following key points:

- Trench and excavation mapping conducted prior to construction of the DCP.P documented that the fault zone is discontinuous, is associated with minimal offset, and does not displace marine terrace deposits that are 120 ka. Thus, the faulting where observed directly is minor and inactive in the late Pleistocene.
- Geologic mapping and interpretation of MBES imagery do not support connecting the Diablo Cove fault offshore to the Shoreline fault zone.
- There is no basis for correlating seismicity with the Diablo Cove fault based on an evaluation of microearthquake locations and consideration of their location uncertainty.
- The short length of the Diablo Cove fault zone—probably less than half a kilometer—is not consistent with a down-dip width of several kilometers that would extend the fault to seismogenic depths.
- Structural analysis of geologic data and high-resolution 3D land seismic data at the DCP.P supports an interpretation, shared by the original mappers of the faults, that the faulting is related to shallow fold deformation and shortening that predates the late Quaternary and probably dates to the Miocene or Pliocene. The faulting may or may not be related to a Miocene diabase intrusion imaged directly north of the north-dipping Diablo Cove fault at shallow depths. Based on this interpretation, the fault extends to only a few tens to hundreds of meters depth.

With respect to Dr. Hamilton's postulated San Luis Range/ IOF thrust fault, we conclude that there is no clear evidence in the available data to support the presence of this fault, and there is evidence that precludes its presence. Accordingly, there is no basis for considering the San Luis Range/ IOF thrust to be a seismic hazard to the DCP.P as proposed by Hamilton (2012a, 2012c). We make this conclusion based on the following key points:

- Analysis of MBES bathymetry data and seismic-reflection data do not support the interpreted uplift rate boundary across the SLRF proposed by Hamilton (2012a, 2012c). Instead, interpretations of the data are consistent with a very low or negligible change in uplift rate where the SLRF is interpreted to impinge on the Shoreline fault zone and where the SLRF is interpreted to diverge from the Shoreline fault zone south of Point Buchon. Interpretations of coastal marine terrace data and offshore marine terraces are consistent with uplift rate boundaries that instead coincide with other structures considered by PG&E (1988, 2011) in past seismic hazard analyses.

- We disagree with the assertion by Dr. Hamilton that the SLRF interpretation is required to fit the observed pattern of coastal terrace uplift and instead suggest the observed pattern of coastal uplift may be matched by several proposed fault geometries, including those proposed by PG&E in past seismic hazard analyses (PG&E, 1988, 2011).
- Based on analyses of the available data, we disagree with the assertion by Dr. Hamilton that the seismicity data beneath the Irish Hills show a clear alignment supporting the SLRF at depth. The seismicity data can be interpreted in different ways to support many different fault models.
- Interpretation of land seismic-reflection data do not show evidence for a gently to moderately dipping SLRF fault beneath the southern Irish Hills in the general location proposed by Hamilton (2012a, 2012c). Instead, interpretations of the seismic-reflection data show steeply north-dipping structures down to approximately 7 km depth or deeper that coincide with recognized faults (the Irish Canyon and San Luis Bay) at the surface. The interpretation of these steeply dipping structures to depth precludes the presence of the SLRF.

Whereas the specific SLRF interpretation by Hamilton is not well supported by the available data, and by no means can be held up as a unique or preferred interpretation, the general solution of a primary, north- or north-northeast-dipping fault beneath the Irish Hills is consistent with several observations, and is a possible fault model that should be considered for seismic hazard analysis to the DCP.P. We note that the interpretations by Hamilton (2012a, 2012c) are being considered for evaluation and integration with other available data following the SSHAC Level 3 process. The SSHAC program for the DCP.P, which is being performed under regulatory review by the NRC, is creating a new SSC model.

8.0 LIMITATIONS

This analysis addresses the Diablo Cove fault and the postulated San Luis Range/ IOF thrust fault and their potential impact on seismic hazards to the DCP.P. The purpose of this analysis is to address the claims by Dr. Hamilton in his testimony using information available from the various cited sources. There are no limitations on the use of the results or conclusions.

9.0 IMPACT EVALUATION

The results and conclusions presented in this report do not have an impact on other Geosciences documents. The Diablo Cove fault has no impact on the seismic hazard at the DCP.P. The findings confirm that the Diablo Cove fault is not a surface-fault rupture hazard and show that it is not a source of potential ground motions for the DCP.P.

As there is no clear evidence indicating that the inferred San Luis Range/ IOF thrust fault as proposed by Dr. Hamilton exists, there is no basis to evaluate seismic hazard from such a structure in a deterministic framework. Dr. Hamilton's proponent model for the fault, and the more general seismic source characterization that a north- or northeast-dipping fault underlies the San Luis Range, is being considered for a PSHA as part of the SSHAC Level 3 program for the DCP.P.

10.0 REFERENCES

AMEC Environment & Infrastructure, Inc. (AMEC), 2012. *Preliminary Reevaluation of Emergent Shoreline Angles, San Luis Range, Diablo Canyon Power Plant, LTSP Update, San Luis Obispo, California*, letter report to William Page, PG&E Geosciences Department, 28 February.

California Energy Commission (CEC), 2008. *An Assessment of California's Operating Nuclear Power Plants: AB 1632 Committee Report*, CEC-100-2008-108-CTF, November.

California State University, Monterey Bay (CSUMB), 2007, 2009, 2010, and 2011. Multibeam echosounder (MBES) data for the California Central Coast. (Available at http://seafloor.csumb.edu/SFMLwebDATA_c.htm; accessed May 16, 2013.)

Fugro Consultants, Inc. (FCL), 2012. PGEQ-PR-07, Validation of the Commercial Software IHS Kingdom Version 8.6 Hotfix 4 2d/3dPAK, VuPAK, and Rock Solid Attributes, Report submitted to Pacific Gas and Electric Company, 18 December.

Fugro Consultants, Inc. (FCL), 2014a. *2012 3D Onshore Seismic Survey Report*, Project Report No. PGEQ-PR-21, Rev. 0, submitted to Pacific Gas and Electric Company, June.

Fugro Consultants, Inc. (FCL), 2014b. *2011-2012 Onshore 2D-3D Data Processing Report*, PGEQ-PR-08, Revision 0, submitted to Pacific Gas and Electric Company, July.

Hall, C.A., 1973. Geologic Map of the Morro Bay South and Port San Luis Quadrangles, California, U.S. Geological Survey Miscellaneous Field Studies Map FM—511, scale 1:24,000.

Hamilton, D.H., 2010. Dual System Tectonics of the San Luis Range and Vicinity, Coastal Central California, poster presentation at the American Geophysical Union Fall Meeting, San Francisco, Calif., 15 December, 20 pp. plus figures.

Hamilton, D.H., 2012a. Direct Testimony of Douglas Hamilton, February 10, 2012, Before the Public Utilities Commission of the State of California, Application of Pacific Gas and Electric Company for Approval of Ratepayer Funding to Perform Additional Seismic Studies Recommended by the California Energy Commission (U 39), Application No. 10-01-014.

Hamilton, D.H., 2012b. The Diablo Canyon Nuclear Power Plant in South Central Coastal California: Incremental Recognition of Seismic Hazard, 1965–2012: Oral presentation at the Association of Engineering Geologists Annual Meeting, Salt Lake City, UT, September.

Hamilton, D.H., 2012c. Irish Hills/San Luis Range Tectonic and Fault Model, Proponent expert presentation given at the DCP.P SSHAC SSC Workshop #2, San Luis Obispo, California, 6 November.

Hansen, D. M., and Cartwright, J., 2006. The three-dimensional geometry and growth of forced folds above saucer-shaped igneous sills: *Journal of Structural Geology*, vol. 28, p.1520-1535.

Hanson, K.L., Lettis, W.R., McLaren, M.K., Savage, W.U., and Hall, N.T., 2004. Style and Rate of Quaternary Deformation of the Hosgri Fault Zone, Offshore South-Central California: in Keller, M.A. (editor), *Evolution of Sedimentary Basins/Onshore Oil and Gas Investigations—Santa Maria Province*, U.S. Geological Survey Bulletin 1995-BB, 37 p.

Hanson, K.L., Wesling, J.R., Lettis, W.R., Kelson, K.I., and Mezger, L., 1994. Correlation, ages, and uplift rates of Quaternary marine terraces, south-central California: in Alterman, I.B., McMullen, R.B., Cluff, L.S., and Slemmons, D.B. (editors), *Seismotectonics of the Central California Coast Ranges*, Geological Society of America Special Paper 292, pp. 45-72 and 2 plates.

Hardebeck, J.L., 2010. Seismotectonics and fault structure of the California central coast, *Bulletin of the Seismological Society of America* **100** (3), 1031–1050, doi: 10.1785/0120090307.

Hardebeck, J.L., 2013. Geometry and Earthquake Potential of the Shoreline Fault, Central California, *Bulletin of the Seismological Society of America* **103**, 447–462, doi: 10.1785/0120120175.

Hardebeck, J.L., 2014a, Updated seismicity relocation catalog, file hypoDD_combined_update_140218.reloc, written communication to LCI, February 18.

Hardebeck, J.L., 2014b, Seismicity and Fault Structure of Estero Bay and the Irish Hills, Proponent expert presentation given at the DCP.P.SSHAC SSC Workshop #3, San Luis Obispo, California, 26 March.

Husen, S., E. Kissling, N. Deichmann, S. Wiemer, D. Giardini, and M. Baer, 2003, Probabilistic earthquake location in complex 3-D velocity models: Application to Switzerland, *J. Geophys. Res.*, **108**(B2), doi: 10.129/2002JB001778.

Jahns, R.H., 1966. *Geology of the Diablo Canyon Power Plant Site, San Luis Obispo County, California*, consultants report to Pacific Gas and Electric Company, 5 December, in Unit 2 PSAR, Appendix B.

Jahns, R.H., 1967a. *Geology of the Diablo Canyon Power Plant Site, San Luis Obispo County, California, Supplementary Report*, consultants report to Pacific Gas and Electric Company, 3 January, in Unit 2 PSAR, Appendix B.

Jahns, R.H., 1967b. *Geology of the Diablo Canyon Power Plant Site, San Luis Obispo County, California, Supplementary Report II*, consultants report to Pacific Gas and Electric Company, 8 July, in Unit 2 PSAR, Appendix B.

Jahns, R.H., 1968. *Geology of the Diablo Canyon Power Plant Site, San Luis Obispo County, California, Supplementary Report III*, consultants report to Pacific Gas and Electric Company, 19 June, in Unit 2 PSAR, Appendix B.

Jahns, R.H., Johnson, A.M., Blum, R.L., Korbay, S.R., Hamilton, D.H., and Harding, R.C., 1973. Geologic Map of Diablo Canyon Power Plant Site, map based on mapping performed 1966-1973 for Pacific Gas & Electric Company, iterations of map used in PG&E (1974) FSAR for Units 1 and 2, approximate scale 1:500.

Johnson, S.Y., and Watt, J.T., 2012. Influence of fault trend, bends, and convergence on shallow structure and geomorphology of the Hosgri strike-slip fault, offshore central California, *Geosphere* **8** (6), 1632-1656.

Killeen, K., 1989. "Timing of deformation of the Pismo syncline, San Luis Obispo, California," M.S. thesis, University of Nevada, Reno, 90 pp.

Langenheim, V.E., 2014. *Gravity, Aeromagnetic and Rock-property Data of the Central California Coast Ranges*, U.S. Geological Survey Open-File Report 2013-1282, 12 p.

Langenheim, V.E., Watt, J.T., and Denton, K.M., 2012. *Magnetic Map of the Irish Hills and Surrounding Areas, San Luis Obispo County, Central California*: U.S. Geological Survey Open-File Report 2012-1080, scale 1:24,000.

Leonard, M., 2010. Earthquake fault scaling: Self-consistent relating of rupture, length, width, average displacement, and moment release, *Bulletin of the Seismological Society of America* **100** (5a): 1971–1988.

Lettis, W.R., and Hall, N.T., 1994. Los Osos fault zone, San Luis Obispo County, California: in Alterman, I.B., McMullen, R.B., Cluff, L.S., and Slemmons, D.B. (editors), *Seismotectonics of the Central California Coast Ranges*, Geological Society of America Special Paper 292, pp. 73-102 and Plate 5.

Lettis, W.R., Kelson, K.I., Wesling, J.R., Angell, M., Hanson, K.L., and Hall, N.T., 1990. Quaternary deformation of the San Luis Range, San Luis Obispo County, California: in Lettis, W.R., Hanson, K.L., Kelson, K.I., and Wesling, J.R. (editors), *Neotectonics of South-Central Coastal California*, Friends of the Pleistocene Pacific Cell 1990 Fall Field Trip Guidebook, pp. 259–290.

Lettis, W.R., Kelson, K.I., Wesling, J.R., Angell, M., Hanson, K.L., and Hall, N.T., 1994. Quaternary deformation of the San Luis Range, San Luis Obispo County, California: in Alterman, I.B., McMullen, R.B., Cluff, L.S., and Slemmons, D.B. (editors), *Seismotectonics of the Central California Coast Ranges*, Geological Society of America Special Paper 292, pp. 111–132.

Lewandowski, N. and Unruh, J., 2014. Analysis of Stress and Strain in the Central Coast, California: Proponent expert presentation given at the DCP.P SSHAC SSC Workshop #3, San Luis Obispo, California, 25 March.

- Luyendyk, B.P., 1991. A model for Neogene crustal rotations, transtension, and transpression in southern California: *Geological Society of America Bulletin*, **103**: 1528–1536.
- Nitchman, S.P., 1988. “Tectonic Geomorphology and Neotectonics of the San Luis Range, San Luis Obispo County, California,” M.S. thesis, University of Nevada, Reno, 120 pp.
- Nitchman, S.P., and Slemmons, D.B., 1994. The Wilmar Avenue fault: A late Quaternary reverse fault near Pismo Beach, California: in Alterman, I.B., McMullen, R.B., Cluff, L.S., and Slemmons, D.B. (editors), *Seismotectonics of the Central California Coast Ranges*, Geological Society of America Special Paper 292, pp. 103–110.
- Nuclear Regulatory Commission (NRC), 1991. Supplement No. 34 to NUREG-0675, Safety Evaluation Report Related to the Operation of Diablo Canyon Nuclear Power Plant, Units 1 & 2, July.
- Ouillon, G., C. Ducorbier, and D. Sornette, 2008. Automatic reconstruction of fault networks from seismicity catalogs: Three-dimensional optimal anisotropic dynamic clustering, *Journal of Geophysical Research* **113**, 15 pp., B01306, doi: 10.1029/2007JB005032.
- Pacific Gas and Electric Company (PG&E), 1974. Units 1 and 2 Diablo Canyon Power Plant, Final Safety Analysis Report, Update 20, U.S. Nuclear Regulatory Commission Docket Nos. 50-275 and 50-323, Also includes Earth Science Associates, 1974, Geologic Map of the Morro Bay South and Point San Luis Quadrangles, San Luis Obispo County, California, and Adjacent Offshore Area, Plate VIII, Appendix 2.5D, scale 1:24,000.
- Pacific Gas and Electric Company (PG&E), 1988. *Final Report of the Diablo Canyon Long Term Seismic Program, Diablo Canyon Power Plant*, U.S. Nuclear Regulatory Commission Docket Nos. 50-275 and 50-323, July.
- Pacific Gas and Electric Company (PG&E), 1990. *Response to Question GSG Q16, Diablo Canyon Long Term Seismic Program, Diablo Canyon Power Plant*, U.S. Nuclear Regulatory Commission Docket No. 50-275 and No. 50-323, Plate GSG Q16-1.
- Pacific Gas and Electric Company (PG&E), 1991. *Addendum to the 1988 Final Report of the Diablo Canyon Long Term Seismic Program*, U.S. Nuclear Regulatory Commission Docket No. 50-275 and No. 50-323, February.
- Pacific Gas and Electric Company (PG&E), 2004. *Final Safety Analysis Report of the Diablo Canyon Independent Spent Fuel Storage Installation*, U.S. Nuclear Regulatory Commission Docket No. 72-26, Figures 2-6.6, 2.6-7, and 2.6-8.
- Pacific Gas and Electric Company (PG&E), 2011. *Report on the Analysis of the Shoreline Fault Zone, Central Coastal California*, Report to the U.S. Nuclear Regulatory Commission, January; <http://www.pge.com/myhome/edusafety/systemworks/dcpp/shorelinereport/>.

Pacific Gas and Electric Company (PG&E), 2013. *Stratigraphic Framework for Assessment of Fault Activity Offshore of the Central California Coast Between Point San Simeon and Point Sal*, Technical Report GEO.DCPP.TR.13.01.

Pacific Gas and Electric Company (PG&E), 2014a. *DCPP 3D/2D Seismic-Reflection Investigation of Structures Associated with the Northern Shoreline Seismicity Sublineament of the Point Buchon Region*, Technical Report GEO.DCPP.TR.12.01, Rev. 1.

Pacific Gas and Electric Company (PG&E), 2014b. *Geologic Mapping and Data Compilation for the Interpretation of Onshore Seismic-Reflection Data*, Technical Report GEO.DCPP.TR.14.01, Rev. 0.

Pacific Gas and Electric Company (PG&E), 2014c. *Offshore Low-Energy Seismic-Reflection Studies in Estero Bay, San Luis Obispo Bay, and Point Sal Areas*, Technical Report GEO.DCPP.TR.14.02, Rev. 0.

Pacific Gas and Electric Company (PG&E), 2014d. *Onshore Seismic Interpretation Project (ONSIP) 2011 Data Report*. Technical Report GEO.DCPP.TR.14.03, Rev. 0.

Satin, L.W., 1960. Apparent-dip computer, *Geological Society of America Bulletin* **71**: p. 231–234.

Shaw, J.H., and Shearer, P.M., 1999. An elusive blind-thrust fault beneath Metropolitan Los Angeles, *Science* **283**: 1516–1518.

Slemmons, D.B., and Clark, D.G., 1991. *Independent Assessment of the Earthquake Potential at the Diablo Canyon Power Plant, San Luis Obispo County, California*, Center for Neotectonic Studies, Mackay School of Mines, University of Nevada, Reno, NV, Appendix D in Supplemental Safety Evaluation Report 34 related to the operation of Diablo Canyon Nuclear Power Plant, Units 1 and 2, Docket Nos. 50-275 and 50-323, April.

Sliter, R.W., Triezenberg, P.J., Hart, P.E., Watt, J.T., Johnson, S.Y., and Scheirer, D.S., 2009 (revised 2010). *High-Resolution Seismic Reflection and Marine Magnetic Data Along the Hosgri Fault Zone, Central California*, U.S. Geological Survey Open-File Report 2009-1100, version 1.1

U.S. Geological Survey (USGS) staff, 1991. *Review of Geological and Geophysical Interpretations contained in Pacific Gas and Electric Co. Final Report of the Diablo Canyon Long Term Seismic Program for the Diablo Canyon Power Plant: A report to the staff of the U.S. Nuclear Regulatory Commission*, Appendix C in Supplemental Safety Evaluation Report 34 related to the operation of Diablo Canyon Nuclear Power Plant, Units 1 and 2, Docket Nos. 50-275 and 50-323, February.

Vittori, E., Nitchman, S.P., and Slemmons, D.B., 1994. Stress pattern from late Pliocene and Quaternary brittle deformation in coastal central California: in Alterman, I.B., McMullen, R.B., Cluff, L.S., and Slemmons, D.B. (editors), *Seismotectonics of the*

Central California Coast Ranges, Geological Society of America Special Paper 292, pp. 133–150.

Willingham, C.R., Rietman, J.D., Heck, R.G., and Lettis, W.R., 2013. Characterization of the Hosgri Fault Zone and adjacent structures: in Keller, M.A. (editor), *The Offshore Santa Maria Basin, South-Central California*, U.S. Geological Survey Bulletin 1995-CC, Evolution of Sedimentary Basins/Onshore Oil and Gas Investigations, Santa Maria Province.

VERIFICATION SUMMARY REPORT

Item	Parameter	Yes	No*	N/A*
1	Purpose is clearly stated and the report satisfies the Purpose.	X		
2	Data to be interpreted and/or analyzed are included or referenced.	X		
3	Methodology is appropriate and properly applied.	X		
4	Assumptions are reasonable, adequately described, and based upon sound geotechnical principles and practices.	X		
5	Software is identified and properly applied. Validation is referenced or included, and is acceptable. Input files are correct.	X		
6	Interpretation and/or Analysis is complete, accurate, and leads logically to Results and Conclusions.	X		
7	Results and Conclusions are accurate, acceptable, and reasonable compared to the Data, interpretation and/or analysis, and Assumptions.	X		
8	The Limitation on the use of the Results has been addressed and is accurate and complete.	X		
9	The Impact Evaluation has been included and is accurate and complete.	X		
10	References are valid for intended use.	X		
11	Appendices are complete, accurate, and support text.			N/A

* Explain "No" or "N/A" entries. (For example, Items 3 thru 7 would be N/A for a data report that simply presents the collected data.)

Comments (use additional pages as necessary):

General: All comments made to earlier drafts of Rev. 0 (submitted on July 14, 2014, July 20, 2014, July 28, 2014, and July 31, 2014) were addressed satisfactorily. There are no outstanding issues to be resolved.

Item 5: This report identifies the software used to analyze geologic and geophysical data and to prepare figures. None of these software required specific validation. The report directs the reader to appropriate reports where pertinent software validation needed to support statements/results cited in this report reside.

Item 11: No appendices are included in this report. This review confirmed that no appendix was referred to in the body of the report.

Verifier (ITR): KATHRYN L. HANSON / Kathryn L. Hanson 07/31/14
(name/signature) (date)

VERIFICATION SUMMARY REPORT

Item	Parameter	Yes	No*	N/A*
1	Purpose is clearly stated and the report satisfies the Purpose.	X		
2	Data to be interpreted and/or analyzed are included or referenced.	X		
3	Methodology is appropriate and properly applied.	X		
4	Assumptions are reasonable, adequately described, and based upon sound geotechnical principles and practices.	X		
5	Software is identified and properly applied. Validation is referenced or included, and is acceptable. Input files are correct.	X		
6	Interpretation and/or Analysis is complete, accurate, and leads logically to Results and Conclusions.	X		
7	Results and Conclusions are accurate, acceptable, and reasonable compared to the Data, interpretation and/or analysis, and Assumptions.	X		
8	The Limitation on the use of the Results has been addressed and is accurate and complete.	X		
9	The Impact Evaluation has been included and is accurate and complete.	X		
10	References are valid for intended use.	X		
11	Appendices are complete, accurate, and support text.			N/A

* Explain "No" or "N/A" entries. (For example, Items 3 thru 7 would be N/A for a data report that simply presents the collected data.)

Comments (use additional pages as necessary):

On this date I have reviewed corrections and modifications made to this report and have found previous comments to be satisfactorily addressed.

Minor, mostly editorial comments have been provided and there are no pending issues to resolve.

No appendices were provided with the report and I have verified that none were referenced in the text.

Verifier (ITR): Carlos Mendoza 7/31/2014
(name/signature) (date)